Induction Motor Parameters Estimation and Faults Diagnosis using Optimisation Algorithms

by

Fang Duan

Bachelor of Engineering,
Southwest Jiaotong University, China, 2005

Master of Engineering,
The University of Adelaide, Australia, 2008

Master of Engineering (Research),
The University of Adelaide, Australia, 2010

Thesis submitted for the degree of

Doctor of Philosophy

in

School of Electrical and Electronic Engineering
The University of Adelaide, Australia

October 2014

ADELAIDE
UNIVERSITY
AUSTRALIA

Contents

Abstract

Induction motors are the most widespread rotating electric machines in industry due to their efficient and cost-effective performance. Induction motors are used to mainly operate at the constant speed since the rotor speed depends on the supply frequency. The development of power electronic devices and converter technologies has revolutionized the adjustable-speed induction motor drives. For most high-performance control methods, the effective motor control requires precise knowledge of the motor's parameters, which are usually obtained from manufacturers. However, the manufacturers describe these parameters under starting or full-loading condition only, instead of the normal operating conditions. It is well known that motor parameters are influenced by not only the load level but also environmental factors, such as temperature, humidity and lubricant viscosity.

The first part of the thesis describes the application of the sparse grid optimisation method in solving the induction motor parameter estimation problem. Kernel of the method is the efficient search in minimising the cost function on the grid created by using the Hyperbolic Cross Points (HCPs). The cost function quantifies the difference between simulation results and measurement results. Within model reference adaptive system (MRAS) framework, a global optimisation algorithm, HCP algorithm (HCPA), runs the motor model and finds the best parameters to minimise the value of the cost function. Since the proposed method requires only voltage and current signals, it is compatible with sensorless control methods, which have the benefits of increasing system reliability and reducing cost. The presented experimental validation shows that the relative errors of the estimated parameter values are less than 10% under various load levels. The estimated parameters can be further refined by applying local search method using global search result as a start point.

On the other hand, an induction motor failure results in severe damage not only to the motor itself but also to motor related equipment devices in an industrial plant. Consequently, motor condition monitoring and fault diagnosis are of great necessity to detect motor faults at the early stage in order to reduce unscheduled downtime, repair costs, and increase life span of machines. Emergence of a fault will cause a gradual drift

of fault-related characteristic model parameters. Therefore, a generic method to detect motor faults developed in this research is based on monitoring these parameters.

In the second part of this thesis, the proposed parameter estimation technique based on the sparse grid optimisation is utilised to detect stator short circuit faults by monitoring two characteristic parameters: fault level and fault location. Experimental results show that the proposed diagnosis method is capable of detecting stator short circuit fault levels and location under different load conditions. Compared to the genetic algorithm, the HCPA shows improved robustness in the case of unbalanced voltage supply. This non-invasive diagnosis method only needs a short length of voltage and current signals recorded at switch board without disrupting the machine's normal operation.

The third part of this thesis demonstrates a multi-motor condition monitoring scheme which can substantially reduce implementation cost for some industrial plants. The proposed multi-motor condition monitoring scheme builds on top of the technology implemented in modern Intelligent Electronic Devices (IEDs) for motor protection and control. The backbone of this scheme is the broadly accepted Ethernet technology and the IEC 61850 communication standard. Due to the widespread use of IEC 61850 in various industries, cost of the technology is significantly reduced while reliability has been improved. Based on the proposed systems, various applications can be developed to achieve remote condition monitoring of induction motors.

Statement of Originality

This work contains no material that has been accepted for the award of any other degree or diploma in any university or other tertiary institution and, to the best of my knowledge and belief, contains no material previously published or written by another person, except where due reference has been made in the text.

I give consent to this copy of the thesis, when deposited in the University Library, being available for loan, photocopying, and dissemination through the library digital thesis collection, subject to the provisions of the Copyright Act 1968.

I also give permission for the digital version of my thesis to be made available on the web, via the University's digital research repository, the Library catalogue, the Australasian Digital Thesis Program (ADTP) and also through web search engines, unless permission has been granted by the University to restrict access for a period of time.

Signed

Date

Acknowledgments

I would like to express my sincere gratitude to my principle supervisor, Dr Rastko Živanović, for the immeasurable amount of support and guidance he has provided throughout this study. His advice on both research as well as on my career have been invaluable. I am indebted to my co-supervisor, Dr Said Al-Sarawi for his valuable suggestions and constructive advice. My sincere thanks goes to Assoc. Prof. Cheng-Chew Lim for his long term help, encouragement and advice. His professionalism and kindness have been always appreciated.

I must thank the office and workshop staff of the School of Electrical and Electronic Engineering, Mr Stephen Guest, Mrs Ivana Rebellato, Mrs Rose-Marie Descalzi, Ms Deborah Koch, Mr David Bowler, Mr Mark Innes, Mr Ryan King, Mr Anthony Schueller and Mr Ian Linke for their kind support throughout my PhD. They always ready to give their timely help whenever required.

Last but not least, I owe my deepest gratitude to my parents for the love and support they have provided through my entire life. A very special thank you to my husband Dr Longfang Zou for his unceasing support, encouragement and inspiration. I cannot present this work without expressing love to my daughter, Emily Chuanqi Zou, who enlightens my life with her sweet smile.

Conventions

Typesetting

This thesis is typeset using the LaTeX2e software. WinEdt build 5.5 was used as an effective interface to LaTeX.

Referencing

Referencing and citation style in this thesis are based on the Institute of Electrical and Electronics Engineers (IEEE) Transaction style.

Units

The units used in this thesis are based on the International System of Units (SI units).

Prefixes

In this thesis, the commonly used numerical prefixes to the SI units are ”p” (pico, 10^{-12}), ”n” (nano, 10^{-9}), ”μ” (micro, 10^{-6}), ”m”,(milli,10^{-3}), ”k”(kilo, 10^{3}), ”M”(mega, 10^{6}), ”G”(giga, 10^{9}), and ”T”(tera, 10^{12}).

Spelling

The Australian English spelling is adopted in this thesis.

Abbreviations

ACSI	Abstract communication service interface
AI	Artificial intelligence
BRB	Broken rotor bar
DDE	Dynamic data exchange
DER	Distributed energy resource
DTC	Direct torque control
EKF	Extended Kalman Filter
ER	Event report
ESPRIT	Estimation of signal parameters via rotational invariance techniques
FFT	Fast Fourier transform
FOC	Field-Oriented Control
GA	Genetic Algorithm
GOOSE	Generic object oriented substation events
HCP	Hyperbolic Cross Point
HCPA	Hyperbolic Cross Point Algorithm
HMI	Human machine interface
IED	Intelligent Electronic Device
I/O	Input/output
LAN	Local area network
LHS	Latin hypercube sampling
LL	Load level

LM	Levenberg-Marquardt
MCC	Motor control centre
MMS	Manufacturing messaging specification
MRAS	Model reference adaptive system
MUSIC	Multiple signal classification
NI	National Instruments
NM	Nelder-Mead
OLE	Object linking and embedding
OPC	OLE for process control
PDE	Partial differential equation
PSA	Pattern search algorithm
RPM	Revolutions per minute
RRTS	Remote relay testing system
SCADA	Supervisory control and data acquisition
SCL	Substation configuration language
SCSM	Specific communication service mapping
SER	Sequence of events recording
SNR	Signal to noise ratio
SR	Squared residual
VUF	Voltage unbalance factor

Author Publications

Journal

[1] F. Duan and R. Živanović, "Condition monitoring of an induction motor stator windings via global optimization based on the Hyperbolic Cross Points," *IEEE Trans. Ind. Electron.*, vol.PP, no.99, pp. 1–9, 2014.

Conference

[1] F. Duan and R. Živanović, "Induction motor stator faults diagnosis by using parameter estimation algorithms," in *9th IEEE International Symposium on Diagnostics for Electrical Machines, Power Electronics & Drives*, Valencia, Spain, Aug. 2013, pp. 274-280.

[2] F. Duan and R. Živanović, "Automated multi-motor condition monitoring based on IEC 61850," in *5th Annual International Energy Conversion Congress and Exhibition Asia DownUnder 2013*, Melbourne, Australia, Jun. 2013, pp. 699-703.

[3] F. Duan and R. Živanović, "Diagnosis of induction machine stator faults by parameter estimation techniques based on direct search on sparse grid," in *The 9th IET International Conference on Advances in Power System Control, Operation and Management*, Hong Kong, China, Nov. 2012, pp. 1-6.

[4] F. Duan and R. Živanović, "A model for induction motor with stator faults," in *AUPEC12 - 22th Australasian Universities Power Engineering Conference*, Bali, Indonesia, Sep. 2012, pp. 1-4.

List of Figures

List of Tables

Chapter 1

Introduction

THIS chapter provides a brief introduction on motor parameters estimation and condition monitoring. The motivation of the research is presented, followed by objectives of the thesis. The original contributions are highlighted. The structure of the thesis is sketched in a diagram and the content of each chapter is overviewed at the end of this chapter.

1.1 Introduction

Induction motors are the most important workhorse of the electrical power industry. They are low-cost, highly efficient, robust and reliable. The power range of induction motors is from a few hundred watts to megawatts, which satisfies the requirement of most industrial processes [1, 2]. Induction motors have been utilised in not only general purpose applications, including machine tools, elevators, pumps, centrifugal machines, conveyors and presses, but also hazardous locations and severe environments, such as grain elevators, shredders and equipments for coal, petrochemical and natural gas plants.

Environmental stress, heavy duty cycles, load conditions, installation and manufacture imperfections can reduce the efficiency or cause a malfunction of induction motors, leading to repair expenses and financial loss due to unexpected downtime. Reducing the operation and maintenance cost is one of the critical requirements in manufacturing industries. If the faults are not prognosticated beforehand, they may result in large revenue loss as well as pose threat to reliability and safety of operation. Condition monitoring is an effective method which can capture the initiation and growth of faults at early stage [3]. Therefore, reliable condition monitoring and fault diagnosis are necessary to lower maintenance cost and increase the productivity of the plant.

Development of the motor condition monitoring and fault diagnosis techniques resulted in an increased demand for induction motor drives. At early stage of application, only simply motor protections were applied, such as over-current, over-voltage and earth-faults to ensure safe and reliable operation. With the increasing demand of uninterrupted operation and system availability, enormous research efforts have been devoted to improve motor condition monitoring and fault diagnosis techniques [3–6].

With the development of power electronic devices, the past few decades have seen a rapid progress in efficient speed control by varying the supply frequency. Speed-sensorless control methods have become an important research area because physical sensors are not usually preferred considering the inherent problems such as fragility, mounting, cost, accuracy, and reliability [7]. Among many high-performance induction motor control methods, field-oriented control (FOC) [8] and direct torque control (DTC) [9] are of particular note in speed sensorless control methods. For both schemes, the effective induction motor control depends on the precise knowledge of the motor parameters. Inaccurate parameters results in a considerable degradation of steady state and transient response of such control system.

Induction motor parameters, provided by manufacturers, are usually obtained under starting or full-load condition, instead of the normal operating conditions. In reality, the motor parameter values might change under different circumstances. For example, temperature has great impact on rotor resistance, magnetic saturation, mutual inductance and stator resistance [10]. Furthermore, fabrication tolerances could lead to variations in the motor parameters even in the same batch. Therefore, accurate motor parameters identification has been a fundamental research field for motor control [10,11].

1.2 Motivation

For the purpose of condition monitoring and parameters estimation, many approaches have been developed so far [3,4,10–13]. Among them, the model-based methods have gained popularity as they have the following advantages [14–17]: low-cost, relative simplicity and flexibility. Such methods are based on an induction machine model that simulates systems behavior under normal and fault conditions when it is fed with the external operating conditions. An estimation algorithm is used to find the best parameters that can match the simulation results with the sensor data. Note that the "sensor data" is used in a broad sense to include voltage, current, angular speed, magnetic flux, temperature, vibration and so on.

The classical induction motor model has been adapted and extended for condition monitoring [14,15,18,19] and parameters estimation [13,16,17]. In the model based condition monitoring and fault diagnosis approaches, induction motor faults are described by characteristic parameters and motor faults can be diagnosed by monitoring these fault related parameters. For example, stator short circuit fault has been detected by monitoring fault level and location [15,18,19] and broken rotor bar fault can be characterised by the ratio of fault and total rotor bars and broken rotor bars location [15,20,21].

The mathematical model of an induction motor is nonlinear. Furthermore, the condition monitoring and parameters estimation are multi-dimensional tasks and typically there are more than four parameters to be estimated. In some methods, the induction motor models have been linearized to enable direct application of a least-squares identification algorithm [15,16]. Otherwise, global optimisation algorithms have to be employed since the results of local optimisation algorithms are dependent on the starting point and the algorithms might be trapped into local minima. The artificial

intelligence (AI)-based global optimisation algorithms, such as expert systems, fuzzy systems, neural networks and genetic algorithm (GA), are the mostly used methods in model based motor condition monitoring [22–25] and motor parameters estimation within model reference adaptive system (MRAS) framework [26–28]. However, the AI-based methods are heuristic search algorithms and require significant computational resources [25, 29]. Furthermore, they do not have any rigorous mathematical description.

The sparse grid approach has been applied in various fields for solving high dimensional and nonlinear tasks since this approach is able to reduce the complexity for a discretization, while maintaining a comparable discretization error [30–35]. Inspired by this fact, this thesis intends to apply the sparse grid approach to solve the high dimensional and nonlinear task of estimating motor parameters and fault related characteristic parameters. In order to find the best matching parameters of the motor model, a global optimisation algorithm, named Hyperbolic Cross Point Algorithm (HCPA) [36], is utilised to conducted effective search on the grid formulated using the Hyperbolic Cross Points (HCPs). Additional heuristics can be easily integrated with the HCPA, which will further reduce the number of search points and hence increase the computation efficiency.

1.3 Objectives of the thesis

In first part of this thesis, the focus is on the investigation of a low-cost, high-performance and flexible induction motor parameters estimation approach. The kernel of the approach is the efficient search of the parameters that enable the best match between the model output and measured results. In order to achieve these goals, several key methods have been employed, including

- **Non-intrusive method**: The approach requires only voltage and current signals without any invasive or additional expensive sensors or hardware circuitry. Consequently, the approach can be implemented during machine's normal operation.
- **Model-based method**: Since the mathematical model of induction motor presented in this approach is replaceable, it is feasible to implement the approach in other types of machines by replacing with corresponding machine mathematical models.

- **Sparse grid**: The motor parameter estimation task includes estimation of five motor parameters and load levels. Furthermore, the motor model and cost function are nonlinear. The sparse grid method is able to reduce the computational complexity for high dimension and non-linear tasks with an acceptable accuracy of the estimated parameters.

- **Adaptive global optimisation algorithm**: The selected global optimisation algorithm, HCPA, guarantees the detection of a global minimum. It conducts search on HCPs instead of the full grid or random search. The adaptiveness of this algorithm significantly reduces the number of evaluated HCPs and improves the computation efficiency.

In the second part of this thesis, the proposed parameter estimation approach is applied in motor condition monitoring and faults diagnosis. Since most of motor faults can be described by characteristic parameters, the motor condition can be assessed by monitoring these fault related characteristic parameters. To this end, the symmetrical motor mathematical model is adapted and extended by including these characteristic parameters. So, the motor condition monitoring task is converted to a model based fault related characteristic parameters estimation. Similar to motor parameter estimation, the selected optimisation algorithm tends to find the best parameters to match model outputs with measured outputs. Thus, it offers a generic method for motor condition monitoring and faults diagnosis by estimating fault related characteristic parameters. As an example, stator short circuit faults are utilised to illustrate and validate the proposed method. The faults can be characterised by two characteristic parameters, fault level and fault location. So, the faults are able to be diagnosed by monitoring these two characteristic parameters.

The third part of this thesis extends the single motor condition monitoring to multi-motor condition monitoring scheme. In order to reduce the implementation and operation cost, the proposed scheme is based on widely used Intelligent Electronic Devices (IEDs) for motor protection and control, Ethernet technology and IEC 61850 communication standard. In the proposed scheme, motors can be remotely monitored and controlled, which will substantially reduce the operating cost of large companies with several plants at different geographic locations. The overall system cost is minimised by utilising the existing IEDs and LAN/WAN infrastructure.

1.4 Statement of original contributions

This thesis presents several original contributions in the three fields of motor parameters estimation, condition monitoring and fault diagnosis, and multi-motor condition monitoring, as declared in this section.

- An induction motor mathematical model is implemented in SIMULINK. Associated MATLAB codes are developed to setup parameters of the motor model and transfer three phase voltage and current signals from abc to $\alpha\beta$ coordinates. The transient and steady state responses of the model are validated by measured voltage, current and rotor speed signals from a three phase 800 W, 380 V induction motor.

- In order to be compatible with the motor model, the HCPA is implemented in MATLAB. The program was validated by using nine widely used test functions in literature.

- An offline induction motor parameters estimation approach is proposed within MRAS framework. Aided by the sparse grid based global optimisation algorithm - HCPA, the approach is able to estimate multiple motor parameters in only one run, which eliminates the error resulting from the assumption of constant machine parameters. The approach also has the advantages of low cost, flexibility and simplicity because it does not require special test signals or configuration of machine. As a generic method, it can be utilised to estimate parameters of other machine types by using the corresponding mathematical model. Based on laboratory measurement, the relative errors of the estimated parameters are in the range of 10%, which can be further improved to 5% through applying a local search method with the global search result as a starting point.

- The sparse grid approach has been utilised in motor condition monitoring and fault diagnosis. The stator short circuit fault is employed to illustrate the proposed approach. The symmetrical induction motor mathematical model is extended by including two characteristic parameters, fault level and fault location. The motor model with stator short circuit faults was presented at the *AUPEC12 - 22th Australasian Universities Power Engineering Conference* [37] and is published in the proceedings. The inter-turn stator winding short circuit fault is detected under different load levels in laboratory environment. Several local and global

optimisation algorithms have been employed to estimate the fault related characteristic parameters. The advantages of HCPA have been highlighted through the comparison with an AI-base algorithm - GA and a direct search algorithm - pattern search algorithm (PSA). The HCPA showed improved robustness in the case of unbalance voltage supply. The initial results of condition monitoring and fault diagnosis of stator short circuit faults were presented at the *9th IET International Conference on Advances in Power System Control, Operation and Management* [38] and *9th IEEE International Symposium on Diagnostics for Electrical Machines, Power Electronics & Drives* [39] and are published in these conferences proceedings. The later comprehensive study is summarised and published in *IEEE Transaction on Industrial Electronics* under the title "Condition Monitoring of an Induction Motor Stator Windings via Global optimisation based on the Hyperbolic Cross Points" [19].

- A multi-motor condition monitoring scheme is demonstrated based on IEDs, Ethernet technology and IEC 61850 communication standard. The condition monitoring cost of a multi-motor industrial plant can be reduced by remote monitoring and control of motors. Using available IEDs and LAN/WAN infrastructure, the implementation cost only relies on the software components, such as manufacturing messaging specification (MMS) and application softwares. The proposed scheme was presented at the *5th Annual International Energy Conversion Congress and Exhibition* [40] and is published in the proceeding.

1.5 Overview of the thesis

A tree diagram of the thesis structure is shown in Fig. 1.1. The thesis overview is provided below.

Chapter 2 starts with a brief overview of the structure and working principle of induction motor. Based on the scope of this thesis, the chapter then describes state-of-the-art technologies for induction motor parameters estimation. It is followed by a review of the published literature on motor condition monitoring and fault diagnosis, including failure rate contribution, corresponding causes and diagnosis methods.

Chapter 3 presents a mathematical model of a generic three phase induction motor. The mathematical model is implemented in MATLAB/SIMULINK program environment. Based on the parameters of a three-phase 800 W, 380 V induction motor and recorded voltage signals from the motor, the simulated current signals and rotor speed

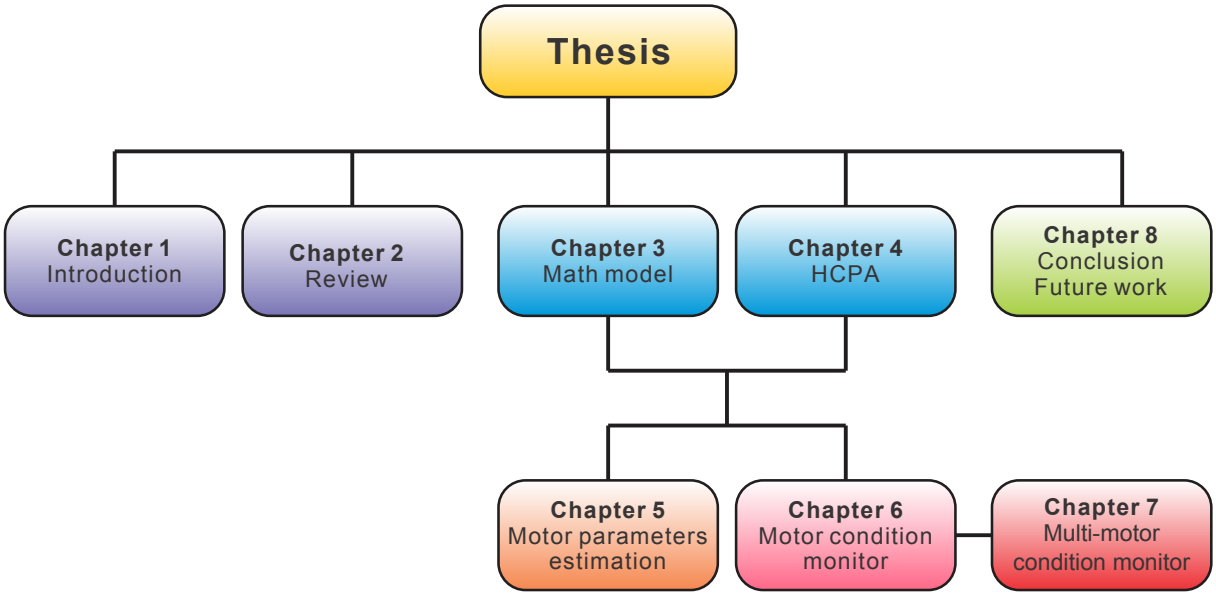

Figure 1.1. The tree diagram of the thesis.

are generated from the SIMULINK model and compared with the recorded values. The good agreement between simulated and measured results validates the proposed model. The model has been utilised in motor parameters estimation in Chapter 5. It has also been employed in motor condition monitoring and faults diagnosis after including fault related characteristic parameters in Chapter 6.

Chapter 4 describes the selected sparse grid based global optimisation algorithm - HCPA. It is able to perform the nonlinear and multi-dimensional parameters estimation tasks required in this thesis in a computation-efficient and accurate way. The algorithm is implemented in MATLAB program environment for the convenience of data exchange between the algorithm and SIMULINK induction model. The algorithm and MATLAB program are evaluated by using nine well known optimisation test functions in literature.

Chapter 5 proposes a low cost offline induction motor parameters estimation method. The proposed method relies on motor mathematical model and optimisation algorithm. In other words, the motor parameters are chosen by an optimisation algorithm to obtain the best matching between measured and simulated results. The difference between measured and simulated results is defined as a cost function. Considering the non-linearity of motor mathematical model and cost function, a global optimisation algorithm has to be employed to avoid being trapped into local minima. Thus, the global optimisation algorithm, the HCPA, is utilised to estimate the following five motor parameters: stator and rotor winding resistance, stator winding leakage and magnetising

inductance, and inertia constant as well as load level. The motor parameters are refined by using the Nelder-Mead local search method with the global search result as a start point. The simulation and experiment results demonstrate that the performance of the proposed method is satisfactory over a wide range of load levels.

In Chapter 6, inter-turn short circuit winding fault is utilised to demonstrate the proposed global optimisation algorithm based motor condition monitoring and fault diagnosis. The symmetrical induction motor mathematical model has been extended by including two characteristic parameters, fault level μ_f and location parameter θ_f. The inter-turn stator short circuit can be diagnosed by monitoring these two parameters. These fault related parameters are estimated by using the similar strategy as motor parameters estimation, i.e. optimising fault related characteristic parameters of motor mathematical model to match simulation with measurement results. Three algorithms, direct search algorithm - PSA, AI-base algorithm - GA and sparse grid based algorithm - HCPA, are respectively employed to search parameters. The condition monitoring has been conducted under unbalanced voltage, low signal to noise ratio (SNR) and different load levels. The evaluated results indicate that the direct search algorithm - PSA is sensitive to the starting point and an additional Latin hypercube sampling (LHS) method [41] had to be employed to generate a proper starting point for the PSA. The efficiency of the HCPA can be further improved by introducing heuristics that concentrates on locations where the fault location parameter θ_f lays. Compared to GA, the HCPA is more robust to supply voltage unbalance and variations in motor loading.

Chapter 7 proposes a concept of multi-motor condition monitoring. The modern IEDs and widely adopted IEC 61850 communication standard provide a cost effective platform for remote condition monitoring and control. After the explanation of IEC 61850 standard, an example based on the enterprise with two factory plants at different locations is employed to demonstrate the system architecture and implementation details. Based on existing IEDs and LAN infrastructure, the remote motor condition monitoring can be realised at low cost. Additionally, various applications can be developed to improve the capabilities for central monitoring, control, information sharing and management across technicians, engineers and managers in the enterprise.

Chapter 8 summarises the results of this thesis and recommends possible directions for future work.

Chapter 2

Induction Motor Parameters Estimation and Condition Monitoring: Literature Review

THE induction motor is an essential element in the industrial world. The controllability and reliability are the major requirements in many applications. The sophisticated controls rely on the accurate motor parameters, while reliable operation demands continuous monitoring of the motor condition and accurate fault diagnosis techniques. In this chapter, the state of the art results on induction motor parameter estimation and condition monitoring are reviewed. To facilitate a clear understanding, the structure and fundamentals of induction motor modelling are firstly presented in brief.

2.1 Introduction

The name of induction motor derives from the fact that the rotor current is induced by the rotating magnetic field from the stator instead of electrical connections. As a result, the induction motor has become the most widely used electrical motor because it is simple, low-cost and robust [2]. Desire to make operation of induction motors even more reliable motivated a considerable research effort in the last few decades.

Fig. 2.1 sketches a typical structure of a three phase induction motor. An induction motor rotor can be either squirrel-cage type or wound type. The rotor consists of a stack of steel laminations, which are clamped together and shrunk onto the steel shaft. In the squirrel-cage type, the conductor bars, evenly placed around a laminated circumference, are mechanically and electrically connected with two rings placed at the two extremities. In the wound type, rotor windings are constructed using insulated hard-drawn copper coils instead of bars. The rotor windings are accessible on the stator side through slip rings. The rotor is supported by two bearings mounted on separate pedestals or incorporated into the enclosure of the motor.

The stator consists of three main parts: frame, core and winding. The frame provides protection and mechanical strength to all the inner parts of the induction motor. It must be strong and rigid to support the stator core and the field winding. Since the space (i.e. airgap) between stator and the rotor is very small, the eccentricity of stator and rotor will lead to unbalanced magnetic pull. The main function of the stator core is

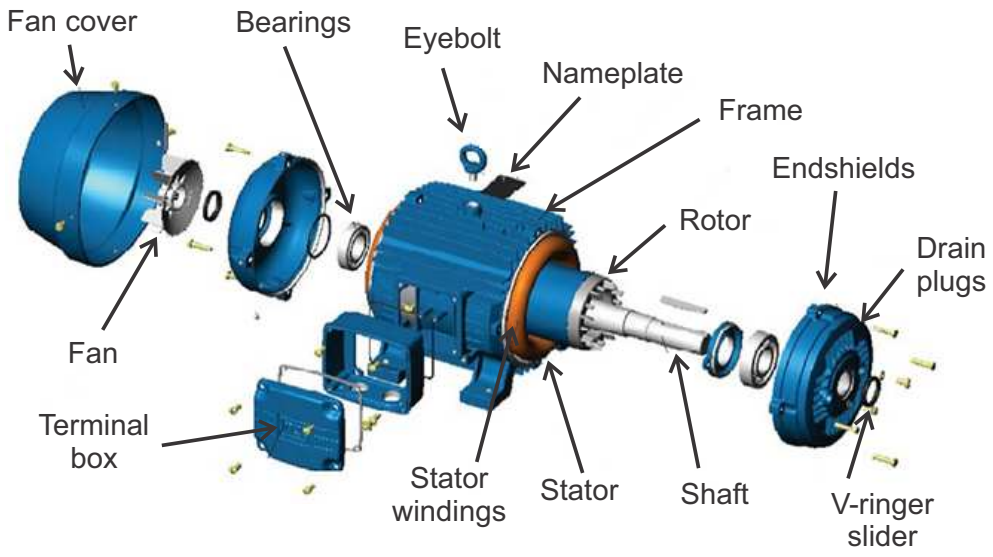

Figure 2.1. A typical structure of three phase induction motor. Adapted from Courtesy of Electromotors WEG SA, Brazil.

to carry the alternating flux. Thus, it must have low levels of vibration when carrying the magnetic flux and have sufficient cohesion to reliably transmit the load torque. In order to reduce the eddy current loss, the stator core is constructed from insulated laminations. The laminations are usually made up of silicon steel to lower hysteresis loss. The slots on the periphery of stator core carry windings, which are made of enameled wire. The three windings are displaced by 120° in space, with respect to each other.

The most fundamental principle of the induction motor is the creation of rotating and sinusoidally distributed magnetic field in the air gap. The stator windings are supplied by a three-phase balanced voltage with angular frequency $\omega_b = 2\pi f$, where f is the electrical supply frequency in Hz. The stator current creates a synchronously revolving magnetic field in the air gap of the machine. Given the number of pole pairs P in each phase, the revolving magnetic field rotates at the synchronous speed of ω_b/P. Fig. 2.2 shows the cross section view of a four-pole induction motor. In terms of revolutions per minute (RPM), the synchronous speed ω_s is

$$\omega_s = 120f/P. \tag{2.1}$$

The rotating magnetic field induces electrical current in the rotor conductors when the magnetic flux from the stator cuts across the rotor conductors. The magnetic field generated by rotor current has an opposite polarity in relation to the stator. The rotor current, considered with respect to electromotive force, produces a torque which acts in the direction of rotated magnetic field. According to the Faraday's and Lenz's laws, currents are induced in rotor's conductors whenever the rotor speed is different from the rotating magnetic field produced by the stator. The difference between the rotor speed ω_r and synchronous speed ω_s is defined as slip s,

$$s = 1 - \omega_r/\omega_s. \tag{2.2}$$

Induction motor usually has a small value of slip, normally less than 5% at full load. Thus, the difference between the rotor speed from the synchronous speed is practically small.

The rotor speed depends on the speed of the rotating magnetic field provided by the stator. The induction motors were traditionally used in fixed speed applications since it was difficult to vary the stator electrical frequency. With the development of power electronics and microprocessors, it became feasible to control rotor speed by using high

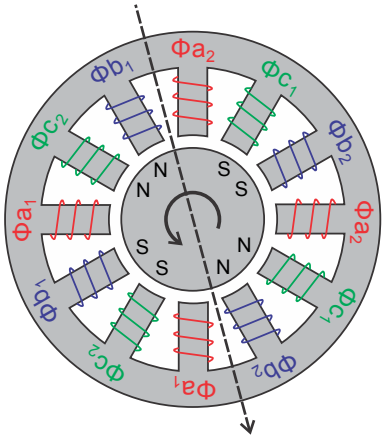

Figure 2.2. Cross section view of a four-pole induction motor.

speed power converters. In the last three decades, significant progress has been made on the topics of sensorless nonlinear observers, adaptive and robust nonlinear controller, output-feedback controller, fault-tolerant controllers, and fault detection and isolation algorithms [42]. The sophisticated and precise motor control relies on accurate motor parameters. Thus, motor parameters estimation has become a fundamental research field in motor control [10,11].

Among the motor performance factors, high reliability and continual services are essential requirements, especially in reliability-critical or safety-critical applications. The reliable performance also implies reduced unscheduled downtime and maintenance cost. The safe and reliable operation of induction motors relies on: built-in reliability in the design & manufacturing phase and condition monitoring during the field operation. Motor manufacturers keep improving design and fabrication techniques to provide high quality and reliability products. On the other hand, the reliable and continuous service are also dependent on installation, field operation and maintenance. The electrical, thermal and mechanical stresses due to environmental and operational conditions may induce catastrophic failure and wear out of induction motors. Therefore, an increasing attention has been paid to induction motor condition monitoring and fault diagnosis. The aim of condition monitoring and fault diagnosis is to detect incipient stage of a fault before serious damage occurs with high associated cost.

This chapter reviews the state-of-the-art motor parameters estimation and condition monitoring methods that have been applied for induction motors. The motivations and expected outcomes of this PhD research work are therefore formulated. The remaining parts of this chapter are organised as follows: Section 2.2 presents the offline

and online motor parameters identification methods. In Section 2.3, four major induction motor faults, i.e. bearing faults, rotor faults, eccentricity faults and stator faults, are presented in terms of failure rate contribution and corresponding causes. In addition, fault diagnosis methods for those fault types have been reviewed.

2.2 Induction motor parameters estimation

The induction motor parameters are usually obtained from full load, no load, and locked rotor test data during commissioning test as per IEEE Standard 112 [43]. However, induction motor parameters vary with temperature, saturation and frequency. The mismatch between the motor parameter values in the motor controller and actual motor parameter values results in a deterioration in the drive performance, eventually leading to unstable operation of the system. The fundamental equivalent circuit parameters of induction motor are stator/rotor resistance, stator/rotor leakage inductance, transient stator inductance and rated magnetising inductance. The operating power factor is also one of the critical parameters for motor control and protection functionalities [44]. Since the power factor can be obtained based on these equivalent circuit parameters [44–46], this thesis focuses on the estimation of equivalent circuit parameters. The motor parameters estimation methods can be generally categorised into two groups, offline identification methods [47–49] and online identification methods [50–52].

Depending on the control scheme, the required motor parameters are some or all of the following: The offline motor parameters identification is normally conducted during the commissioning session. In some methods, the motor is kept at standstill with a single phase supply. The stator resistance is usually determined by applying DC voltage, i.e. resistance is calculated by voltage-to-current ratio. The remaining parameters are then identified by the transient response when DC voltage pulse is applied [53]. In order to improve the accuracy, special excitation signals, adaptive observers, complicated mathematical processing methods are employed in [48,54]. Few research has been carried on the AC voltage excitation since the test voltage and current signals have to be carefully designed [47,55]. In other methods, motor parameters are estimated while rotor rotates. The standard DC, no-load and the pseudo-locked rotor testes are utilised in the laboratory experiments [56–58].

In the online motor parameters estimation, motor parameters are continually updated to the sensorless control algorithms. There are three major types of online motor parameters identification techniques.

1. **Spectral Analysis Techniques**: This type of techniques is based on the analysis of characteristic frequency components in the voltage/current spectrum. The frequency components are usually the consequent response to deliberately injected test signals, such as negative sequence components [59], pseudo-random binary sequence signal [60], and sinusoidal perturbation [61]. Since this type of techniques cannot be applied during normal operating conditions, it has hardly been utilised in practice.

2. **Observer-Based Techniques**: The observer-based techniques are able to estimate parameters during the normal operating conditions. Among several proposed techniques, Extended Kalman Filter (EKF) [62–65] and the adaptive observer [51, 66, 67] are of particular notice. The EKF method can achieve high accuracy estimation under noisy conditions at the cost of heavy computation.

3. **Model Reference Adaptive System (MRAS)-Based Techniques**: The MRAS approach has attracted considerable research interest because of low-cost and simplicity of implementation. It is a generic approach based on a principle of model reference adaptive control [68]. The kernel of this method is to optimise parameters for model so that the model outputs closely match the measured outputs. The accuracy is therefore heavily dependent on the accuracy of the applied model and the selected optimisation method [13, 19, 69]. The local optimisation algorithms might converge to local minima or even diverge when initial values of the parameters are far away from their real values. Thus, global optimisation algorithms are highly preferred in the MRAS based approach.

2.3 Induction motors faults and corresponding diagnosis methods

Depending on the region of fault occurrence, induction motor faults are generally classified into four categories: bearing faults, rotor faults, stator faults and eccentricity faults [12, 70]. The early work on fault diagnosis of induction motors dates back to

1970s to 1980s [71–73]. Since 1990s, it has seen the rapid developments in this topic. The pace to seek for cost-effective and accurate fault diagnosis solutions is still continuing due to the limitations of the prior-art methods and new change introduced by complex motor control systems, in which some faults related signatures are suppressed [12, 42]. Several papers have been devoted to addressing the induction motor condition monitoring and fault diagnosis methods [12, 70, 74–77]. In the following subsections, the diagnosis methods of bearing, rotor and eccentricity related faults are briefly presented first. Then, the methods for the stator related faults are discussed in detail, which are the most relevant to the research work presented in this dissertation.

2.3.1 Bearing faults

The bearing consists of an inner and an outer ring, where a set of balls or rolling elements are placed inside of raceways of these rings. Bearings can be spoiled by internal failures, such as spalls, pits and cracks on the rolling surfaces or external causes including contamination, corrosion, improper lubrication, misalignment and overloading operation [78–80]. Almost 40-50% of all motor failures are bearing related and these faults may lead to increased vibration and noise levels [81].

Among various bearing faults related signals (e.g., vibration, current, acoustic emission, sound pressure), vibration is the most widely used signal for diagnosing the faults [82–88]. In some cases, when the mechanical vibrations are not easily sensed (e.g. under harsh environments), current is more preferable as a non-intrusive diagnosis method [89–92]. However, the physical mechanism that links vibration and motor current is still somehow unclear [93]. Vibration effects on motor current are believed to be related to the air-gap variations, implying a correlation with displacement faults [94]. The study in [93] intended to compare the performance of vibration based methods and current based methods. It is concluded that the diagnosis of bearing faults by using current signal analysis is effective only for faults of low characteristics frequency, while vibration is a robust indicator for all the analyzed conditions. In [95, 96], both vibration and current have been used to provide an improved indication for bearing faults.

2.3.2 Rotor related faults

The rotor related faults include broken rotor bars and end-ring faults. The faults account for about 5-10% of total induction motor failures [97, 98]. The faults can be caused by excessive thermal, magnetic, residual or/and dynamic stresses; corrosion due to chemical or moisture; mechanical stress due to loose laminations and fatigued part [12].

The faults result in speed oscillation and abnormal frequent components in current spectrum. When broken rotor bar or end-ring occurs, the current cannot flow through the broken rotor bar, resulting in an unbalanced rotor flux. This unbalance is a combination of positive- and negative-sequence rotor flux, rotating at slip frequency in the opposite direction. Consequently, the faults give rise to a sequence of the sideband components $f_b = (1 \pm 2ks)f$ around the fundamental frequency component f, where $k = 1, 2, 3....$ The harmonics can be utilised as an indicator of broken rotor bar faults [90, 98, 99].

The issue of using the sideband frequency components as fault indicator is that load oscillations and non-ideal power supply (e.g. harmonic voltages and voltage unbalance) could also induce the same frequency harmonic, which cannot be differentiated from the one caused by rotor broken bar. Hence, different signal processing techniques have been applied to extract useful current spectrum information, such as motor current zero crossing instants [100], stator current envelope [101, 102], multiple discriminant analysis [103], wavelet decomposition [104, 105], multiple signal classification (MUSIC) [106], and estimation of signal parameters via rotational invariance techniques (ESPRIT) [107].

Apart from current based methods, other diagnostic methods are also proposed such as instantaneous power [108–111], external magnetic field [112], and air-gap torque [113]. In order to remove effects from non-ideal power supply and load oscillations, open terminal test method is demonstrated in [114]. Specifically, when all the three stator voltages are removed, the stator currents rapidly die down to zero and the rotor currents induce voltages in stator windings. Thus, broken bars faults can be diagnosed by monitoring harmonic frequency components in spectrum. In [115], a model-based diagnostic method is introduced for closed-loop controlled induction motors. The concept lies on the measurement of the oscillations at a frequency of $2sf$ presented in the d-axis component of the estimated rotor flux. Then, a virtual magnetising current component associated with the fault is reconstructed, which allows the detection and

quantification of the extension of rotor faults in the motor. It establishes a clear mathematical relationship between the obtained severity factor and number of broken rotor bars. The proposed method is claimed to be independent of the load level, speed, and control loop bandwidth of the motor drives. However, it requires an accurate mathematical model of the entire driving system, including the control loop parameters, which may be not available or of which the parameters are time varying due to aging or change of operating conditions. The latest study [116] shows that the axis ducts can produce frequency components identical to broken rotor bar frequency components of $(1 \pm 2s)f$. Accordingly, the startup transient is utilised to solve this challenge in this study.

The sensitivities of different diagnostic signals are compared in [117]. It has been found that even though stator current is popularly used for the broken bars diagnosis, it has the highest sensitivity among the partial power, torque, and total power. The partial power referred to the DC component has the best performance in term of sensitivity. The instantaneous powers, both total and partial, appear to be better suited for diagnosis of rotor abnormalities than the stator current. This is consistent with the conclusion in [109, 110].

2.3.3 Eccentricity related faults

Machine eccentricity is the condition that unequal air gap exists between the stator and rotor [3, 70]. The eccentricity faults can be the types of static air-gap eccentricity, dynamic air gap eccentricity or mixture of both forms, called mixed eccentricity. Static eccentricity is usually due to the stator core ovality or incorrect positioning of the rotor or stator during manufacturing process, and therefore may exist in new induction motors [118]. Although 10% is the maximum level of permissible eccentricity for most industrial plants [12], motor manufacturers make substantial effort to reduce the eccentricity level in order to minimise vibration, noise and unbalanced magnetic pull. Dynamic eccentricity is space and time dependent due to bent shaft, bearing wear, misalignment, mechanical resonance at critical speed, etc. The large eccentricity results in unbalanced radial forces and thus leads to stator to rotor rub, which causes serious damage of the stator and rotor.

The vibration and current signals were usually selected to diagnose the presence of eccentricity since the eccentricity variations lead to unique signature patterns in the

vibration and current spectra [12,119]. Few research results are based on vibration signals because vibration transducers are delicate, expensive and difficult to install [119]. Furthermore, the variation of the speed and mechanical load of the motor might result in the variation and lead to false alarm. On the contrary, current transformers can be readily installed in an industrial environment to acquire current signals without invasive components. Thus, the most eccentricity diagnosis methods are based on stator current spectral analysis, as discussed in follows.

The static and dynamic eccentricity related frequency components in the motor stator currents spectrum are [12]

$$f_e = [(kN_s \pm n_d)\frac{1-s}{P} \pm v]f, \tag{2.3}$$

where k is a non-zero positive integer; N_s is number of rotor slots; n_d is eccentricity order ($n_d = 0$ and $n_d = 1, 2, 3, ...$ respectively represent for static and dynamic eccentricity); $v = \pm 1, \pm 3, \pm 5$ is the order of the stator time harmonics. Since there is always some degree of both static and dynamic eccentricities in induction motors, the studies presented in [118, 120] investigate the models and diagnostic methods that are applicable to the presence of this mixed eccentricity. The mixed eccentricity can be detected by diagnosing low-frequency components near the fundamental [121]

$$f_L = |f \pm kf_r|, k = 1, 2, 3, ..., \tag{2.4}$$

where f_r is the rotational frequency of the rotor.

The limitation of the current spectrum analysis is that not all three phase induction motors have the featured harmonics in the stator current spectrum. The presence of these harmonics is dependent on the number of rotor slots and the number of fundamental pole pairs. Furthermore, some of these harmonics might appear in a healthy machine due to machine power supply and constructional unbalances [121]. In addition, the widely used motor control systems might suppress some fault signatures [122]. In order to improve the diagnosis accuracy, neural network based diagnosis method is trained and tested with data collected from a closed-loop drive-connected induction motor. Then, the trained network is able to diagnose the motor condition by estimating a threshold corresponding to an operating condition [123]. In [124], it is shown that the harmonics of the instantaneous power can also be utilised to diagnose the presence of eccentricity since the instantaneous power is the product of an instantaneous

line voltage and line current. An inverter-embedded test approach is proposed for offline eccentricity monitoring in [125]. When motor is at standstill, the inverter injects a small pulsating AC field superimposed on varying levels of the DC field. The measured equivalent differential inductance can be used as an indicator for detecting the present of eccentricity. The proposed method can be integrated with inverter without additional hardware, software and computational cost. Since the method diagnoses the fault at motor standstill, it cannot be utilised as on-line condition monitoring.

2.3.4 Stator related faults

The stator related faults are mostly responsible for 30-40% of all reported induction motor failures [126]. The faults usually result from the degradation of the stator insulation system mainly due to high temperature in stator core or winding; loose bracing for end winding, slack core lamination, slot wedges, and joints; short circuit or starting stresses; contamination from oil, moisture, and dirt; electrical discharges; leakage in cooling systems, etc. [6,76]. One of the dominant incipient failure stages is the interturn short circuit of windings. The local heat in these short-circuited windings will expand to adjacent windings and to stator core, resulting in stator core-ground insulation failure. The propagation of this process is typically as fast as 1-2 s from turn-to-turn short circuit to phase-to-ground or phase-to-phase faults when the breakdown temperature of the insulation is reached [127]. Therefore, reliable detection of the interturn short circuit fault in early stage would eliminate subsequent damage to adjacent windings and stator cores.

Intensive research efforts have been devoted to diagnosing stator interturn short circuit faults. The diagnosis methods can be broadly classified into three categories: analysis of fault signatures in recorded signals, model-based techniques and artificial intelligence (AI) techniques.

In the first class, the condition monitoring is achieved by identifying the variations of fault related signatures from recorded signals in time and/or frequency domain. Features extracted from recorded signals are employed to diagnose faults. Table 2.1 summaries some commonly used signatures based diagnosis methods. For example, the stator short circuit faults result in the asymmetry in the machine impedance. The

Table 2.1. Induction motor stator short circuit faults diagnosis methods based on fault signatures

Fault indicator	Non-Invasive	Online	Robust to power supply unbalance	Robust to intrinsic unbalance	References
Negative-sequence current	•	•			[72, 104, 105, 130–132]
Negative-sequence voltage	•	•	•		[133]
Zero-sequence voltage	•	•	•		[134]
Negative-sequence impedance	•	•	•		[128, 135, 136]
Stator induced voltage			•		[137]
Impedance matrix	•	•	•	•	[138, 139]
Instantaneous power	•	•	•	•	[140, 141]
Air-gap torque	•	•			[74]
Swing angle	•	•		•	[142, 143]
Stator current zero crossing instants	•		•	•	[144]

asymmetrical impedance leads to unbalanced phase currents, which cause negative-sequence currents [128]. This negative-sequence currents can be used as an indicator of the stator related faults [72].

Apart from low cost and technical simplicity, this type of methods does not require physical access to the motor because the current can be measured from the switchboard. However, these methods are only applicable to symmetrical rotating machines under constant power supply conditions [129]. The featured frequency components of the stator current spectrum used for the stator short circuit detection could also be caused by the intrinsic asymmetry of the motors, the power supply unbalance, machine saturation and so on, which is the common drawback of fault signatures based methods [12]. In order to improve the accuracy of faults detection, advanced signal processing techniques have been employed, such as wavelet transform [104, 105], extended Park's vector [130], multiple reference frames theory [131], and stator current envelope [132].

The second class is based on machine mathematical modelling that includes models of faults. Enabled by powerful computers, various approaches have been proposed to model the behaviour of induction motor under fault conditions [85]. The

winding function approach provides a deep understanding of frequency components under inter-turn short circuit faults [145, 146]. However, due to its complexity, it is not attractive in practical industrial applications. Other schemes are based on comprehensive mathematical models of induction motor and characteristic parameters of faults [14, 20, 37]. These schemes require specification of the fundamental motor parameters as well as initial values of the parameters that characterise machine condition. Measured stator voltage is utilised as input of the induction motor model to produce stator current as output. The squared value of the residual between the model output and measured stator current is defined as the objective function. If the value of the objective function is larger than a specified threshold, a new set of characteristic parameters will be estimated to reduce this value [14, 37]. New model output will be produced based on the new set of parameters. The process iterates until the objective function drops below the threshold. The motor condition can be determined according to these characteristic parameters. Since an induction motor model is highly nonlinear, local search algorithm might be trapped into local minima. Thus, the parameter estimation result of local search algorithm is highly dependent on the starting point [39]. In contrast, global optimisation algorithms are less sensitive to a starting point. The estimated result is close to global minimum at the cost of slightly increased computation time [19]. An alternative choice of direct parameter estimation is a stator-fault detection and identification strategy based on the generation of a residual by using a state observer [18, 147]. In this method, the negative sequence component of the current estimation error is utilised as a fault detector to lower the sensitivity of parameter change.

The third class is based on the artificial intelligence (AI) techniques [148]. The AI techniques are of great practical significance and have been utilised to solve complex problems in engineering and science. In the AI-based induction motor monitoring schemes, stator currents and voltages are usually the preferred inputs due to the noninvasive signal acquisition and elimination of expensive sensors [149]. Substantial research has been carried out on using AI-based techniques, including neural networks [24,150], expert systems [22], fuzzy systems [82,151,152], and genetic algorithm (GA) [25,26]. The AI-based diagnostic procedure can be divided into three steps, choosing the targeted failures, defining the cause effect relationships, and computing the diagnostic indices linked to the fault [29]. Compared to the signature analysis based approaches, the AI-based methods are robust to intrinsic motor asymmetry and power supply unbalance at the expense of significantly increased computation burden. Moreover, training data

or a set of existing operation data are usually required to improve the accuracy of the diagnostic results. With advancement in computation capability and cost reduction of digital signal processors [153], AI-based techniques are still very promising in future diagnosis of induction motors.

2.4 Conclusion

In this chapter, two major aspects of induction motor parameters estimation and faults diagnosis are reviewed. The description of induction motor structure and operation principle provides an in-depth understanding of the motor parameters, faults location and corresponding diagnosis methods. The motor parameters estimation methods are introduced in two categories, offline and online. The four major induction motor faults are presented in terms of failure rate contribution, corresponding causes and diagnosis methods.

The provided literature review presents the background material for this thesis. Based on a thorough understanding of the motor working principle and state-of-the-art technologies, a sparse grid based induction motor parameters estimation and fault diagnosis approach is proposed and presented in the following parts of the thesis.

Chapter 3

Three Phase Induction Motor Model

THIS chapter presents a dynamic MATLAB/SIMULINK model of three phase induction motor. The transient response of the model is examined in terms of stator current and rotor speed under various load levels. The model is validated by comparing simulated signals with measured voltage and current signals from a three phase 800 W, 380 V induction motor. The model has been utilised in motor parameters estimation and condition monitoring in the subsequent parts of the thesis.

3.1 Introduction

A large number of mathematical models for three phase induction motors have been intensively studied in the past decades [2, 14, 85, 154]. Induction motor models are constructed based on a suitable mathematical descriptions, which have relevant dynamic characterisation of the processes associated with induction motor operation in healthy and fault conditions. Model based methods have been widely implemented for induction motor parameters estimation [13, 69], condition monitoring and protection [15, 131, 145]. The advantages of model based methods are: they are no-intrusive and application cost tends to be low.

Verification and validation processes are of significant importance for the model development. Model verification involves checking the mathematics consistency, the solution procedure and the underlying assumptions. Validation is usually performed by comparing simulated and measured data.

This chapter aims at providing a three phase induction motor mathematical model to be used in motor parameter estimation and condition monitoring in the subsequent parts of the thesis. In particular, the three main goals of this chapter are:

1. to build a mathematical model, which is able to present both transient and steady state machine response under various load levels;

2. to realise the mathematical model in SIMULINK/MATLAB environment;

3. to validate the model using experimental data.

This chapter is organised as follows: a mathematical model for a three phase induction motor is presented in Section 3.2. Then, the model is transferred from *abc* to $\alpha\beta$ coordinates to reduce computational complexity. In Section 3.3, the dynamic model is implemented in SIMULINK/MATLAB environment. The model is then validated under both transient and steady state conditions. In the validation process, recorded currents from a three phase 800 W induction motor operated at different conditions are used and results are provided in Section 3.4. The analysis presented in this chapter serves as a common base for all the investigations and results presented later in Chapter 5 (model based parameter estimation) and Chapter 6 (model based condition monitoring).

3.2 Mathematical model of induction motor

The modelling of the three-phase induction machine relies on the following hypotheses and assumptions [155],

1. The machine air gap has supposed constant thickness. So, the notching effects and generating space harmonic can be ignored;
2. The magnetomotive forces created by stator and rotor phases are spread in a sinusoidal way along the air gap;
3. The slotting in stator and rotor produces negligible variation in respective inductances;
4. The magnetic field is not saturated and has a constant permeability;
5. The skin effect, hysteresis and eddy effects are not taken into account;
6. The harmonics in voltages and currents are neglected;
7. The temperature of motor stays constant resulting in constant parameters in the mathematical models.

These hypotheses allow the development of a practical mathematical model with a limited complexity.

3.2.1 Induction motor model in abc coordinates

The proper selection of an induction motor model structure and its parametrisation are critical since they influence both the observability and identifiability. The dynamic mathematical model of an induction motor is usually represented in the stationary a, b and c reference frame in terms of voltage, current and flux linkage as follows [2, 156],

$$\begin{bmatrix} v_{as} \\ v_{bs} \\ v_{cs} \end{bmatrix} = R_s \begin{bmatrix} i_{as} \\ i_{bs} \\ i_{cs} \end{bmatrix} + \frac{d}{dt} \begin{bmatrix} \lambda_{as} \\ \lambda_{bs} \\ \lambda_{cs} \end{bmatrix}, \tag{3.1}$$

$$0 = R_r \begin{bmatrix} i_{ar} \\ i_{br} \\ i_{cr} \end{bmatrix} + \frac{d}{dt} \begin{bmatrix} \lambda_{ar} \\ \lambda_{br} \\ \lambda_{cr} \end{bmatrix}, \tag{3.2}$$

$$\begin{bmatrix} \lambda_{as} \\ \lambda_{bs} \\ \lambda_{cs} \end{bmatrix} = \boldsymbol{L}_{sr} \begin{bmatrix} i_{ar} \\ i_{br} \\ i_{cr} \end{bmatrix} + \boldsymbol{L}_{ss} \begin{bmatrix} i_{as} \\ i_{bs} \\ i_{cs} \end{bmatrix}, \tag{3.3}$$

$$\begin{bmatrix} \lambda_{ar} \\ \lambda_{br} \\ \lambda_{cr} \end{bmatrix} = \boldsymbol{L}_{rr} \begin{bmatrix} i_{ar} \\ i_{br} \\ i_{cr} \end{bmatrix} + \boldsymbol{L}_{rs} \begin{bmatrix} i_{as} \\ i_{bs} \\ i_{cs} \end{bmatrix}, \tag{3.4}$$

where

v_{abcs}, i_{abcs} and λ_{abcs}	stator voltage, current and flux,
i_{abcr} and λ_{abcr}	rotor current and flux,
R_s and R_r	stator and rotor resistance.

The stator-to-stator winding inductances $\boldsymbol{L}_{ss}$, rotor-to-rotor winding inductances $\boldsymbol{L}_{rr}$ and stator-to-rotor mutual inductances $\boldsymbol{L}_{sr}$ are presented as [154],

$$\boldsymbol{L}_{ss} = \begin{bmatrix} L_{ls} + L_s & L_{sm} & L_{sm} \\ L_{sm} & L_{ls} + L_s & L_{sm} \\ L_{sm} & L_{sm} & L_{ls} + L_s \end{bmatrix}, \tag{3.5}$$

$$\boldsymbol{L}_{rr} = \begin{bmatrix} L_{lr} + L_r & L_{rm} & L_{rm} \\ L_{rm} & L_{lr} + L_r & L_{rm} \\ L_{rm} & L_{rm} & L_{lr} + L_r \end{bmatrix}, \tag{3.6}$$

$$\boldsymbol{L}_{sr} = L_{sr} \begin{bmatrix} \cos(\theta_r) & \cos(\theta_r + \frac{2\pi}{3}) & \cos(\theta_r - \frac{2\pi}{3}) \\ \cos(\theta_r - \frac{2\pi}{3}) & \cos(\theta_r) & \cos(\theta_r + \frac{2\pi}{3}) \\ \cos(\theta_r + \frac{2\pi}{3}) & \cos(\theta_r - \frac{2\pi}{3}) & \cos(\theta_r) \end{bmatrix}, \tag{3.7}$$

where L_{ls}, L_s and L_{sm} are the per phase stator leakage inductance, self inductance of the stator winding and mutual inductance between stator windings, respectively; L_{lr}, L_r and L_{rm} are the per phase rotor leakage inductance, self inductance of the rotor winding and mutual inductance between rotor windings, respectively; L_{sr} is the mutual inductance between stator and rotor windings; θ_r is rotor angular position. The peak value of stator-to-rotor mutual inductances $\boldsymbol{L}_{sr}$ is equal to the transpose of rotor-to-stator mutual inductances $\boldsymbol{L}_{rs}$, i.e. $\boldsymbol{L}_{sr} = \boldsymbol{L}_{rs}^T$.

Based on the hypotheses at the beginning of this section, the inductances of induction motor can be expressed in terms of the per phase total equivalent stator winding turns N_s, equivalent rotor winding turns N_r and airgap permeance P_g [2],

$$\begin{aligned} L_s &= N_s^2 P_g; \\ L_{sm} &= N_s^2 P_g \cos(\frac{2\pi}{3}); \quad L_{rm} = N_r^2 P_g \cos(\frac{2\pi}{3}); \\ L_{sr} &= N_s N_r P_g \qquad\qquad L_r = N_r^2 P_g. \end{aligned} \tag{3.8}$$

Thus, the some of inductances can be represented by L_s to reduce the number of variables,

$$\begin{aligned} L_{sm} &= -\frac{L_s}{2}; \quad L_{rm} = -(\frac{N_r}{N_s})^2 \frac{L_s}{2}; \\ L_{sr} &= \frac{N_r}{N_s} L_s; \qquad L_r = (\frac{N_r}{N_s})^2 L_s. \end{aligned} \tag{3.9}$$

In literature, the above induction machine model are usually simplified to reduce the computational requirement, for example, using reduced-order motor model [157] or considering the steady state and neglecting the dynamic models [11]. In this thesis, the motor parameters are estimated based on both transient response and steady state condition.

3.2.2 Induction motor model in $\alpha\beta$ coordinates

The three-phase quantities (voltages and currents) are transformed from *abc* to $\alpha\beta$ coordinates to reduce computational complexity. The transformation matrices of stator and rotor variables from *abc* to $\alpha\beta$ are defined as follows [158],

$$\begin{aligned} X_{\alpha\beta s} &= T_{\alpha\beta} X_{abcs} \qquad\quad : \textit{stator variables} \\ X_{\alpha\beta r} &= T_r(\theta_r) T_{\alpha\beta} X_{abcr} \;\; : \textit{rotor variables}, \end{aligned} \tag{3.10}$$

where

$$T_{\alpha\beta} = \sqrt{\frac{2}{3}} \begin{bmatrix} 1 & -1/2 & -1/2 \\ 0 & \sqrt{3}/2 & -\sqrt{3}/2 \end{bmatrix}, \tag{3.11}$$

$$T_r(\theta_r) = \begin{bmatrix} \cos\theta_r & -\sin\theta_r \\ \sin\theta_r & \cos\theta_r \end{bmatrix}. \tag{3.12}$$

Applying these two transformation matrices to Eqs. (3.1)-(3.4) and replacing L_{sm}, L_r, L_{rm} and L_{sr} with L_s using Eq. (3.9), the mathematical model of an induction motor in the $\alpha\beta$ reference frame is presented as,

$$\begin{bmatrix} v_{\alpha s} \\ v_{\beta s} \end{bmatrix} = R_s \begin{bmatrix} i_{\alpha s} \\ i_{\beta s} \end{bmatrix} + \frac{d}{dt} \begin{bmatrix} \lambda_{\alpha s} \\ \lambda_{\beta s} \end{bmatrix}, \tag{3.13}$$

$$0 = R_r' \begin{bmatrix} i_{\alpha r}' \\ i_{\beta r}' \end{bmatrix} + \frac{d}{dt} \begin{bmatrix} \lambda_{\alpha r}' \\ \lambda_{\beta r}' \end{bmatrix} - \omega_r T_r \left(\frac{\pi}{2}\right) \begin{bmatrix} \lambda_{\alpha r}' \\ \lambda_{\beta r}' \end{bmatrix}, \tag{3.14}$$

$$\begin{bmatrix} \lambda_{\alpha s} \\ \lambda_{\beta s} \end{bmatrix} = L_{ls} \begin{bmatrix} i_{\alpha s} \\ i_{\beta s} \end{bmatrix} + L_m \left(\begin{bmatrix} i_{\alpha s} \\ i_{\beta s} \end{bmatrix} + \begin{bmatrix} i_{\alpha r}' \\ i_{\beta r}' \end{bmatrix} \right), \tag{3.15}$$

$$\begin{bmatrix} \lambda_{\alpha r}' \\ \lambda_{\beta r}' \end{bmatrix} = L_{lr}' \begin{bmatrix} i_{\alpha r}' \\ i_{\beta r}' \end{bmatrix} + L_m \left(\begin{bmatrix} i_{\alpha s} \\ i_{\beta s} \end{bmatrix} + \begin{bmatrix} i_{\alpha r}' \\ i_{\beta r}' \end{bmatrix} \right), \tag{3.16}$$

where $R_r' = (\frac{N_s}{N_r})^2 R_r$, $i_{\alpha\beta r}' = \frac{N_r}{N_s} i_{\alpha\beta r}$, $\lambda_{\alpha\beta r}' = \frac{N_s}{N_r} \lambda_{\alpha\beta r}$, $L_{lr}' = (\frac{N_s}{N_r})^2 L_{lr}$ and $L_m = \frac{3}{2} L_s$.

The equation of motion of a rotor can be expressed as [2],

$$\frac{2H}{\omega_b} \frac{\mathrm{d}\omega_r}{\mathrm{d}t} = T_{EM} + T_{Ex}, \tag{3.17}$$

where H is the inertia constant, ω_b and ω_r are base electrical radians per second and instantaneous angular speed of the rotor, respectively. The electromagnetic torque T_{EM} can be calculated by

$$T_{EM} = \frac{3P}{4} (\lambda_{\beta s} i_{\alpha s} - \lambda_{\alpha s} i_{\beta s}), \tag{3.18}$$

where P is the number of pole pairs in each phase. The externally-applied mechanical torque, T_{Ex}, is related to the load level LL,

$$T_{Ex} = LL \times \frac{P_B}{(2/P)\omega_b}, \tag{3.19}$$

where P_B is the rated power output of the machine.

Fig. 3.1 shows the equivalent circuit model of a three phase induction motor in the $\alpha\beta$ reference frame. Based on the mathematical equations and equivalent circuit, a MATLAB/SIMULINK model is constructed in the next section.

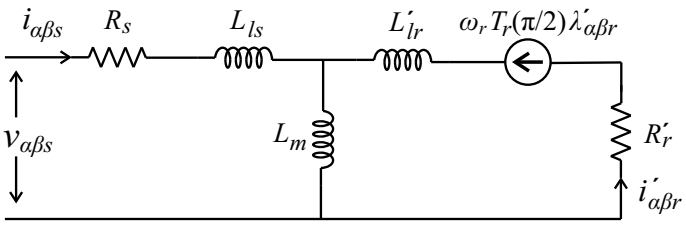

Figure 3.1. Equivalent circuit representation of an induction motor in the $\alpha\beta$ reference frame.

Table 3.1. Inputs and outputs of each block in the SIMULINK model.

Block name	Input	Output
Alpha	$v_{\alpha s}$, $\lambda'_{\beta r}$, ω_r	$I_{\alpha s}$, $\lambda_{\alpha s}$, $\lambda'_{\alpha r}$
Beta	$v_{\beta s}$, $\lambda'_{\alpha r}$, ω_r	$I_{\beta s}$, $\lambda_{\beta s}$, $\lambda'_{\beta r}$
Synchronisation	$I_{\alpha s}(t)$, $I_{\beta s}(t)$	$I_{\alpha s}(t+T_d)$, $I_{\beta s}(t+T_d)$
Rotor speed	$I_{\alpha s}$, $\lambda_{\alpha s}$, $I_{\beta s}$, $\lambda_{\beta s}$	ω_r

3.3 SIMULINK model of induction motor

MATLAB / SIMULINK has been chosen for the implementation of the induction motor model proposed in the Section 3.2.2. SIMULINK offers a convenient graphical user interface to implement continuous and discrete systems in the input-state-output form. Apart from the mathematical representation of the induction motor model and configuration of the operation conditions, SIMULINK/MATLAB can be expediently used to setup a suitable solution method and analyse results.

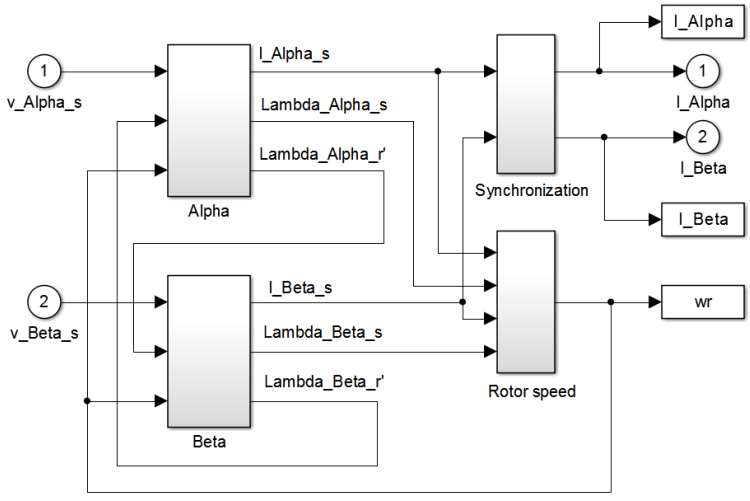

Figure 3.2. SIMULINK model of induction motor.

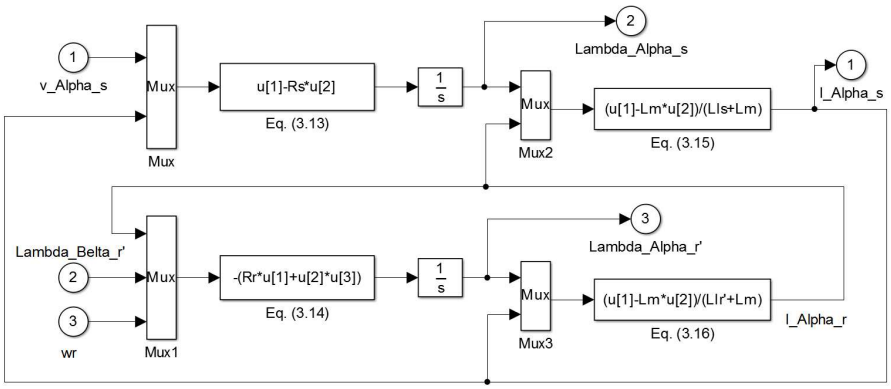

Figure 3.3. SIMULINK block diagram of *Alpha* block in Fig. (3.2).

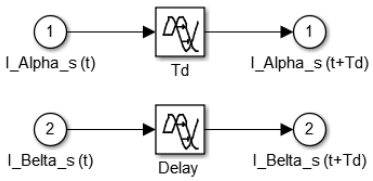

Figure 3.4. SIMULINK block diagram of *Synchronisation* block in Fig. (3.2).

For the sake of simplicity, a MATLAB code is written to initialize induction motor (i.e. calculate initial values) and transfer three phase voltage signals from *abc* to $\alpha\beta$ coordinates using Eq. (3.10) before incorporated in the SIMULINK model. In SIMULINK, the system is drawn on screen as block diagrams, as shown in Fig. 3.2. The model is composed of four blocks and the inputs and outputs for each block are listed in the Table 3.1. Blocks *Alpha* and *Beta* are utilised to calculate stator and rotor currents and flux vectors in *Alpha* and *Beta* axis, respectively. The diagram of block *Alpha* and related equations are shown in Fig. 3.3. The corresponding equation is marked on the each block. The diagram of block *Beta* is omitted because it is similar to the *Alpha* block. The generated current signals are synchronised with the measured voltage signals. The unsynchronised measured voltage and current signals, which results from

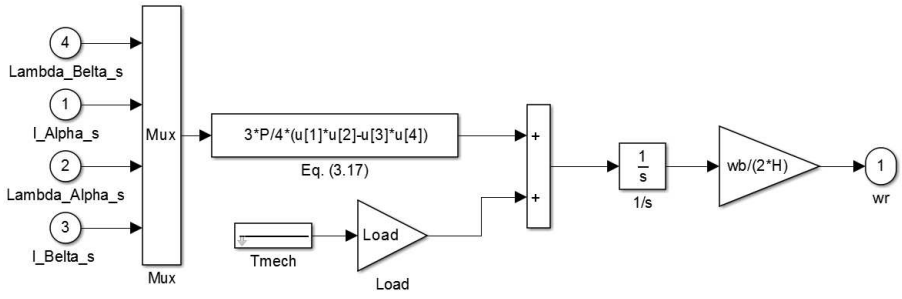

Figure 3.5. SIMULINK block diagram of *Rotor speed* block in Fig. (3.2).

measurement error, leads to a time offset between simulated and measured current signals. Therefore, a parameter T_d is defined to synchronise simulated and measured currents in *Synchronisation* block, as shown in Fig. 3.4. Rotor speed is calculated based on the load level in block *Rotorspeed*. In Fig. 3.5, the block *Tmech* is utilised to dynamically change the load level, which will be illustrated in the next section.

3.4 Model validation

The proposed induction motor model is experimentally validated by using a three phase 800 W induction motor. The motor parameters, provided by the machine manufacturer, are tabulated in Table 3.2. The experiment setup is shown in Fig. 3.6. The stator voltage and current of the induction motor are measured by the voltage transducer LEM LV 25-P [159] and the current transducer LEM HY-15 [160], respectively. The signals from these two transducers are recorded using National Instruments (NI) 16-bit PCMCIA DAQCard-6036E card [161]. The sampling frequency is 10 kHz. Another motor is utilised as a load and the load level was varied by adjusting a clutch between the motor and the loading motor.

The simulated stator currents are generated from the SIMULINK model based on the recorded stator voltage. The recorded current signals $i_{a,b,c}$ are transferred to $i_{\alpha\beta}$ in $\alpha\beta$ coordinates by using transform matrix Eq. (3.10). Figs. 3.7(a) and (b) show simulated and recorded currents in $\alpha\beta$ coordinates from the 0% load of the symmetrical induction motor after synchronisation. As explained in the Section 3.3, the inset of Fig. 3.7 shows a time offset between the recorded and simulated currents before synchronisation due to the measurement error. Therefore, an additional parameter, T_d, is defined in the SIMULINK model to calibrate the time offset, as shown in Fig. 3.4. The simulated and recorded currents have a good agreement in both transient state (i.e. from 0 - 0.2 s) and steady state (after 0.2 s). The squared residual (SR) of simulated and recorded currents

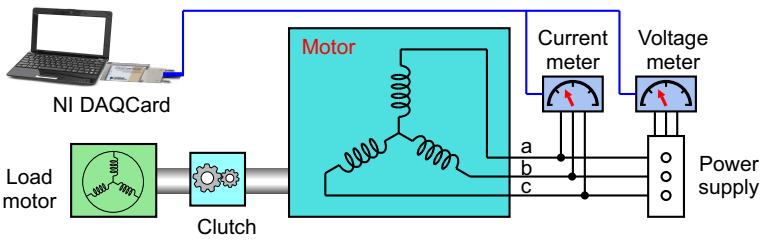

Figure 3.6. The experiment setup of motor parameters estimation.

Table 3.2. Induction motor parameters.

Parameter name	Value
Ouput power	800 W
Line voltage	380 V
Rotor inertia	0.0025 Kg m^2
Rated frequency	50 Hz
Number of poles	4
No load speed	1492 RPM
Rated power factor	0.74
Stator winding resistance (R_s)	8.4 Ω
Referred rotor winding resistance ($R_r^{'}$)	8.2 Ω
Stator winding leakage inductance (L_{ls})	0.0328 H
Stator magnetising inductance (L_s)	0.4377 H
Referred rotor winding leakage inductance ($L_{lr}^{'}$)	0.0328 H
Inertia constant (H)	1.8 s

is defined as,

$$SR = \left[i_{\alpha s} - i'_{\alpha s}\right]^2 + \left[i_{\beta s} - i'_{\beta s}\right]^2. \tag{3.20}$$

In order to double check the model and transform, the simulated currents are transferred to abc coordinates by using the matrix T_{abc}

$$T_{abc} = \sqrt{\frac{2}{3}} \begin{bmatrix} 1 & 0 \\ -1/2 & \sqrt{3}/2 \\ -1/2 & -\sqrt{3}/2 \end{bmatrix}. \tag{3.21}$$

Fig. 3.8 shows the simulated and measured stator currents in abc coordinates. As expected, they coincide with each other in both transient and steady state. Thus, the study is conducted in $\alpha\beta$ coordinates to avoid unnecessary transformation in the following parts of the thesis.

The model is further examined by adding different load levels while motor is running. Fig. 3.9 shows the simulated stator current with various load level. The motor starts without load (Fig. 3.9(a,c)). The 50% load is added at 1 s and the load is increased to 100% at 1.5 s (Fig. 3.9(b,d)). The simulated steady state currents of the motor with 0%, 50% and 100% load are respectively 1.45, 2.01 and 2.47 A, which is close to the corresponding measured values of 1.47, 2.00 and 2.48 A. The simulated rotor speeds at

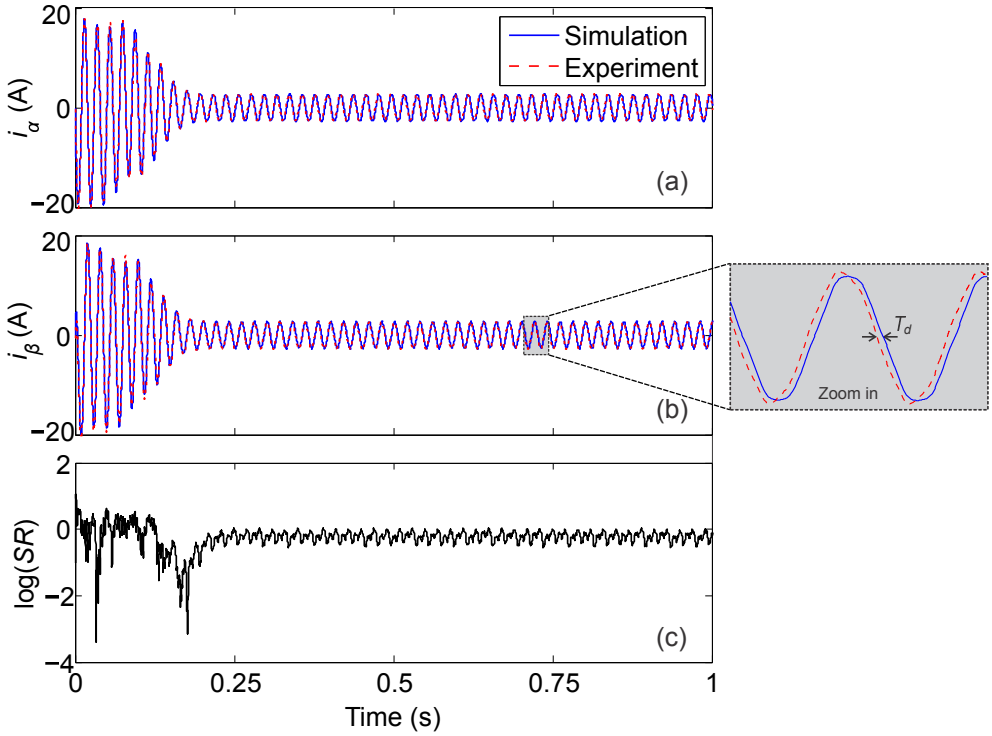

Figure 3.7. Comparison between simulated and measured stator currents in $\alpha\beta$ coordinates after synchronisation. The simulated and measured stator currents i_α (a) and i_β (b) from the 0% load of the symmetrical induction motor ; The squared residual (SR) of simulated and recorded stator currents in logarithmic scale (c). Inset: Zoomed figure shows the time offset without synchronisation. A parameter T_d is defined to synchronise the simulated and measured currents.

load levels of 0%, 50% and 100% are shown in Fig. 3.10. The rotor is at standstill at the beginning. After the three phase current is supplied to the stator, the magnetic field produces starting torque. The rotor speed reaches the steady state when it revolves at the same speed of the rotating magnetic field. The synchronous speed (ω_s) and measured rotor speed (ω_r) are 1500 RPM and 1942 RPM, respectively. According to the definition of slip (s) in Eq. (2.2), the slip of the unloaded motor is 0.53%. When a load is applied to the motor, the rotor speed decreases to develop torque to drive the load, as shown in Fig. 3.10. The speed reaches a constant speed again until the new balance of induced emf and torque. The simulated rotor speed with 50% and 100% load levels are 1437 RPM and 1401 RPM, respectively. These values are close to the corresponding measured rotor speed of 1435 RPM and 1400 RPM.

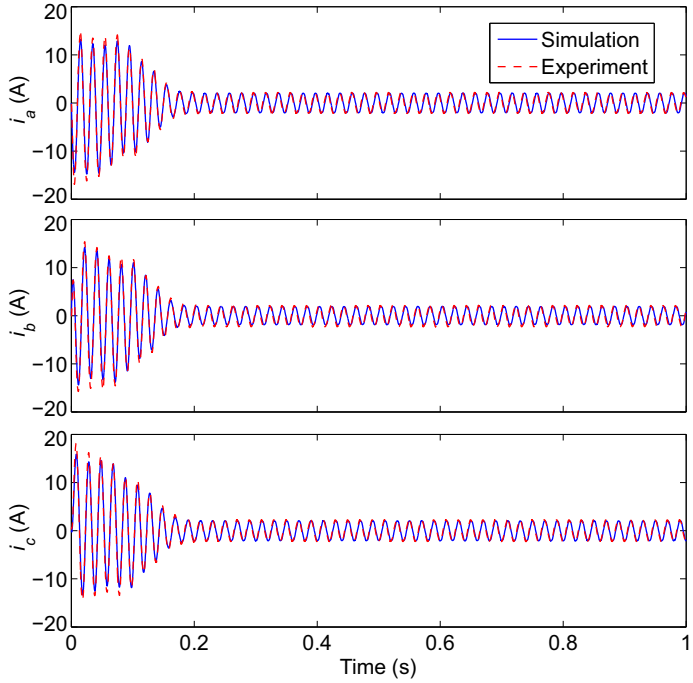

Figure 3.8. Comparison between simulated and recorded stator currents from the 0% load of the symmetrical induction motor in *abc* coordinates after synchronisation.

3.5 Conclusion

In this chapter, a mathematical model for a three phase induction motor is presented. The model is able to simulate an induction motor in both transient and steady state conditions with various load levels. The proposed model is realised in MATLAB/SIMULINK and examined by using recorded voltage and current signals from a three phase 800 W, 380 V induction motor. The good agreement between simulated and measured results validates the proposed mathematical model. The model is utilised to conduct motor parameters estimation and condition monitoring in the subsequent parts of the thesis.

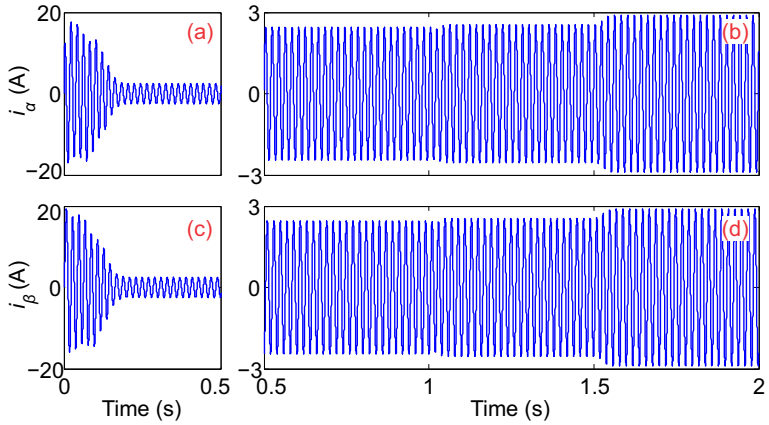

Figure 3.9. Simulated stator current in $\alpha\beta$ coordinates with dynamic load level. From 0 to 1 s, 0% load; From 1 to 1.5 s, 50% load; From 1.5 to 2 s, 100% load.

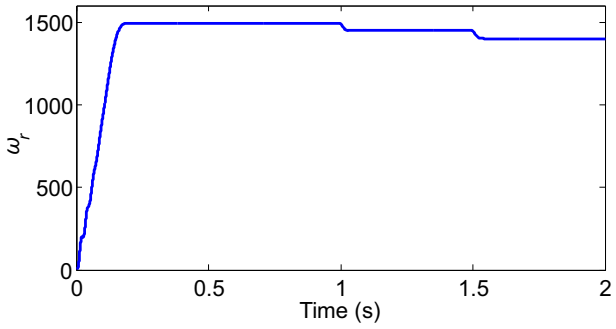

Figure 3.10. Simulated rotor speed with dynamic load level. From 0 to 1 s, 0% load with steady state rotor speed of 1942 RPM; From 1 to 1.5 s, 50% load with steady state rotor speed of 1437 RPM; From 1.5 to 2 s, 100% load with steady state rotor speed of 1401 RPM.

Chapter 4

Hyperbolic Cross Point Algorithm

THE sparse grid approach has been applied in various fields in solving high dimensional optimisation tasks. In this chapter, one of the types of sparse grids, named Hyperbolic Cross Points (HCPs), is described. An algorithm based on HCPs, named the HCP Algorithm (HCPA), is presented for induction motor parameters estimation and condition monitoring in the subsequent chapters of this thesis. As a global optimisation algorithm, the HCPA is ensured to conduct global search for nonlinear and multi-dimensional parameters estimation tasks in a computation-efficient and accurate way. Furthermore, the adaptiveness of this algorithm significantly reduces the number of points to be evaluated and further improves the efficiency. The HCPA is implemented using the MATLAB as a programming tool and examined by using nine well-known test functions available in literature.

4.1 Introduction

The sparse grid approach is derived from a 1-dimensional multi-scale basis by a tensor product construction. This approach is originally developed for solving the high dimensional partial differential equations (PDEs) because the conventional discretisation methods can only deal with the PDEs up to three or four dimensions due to storage requirements and computational complexity [162, 163]. Given a prescribed accuracy, the computational cost exponentially increases with an increase of the dimensionality d of the considered problem. For a d-dimensional function, a full grid includes $O(N^d)$ points, where N is the number of grid points in one coordinate direction. Whereas, the sparse grid method only employs $O(N \cdot (\log N)^{d-1})$ grid points and the accuracy $O(N^{-2} \cdot (\log N)^{d-1})$ is nearly as good as the conventional full grid methods [164]. The sparse grid method provides acceptable accuracy with less number of evaluated points for high dimensional functions.

Although the sparse grid approach is originally developed for the solution of PEDs, the applications have been significantly extended in various fields. It is particularly attractive for the numerical solution of moderate and higher dimensional tasks, such as integral equations [165,166], interpolation and approximation [167,168], integration problems [30], eigenvalue problems [169], data mining [32], option pricing [33], finance and insurance [31], and global optimisation [21,38]. The sparse grid approach results in reducing the complexity for a discretization, while maintaining a comparable discretization error. Thus, it is possible to tackle high dimensional optimisation problems.

In this thesis, one of the types of sparse grid, named Hyperbolic Cross Points (HCPs), is applied in global optimisation problems of motor parameters estimation and motor condition monitoring. The global optimisation algorithm, conducting search on HCPs, is thus named HCP algorithm (HCPA) [36]. The proposed method is based on the three phase induction motor mathematical model presented in Chapter 3 [37]. Since the induction motor model is highly nonlinear, local search algorithm might be trapped into local minima. The parameter estimation result of local search algorithm is highly dependent on the start point [39]. Therefore, the global optimisation algorithm based on HCP is selected to enable the global minimum search for this nonlinear and multi-dimension parameter estimation task in a computation-efficient and accurate way. Furthermore, the adaptiveness of this algorithm significantly reduces the number of evaluated points and improves the efficiency as explained in Section 4.4. In

addition, the efficiency of the HCPA can be further improved by introducing very simple heuristics that concentrate points in a region where a solution lays. These heuristic techniques reduce the required number of sampling points while preserving rigorous mathematical function approximation properties, which is further discussed in Chapter 6.

The work performed in this chapter aims at introducing the sparse grid based global optimisation algorithm, the HCPA. This chapter is organised as follows, the sparse grid approach and types of sparse grids are reviewed in Section 4.2. Section 4.3 presents the definition of the HCPs and the HCPA. The HCPA is implemented in MATLAB. In Section 4.4, the implemented HCPA is verified using nine well-known test functions from literature [36,170]. Combined with the induction motor model presented in Chapter 3, the algorithm is used for induction motor parameters estimation and condition monitoring in Chapters 5 and 6, respectively.

4.2 Sparse grids

In one dimension (d=1), a set of equidistant grid points in the internal $\Omega_l := [-0.5, 0.5]$ of *Level* L is given by

$$\Omega_L := \{x_{i,L} = i \cdot h\}, i = \pm\{0, 1, 2, ..., 2^L - 1\}. \tag{4.1}$$

where $h = 2^{-(L+1)}$ is the mesh size.

The scheme of 1-dimensional grid points with *Level* $L = 0, 1, 2, 3, 4$ and 5 are shown in Fig. 4.1. Based on the 1-dimensional grid points, the d-dimensional grid is defined as

$$\Omega_L = \Omega_{L_1} \times \Omega_{L_2} \times ... \times \Omega_{L_d} \ , \tag{4.2}$$

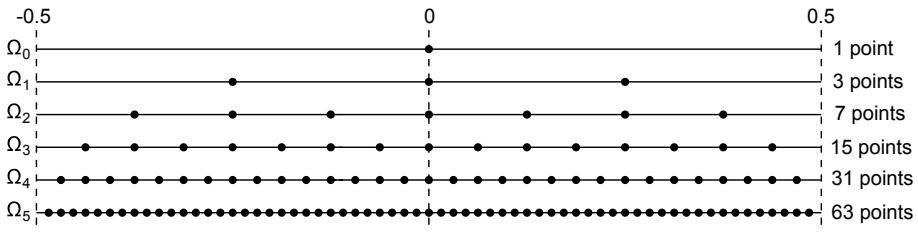

Figure 4.1. Scheme of 1-dimensional grid points with *Level* L=0, 1, 2, 3, 4 and 5.

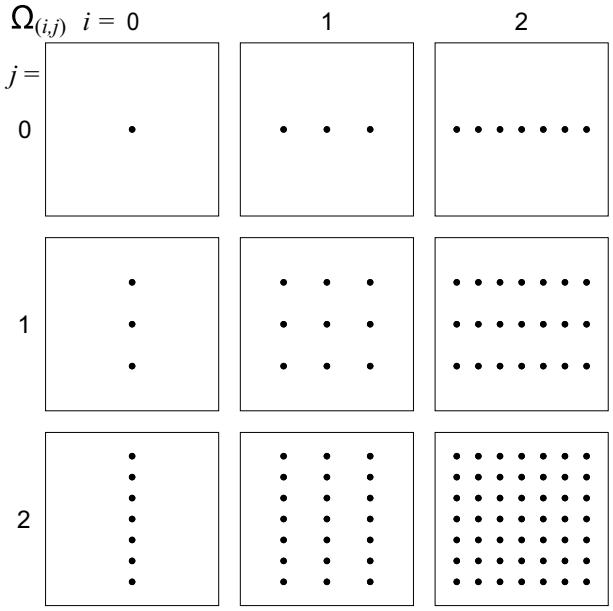

Figure 4.2. The quadratic scheme of grids contained in the full grid points for $d = 2$.

where the array $L = [L_1, ..., L_d]$ denotes the *Levels* of the d-dimensional grid. A mesh size h_i of grid is equal to $2^{-(L_i+1)}$ in i direction. Fig. 4.2 shows the discretization of a 2-dimensional grid with respect to each direction. The discretization of the full grid of *Level* $L = 2$ includes 49 points with the space between points of $2^{-3} = 0.125$.

Compared to the linear subspace discretization, the sparse grid approach constructs a multi-dimensional basis by a special truncation of the tensor product. According to specific tasks, various types of spare grids have been developed, such as the Clenshaw-Curtis [171], Gauss-Patterson [172], Gauss-Chebyshev [173], Hyperbolic Cross Point (HCP) [36], and no boundary nodes grid [174]. These sparse grids are constructed by combining the tensor product of 1-dimensional quadrature rules. To give an example, Fig. 4.3 shows one of the types of sparse grids, namely the no-boundary-nodes grid, which includes only 17 points. This grid is based on a combination of anisotropic full grid solutions [174]. For $d = 2$ within the area $S = [-0.5, 0.5] \times [-0.5, 0.5]$, no-boundary-grid with *Level* $L = 5$ has 321 points, while full grid (without boundary points) has $(2^6 - 1)^2 = 3969$ points, as show in the Fig. 4.4. Compared with full grid method, sparse grid method could significantly reduce the number of grid points in high dimensional problems.

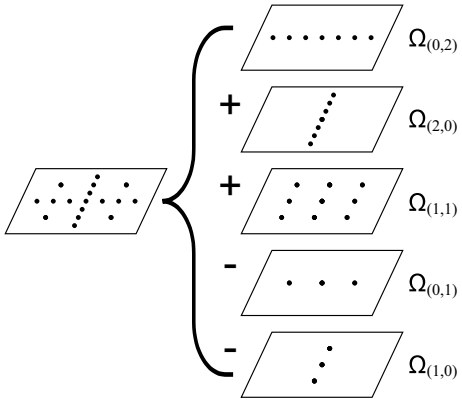

Figure 4.3. The combination technique in generating a 2-dimensional no-boundary-nodes grid with *Level* $L = 2$.

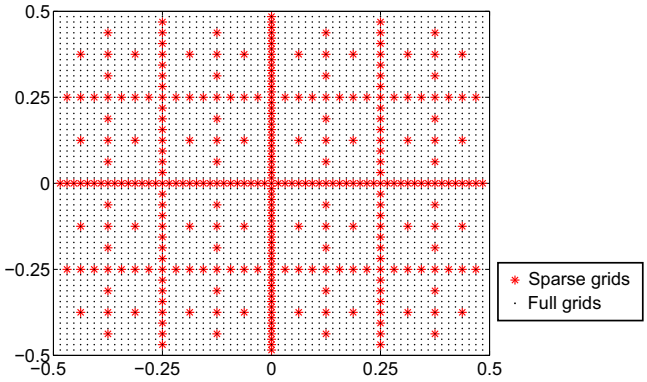

Figure 4.4. The comparison between no-boundary-grid and full grid with *Level* $L = 5$.

4.3 Hyperbolic Cross Point Algorithm

The explanation of the HCPA starts from the definition of the HCPs. The domain of HCP is defined as $[-0.5,\ 0.5]$. In one dimension, any point $x \in [-0.5,\ 0.5]$ with dyadic coordinates

$$x = \pm \sum_{i=1}^{L} a_i 2^{-i}, \quad a_i \in \{0, 1\} \tag{4.3}$$

is a HCP, where L is the *Level* of the HCP. The representation of Eq. (4.3) is unique except at $x = 0$. The *Level* of the point 0 is defined as 0. For example, the *Level* L of a HCP 0.375 is equal to 3 since it can be expressed as $0.375 = 0 \times 2^{-1} + 1 \times 2^{-2} + 1 \times 2^{-3}$. In a d dimension $X = [x_1, x_2, ..., x_d]$, the *Level* L is the sum of levels for all coordinates x_i,

$$Level(X) = \sum_{i=1}^{d} Level(x_i). \tag{4.4}$$

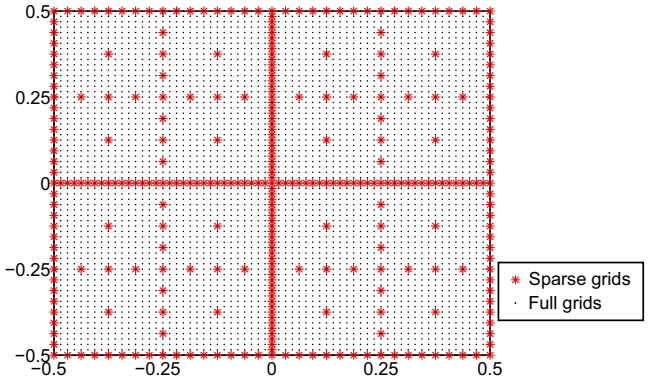

Figure 4.5. The comparison between full grid and HCPs with $L = 5$.

For example, the *Level* L of a 1-dimensional HCP 0.25 is 2; L of a 3-dimensional HCP [0.25, 0.375, 0] is 5.

As an example, Fig. 4.5 shows the 2 dimension full grid points and HCPs with $L = 5$. The total number of points of full grid (with boundary points) is $(2^5 + 1)^2 = 1089$. Compared with full grid, the number of HCPs has been significantly reduced to 147. However, the total number of HCPs can be very large in high dimension. It is wasteful and inefficient to evaluate all HCPs. In order to conduct an effective search on HCPs, an algorithm, named HCPA has been proposed in [36]. The HCPA is described as follows.

An example of a function $Z = F(X)$ with a set of d variables ($X = [x_1, x_2, ..., x_d]$) is utilised to explain the HCPA. The algorithm conducts search on HCPs instead of the full grid or random search [36]. The following definition and discussion are all based on HCPs. The HCPA records all evaluated HCPs (denoted as $\mathbf{X}$) and the corresponding function values (denoted as $\mathbf{Z}$). Each evaluated HCP X^i has a property matrix $P^i = [L^i, D^i, R^i]$, where L is the *Level*; R is the *Rank*, presenting the order of Z^i in the $\mathbf{Z}$. In other words, $R(X^i) = 1$ if Z^i is the minimum value in the $\mathbf{Z}$; $R(X^i) = n$ if Z^i is the maximum among all evaluated points. The D is the *Degree*, presenting how many times the point X^i has been the best point $\widetilde{X}$. The D of a new generated HCP is 0. The value is increased by 1 each time when a HCP is chosen as the best point. The best point is selected based on the *Goodness-Criterion* G, denoted as [36]

$$G(X^i) = [L^i + D^i]^{\alpha} \cdot [R^i]^{(1-\alpha)}. \tag{4.5}$$

where $\alpha \in [0, 1]$ is the adaptiveness parameter [36]. The HCP with the minimal value of *Goodness-Criterion* is the best point $\widetilde{X}$. The *Goodness-Criterion* G provides an adaptive

way to control search regions where small function values have been detected (local search, $\alpha = 0$) or few samples have been selected (global search, $\alpha = 1$). The effect of α on search region is discussed further in the Subsection 4.4.1. The major drawback of the conventional sparse grid methods is that they do not support local adaptivity, which is highly desirable in the field of optimisation. With the *Goodness-Criterion* function, the HCPA can conduct both global and local searches.

The next generation of generated knots are the neighbors of the best point $\widetilde{X}$. Each neighbor of $\widetilde{X}$ only differs in one coordinate. A neighbor Y is defined as

$$y_i = x_i \pm 2^{-Level(x_i)-\widetilde{D}}, \quad i \in \{1, ..., d\}, \tag{4.6}$$

where $\widetilde{D}$ is the *Degree* of $\widetilde{X}$. These neighbors have the same *Level* of $\widetilde{L} + \widetilde{D}$, where $\widetilde{L}$ is the *Level* of $\widetilde{X}$. Since the boundaries of variables are scaled into the d dimension box $[-0.5, 0.5]^d$, any new generated neighbours beyond this box are discarded. To give an example, the neighbors of a best points [0, 0.5] with property matrix $\widetilde{P}$ of $[\widetilde{L} = 1, \widetilde{D} = 2, \widetilde{R} = 2]$ are [$\pm$0.25, 0.5] and [0, 0.375]. The point of [0, 0.625] is discarded since it exceeds the boundary of [-0.5, 0.5]. These neighbors all have the same *Level* $L = \widetilde{L} + \widetilde{D} = 3$.

The flowchart of the HCPA is shown in Fig. 4.6. The steps in the flowchart are discussed as follows:

1. The HCPA begins with $X = \underbrace{[0, 0, ..., 0]}_{d}$ (denoted as $[0]^d$) because it has the lowest *Level* $L = 0$. Since there is only one point in the **X** and **Z**, the point is automatically selected as the best point $\widetilde{X}$. So, the property matrix of $X = [0]^d$ is $P = [0, 1, 1]$;

2. The iteration of the algorithm starts with the best point $\widetilde{X}$;

3. All neighbors of $\widetilde{X}$ with *Degree* $\widetilde{D}$ are calculated by using Eq. (4.6);

4. All these neighbors have the same *Level* of $\widetilde{L} + \widetilde{D}$. The D of these new generated knots are equal to 0. The L and D are assigned to each new HCP. The rank R will be calculated in the Step 7;

5. The function values of the new knots are computed;

6. The new generated knots and their corresponding function values are stored into the **X** and **Z**, respectively;

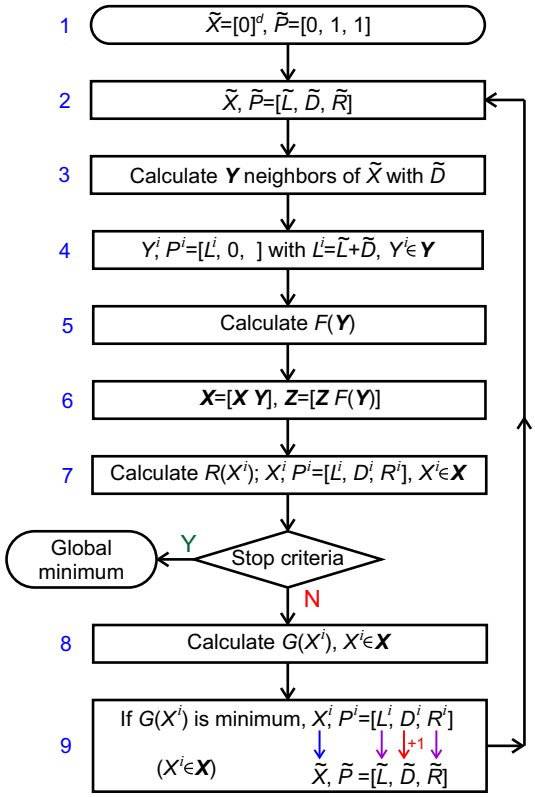

Figure 4.6. The flowchart of the HCPA.

7. The order of all evaluated HCPs are resorted after their function values are added in **Z**. Accordingly, the R of each HCP is recalculated based the function value. The algorithm stops if it reaches one of the stop criteria (e.g. maximum search time, maximum *Level*). Otherwise, the algorithm continues to the next step;

8. The algorithm calculates the G as in Eq. (4.5) of each HCP;

9. The algorithm assigns the HCP with minimal G as the best point $\widetilde{X}$ and the D of this point is increased by 1. Then, the algorithm goes to the second step and iterates until it reaches the stop criteria.

It is worthwhile to note that in the property matrix only the L is fixed while the D and R change during the computation.

Apart from the adaptiveness parameter α, there are another two parameters of the HCPA. Firstly, the parameter L_0 is defined as the fineness [36]. The algorithm only considers points with *Level* $L < L_0$. The large number of L_0 will increase the accuracy and of course the search time. Secondly, in order to reduce unnecessary search around a local minimum, the algorithm will exclude a box with side length of ϵ around the

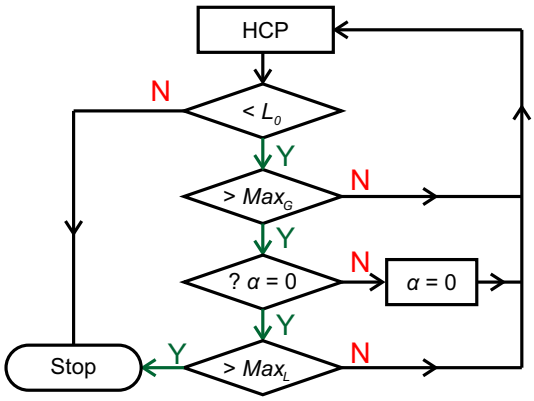

Figure 4.7. The stop criteria of the HCPA.

local minimum [36]. The parameters of α and ϵ are extremely useful in solving high dimensional functions. Small value of α and large value of ϵ are usually employed to avoid the excessively long running time in optimising high dimensional functions.

The stop criteria of the HCPA are L_0, Max_G and Max_L, where Max_G and Max_L are maximum global and local search points, respectively. In order to improve the accuracy, the complex stop criteria are employed, as shown in Fig. 4.7. The algorithm stops when all HCPs with $Level < L_0$ have been evaluated. Otherwise, the total number of evaluated HCPs will be checked. If the number of evaluated HCPs is smaller than Max_G, the algorithm continues and generates new HCPs. If it is bigger than Max_G, the adaptiveness parameter α is set to 0 to conduct local search. The algorithm iterates until all HCPs with $Level < L_0$ have been evaluated or the Max_L is reached.

4.4 HCPA evaluation

As mentioned in Section 4.3, three parameters L_0, ϵ and α are employed to make the HCPA flexible according to the objective function. The proper selection of these parameters has great impact on the performance of the algorithm. As a rule of thumb, recommended parameters are given by Novak and Ritter [36], as shown in Table 4.1. In general, large α and small ϵ are employed to have more accurate results in low dimensional functions. On the other hand, small α and large ϵ are selected to obtain results with reasonable accuracy and computational cost in high dimensional functions. This is a tradeoff between accuracy and computational cost. The essence is the affordable number of function evaluations, depending on the dimension of the function and the available resources.

Table 4.1. The recommended parameters of HCPA. [36]

d	L_0	ϵ	α
2	14	0.02	0.5
3	7	0.05	0.4
4	5	0.08	0.2
5	4	0.15	0.15
≥ 6	3	0.3	0.1

In this thesis, the HCPA is implemented using the MATLAB as a programming tool. Nine well-known test functions in literature [36, 170] are utilised to verify the HCPA and MATLAB code. Except special cases, the parameters of the HCP are chosen based on the recommended parameters in Table 4.1 and the maximum global and local function evaluations are respectively set to $Max_G = 500$ and $Max_L = 500$.

4.4.1 Goldstein-Price Function, Dim=2

The Goldstein-Price function F_{GP} is defined as

$$\begin{aligned} F_{GP}(x) = &\left[1 + (1 + x_1 + x_2)^2(19 - 14x_1 + 3x_1^2 - 14x_2 + 6x_1x_2 + 3x_2^2)\right] \times \\ &\left[30 + (2x_1 - 3x_2)^2(18 - 32x_1 + 12x_1^2 + 48x_2 - 36x_1x_2 + 27x_2^2)\right] \\ &-2 \leqslant x_i \leqslant 2, i = 1, 2 \end{aligned} \tag{4.7}$$

The Goldstein-Price function has several local minima, as shown in Fig. 4.8(a). The function values are plotted in logarithmic scale for better visualization. The global minimum is $F_{GP}(\widehat{x}) = 3$ at the point $\widehat{x} = (0, -1)$.

The Goldstein-Price function is utilised to illustrate the effect of the parameter α on the evaluated HCPs. Fig. 4.8(b) shows the contour plot of the function and the evaluated HCPs with $\alpha = 1$. The evaluated HCPs are indicated as blue dots. In this case, the algorithm is non-adaptive and conducts global search. The algorithm starts from the HCP with the lowest *Level*. The *Level* is increased by 1 each time after all the HCPs with lower *Level* have been evaluated. The algorithm stops after it reaches one of the stop criteria. Although it avoids being trapped into local minima, it is not an effective search. With $\alpha = 0$, the algorithm is highly adaptive and it conducts search around the region with small function values, as shown in Fig. 4.8(c). In this case, the algorithm can be regarded as a local search algorithm and it might be trapped into local minima. To optimise the search, $\alpha = 0.5$ is selected as recommended in [36]. The evaluated

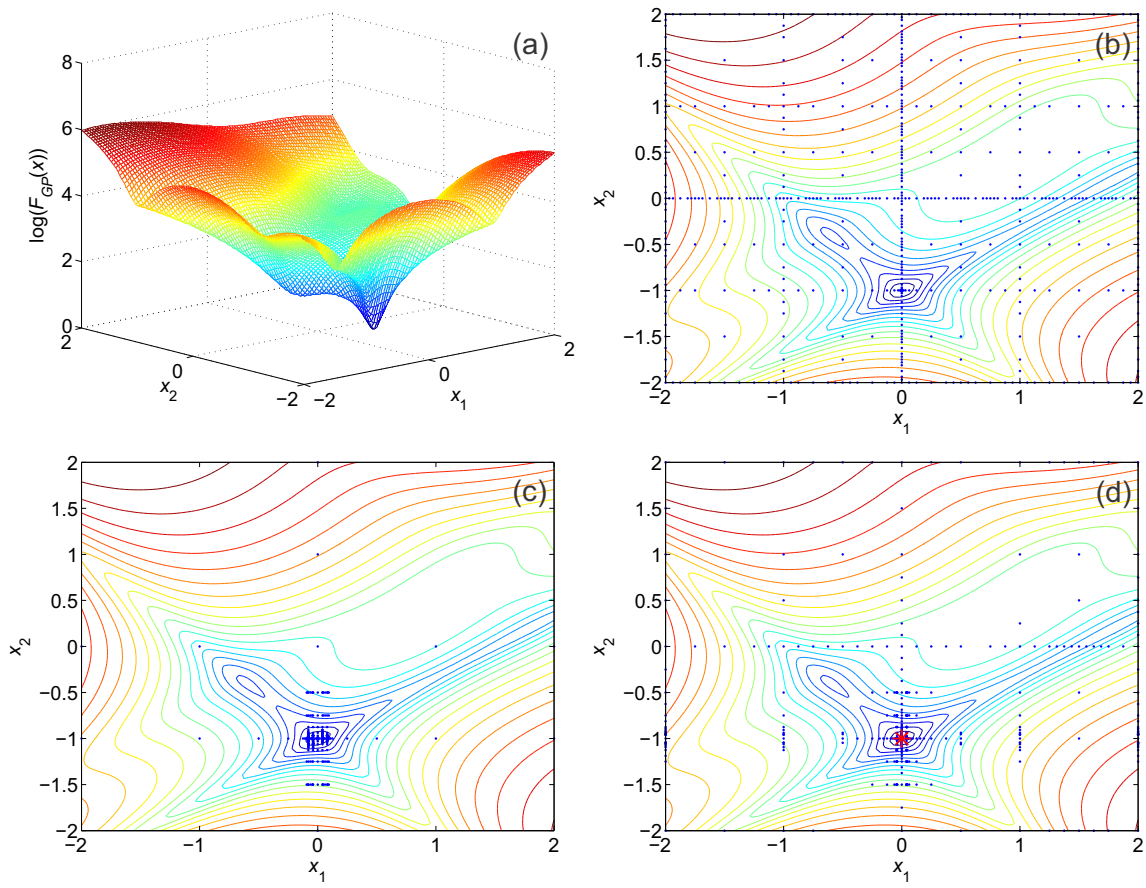

Figure 4.8. Goldstein-Price Function. 3-dimensional plot (a); Contour plot and evaluated HCPs with $\alpha = 1$ (b), $\alpha = 0$ (c) and $\alpha = 0.5$ (d). The evaluated HCPs and global minimum point found by HCP are indicated with blue dots and red star, respectively.

HCPs are reasonably distributed in the whole region and more searches have been conducted around the global minima, as shown in Fig. 4.8(d). The effective search can be achieved by adjusting the value of α according to the given optimisation task. The estimated global minimum (indicated as red star) is in agreement with the value given in [175].

4.4.2 Rastrigin Function, Dim=d

The Rastrigin function is highly multimodal with several local minima. The global minimum is located at $\widehat{x} = (0, 0, .., 0)_d$ with the value of $F_R(\widehat{x}) = 0$, given in [175]. The 2-dimensional Rastrigin function F_R is defined as

$$F_R(x) = x_1^2 - \cos(18x_1) + x_2^2 - \cos(18x_2) \qquad -1 \leqslant x_i \leqslant 1, i = 1, 2. \tag{4.8}$$

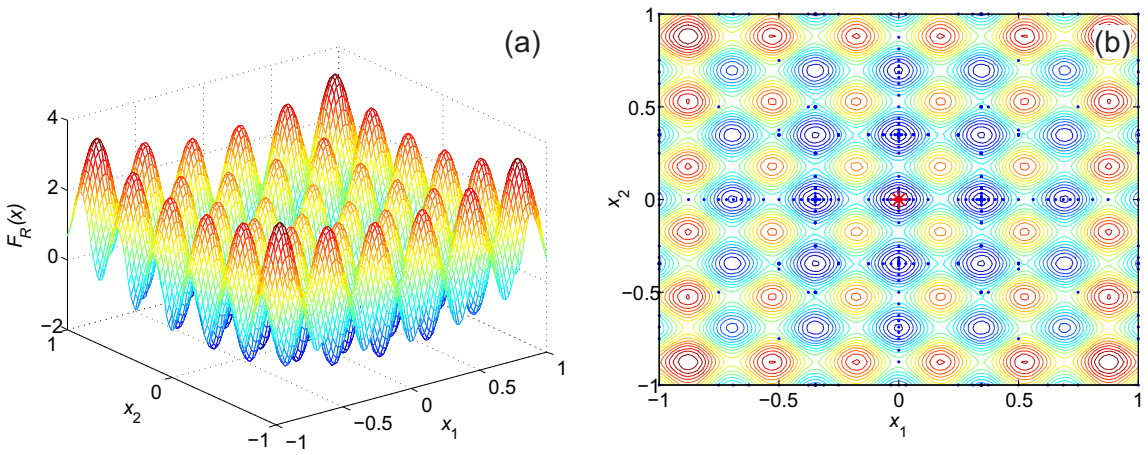

Figure 4.9. 2-dimensional Rastrigin Function. 3-dimensional plot (a); Contour plot and evaluated HCPs with $\alpha = 0.5$ (b). The evaluated HCPs and global minimum point found by HCP are indicated with blue dots and red star, respectively.

Fig. 4.9(a) shows the function in 2-dimensional form (d=2). With the recommended parameters, the global minimum values of $F_R(x^*) = 0$ is found at $(x^*) = (0, 0)$, indicated as a red star in Fig 4.9(b).

4.4.3 Rosenbrock Function, Dim=d

The Rosenbrock function is one of the popular test functions for optimisation algorithms. The Rosenbrock function is unimodal and the global minimum lies in a narrow and parabolic valley. Thus, it is also referred to as the Valley or Banana function. Even though this valley is easy to find, convergence to the global minimum is difficult [176]. The global minimum is located at $\widehat{x} = (1, 1, .., 1)_d$ with the values of $F_{RO}(\widehat{x}) = 0$. The 2-dimensional Rosenbrock function F_{RO} is defined as,

$$\begin{aligned} F_{RO}(x) &= 100(x_2 - x_1^2)^2 + (x_1 - 1)^2 \\ &-2 \leqslant x_1 \leqslant 3, -2 \leqslant x_2 \leqslant 9. \end{aligned} \tag{4.9}$$

Fig. 4.10(a) shows the 2-dimensional form of the function. With the $Max_G = 500$ and $Max_L = 500$, a minimum $F_{RO}(x^*) = 0.2474$ is found at $x^* = (0.5047, 0.2502)$, which is indicated with red star in Fig. 4.10(b). In order to refine the result, both Max_G and Max_L are increased to evaluate more HCPs. Fig. 4.10(c) shows the evaluated HCPs with $Max_G = 1500$ and $Max_L = 1500$. A minimum $F_{RO}(x^*) = 0.0178$ with $x^* = (0.8667, 0.7510)$ is found. The estimated global minimum is closer to the true global minimum $\widehat{x} = (1, 1)$. The value of estimated minimum has not been significantly

reduced even the Max_G and Max_L are further increased to 2000. The estimated global minimum is $F_{RO}(x^*) = 0.0155$ located at $x^* = (1.1245, 1.2646)$, as shown in Fig. 4.10(d).

4.4.4 Branin and Hoo Function, Dim=2

The Branin and Hoo function F_{BR} is defined as

$$F_{BR}(x) = 10\left(1 - \frac{1}{8\pi}\right)\cos(x_1) + \left(x_2 - \frac{5.1}{4\pi^2}x_1^2 + \frac{5}{\pi}x_1 - 6\right)^2 + 10 \qquad (4.10)$$
$$-5 \leqslant x_1 \leqslant 10, 0 \leqslant x_1 \leqslant 15.$$

Fig. 4.11(a) shows the shape of Branin and Hoo function. The function has three identical global minima of $\widehat{x} = (-\pi, 12.275), (\pi, 2.275)$ and $(9.42478, 2.475)$ with minimum value of $F_{BR}(\widehat{x}) = 0.397887$ [175]. With the standard parameters of HCPA,

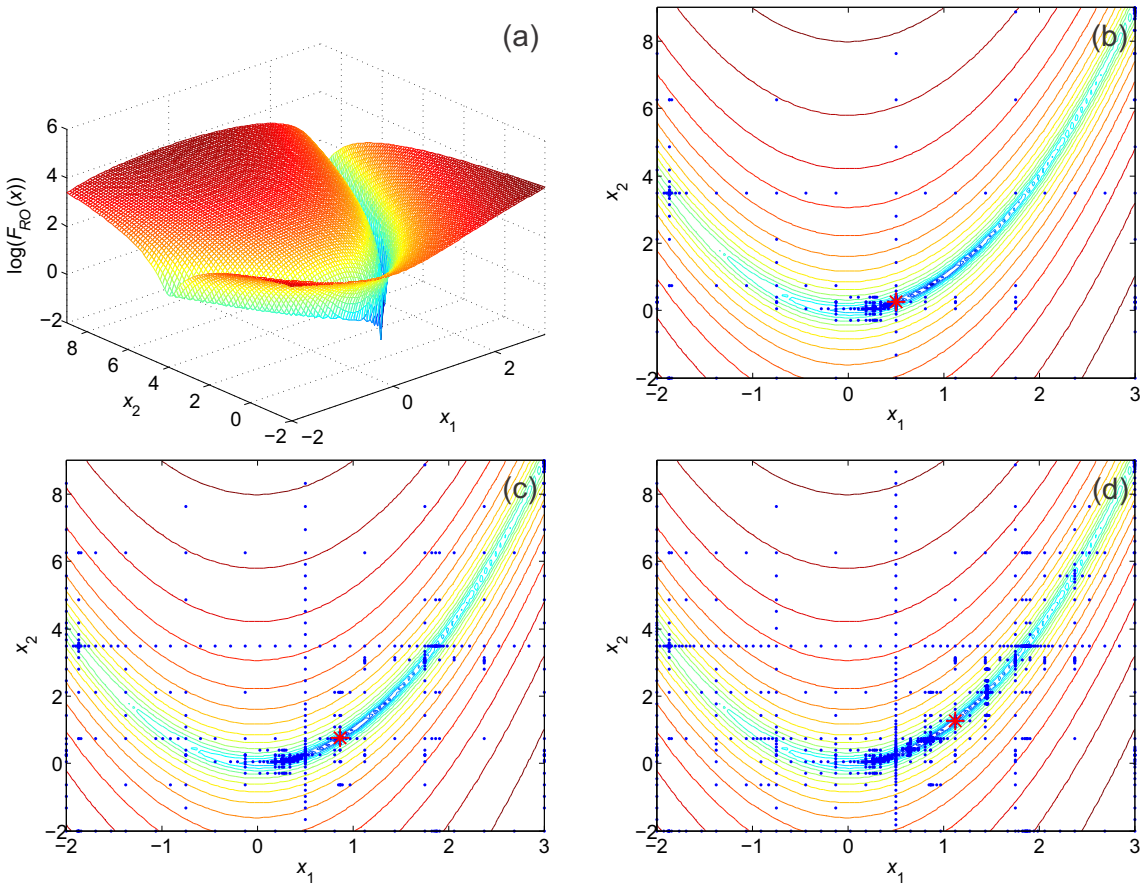

Figure 4.10. 2-dimensional Rosenbrock Function. 3-dimensional plot (a); Contour plot and 500 evaluated HCPs (b); Contour plot and 1000 evaluated HCPs (c); Contour plot and 2000 evaluated HCPs (d). The evaluated HCPs and global minimum found by HCP x^* are indicated with blue dots and red star, respectively.

one of the global minima $x^* = (9.4228, 2.4733)$ is found with the function value of $F_{BR}(x^*) = 0.3979$, as shown in Fig. 4.11(b).

Combined with the fuzzy c-means clustering algorithm [177], the HCPA can be utilised to deal with functions with multiple global minima. The method is described as follows,

1. Increase the maximum evaluated number of HCPs to 1000 and $\alpha = 0.8$ so that HCPs are reasonably distributed in the whole search regime, as shown in Fig. 4.11(c);

2. Use fuzzy c-means clustering algorithm to divide HCPs into clusters, as shown in Fig. 4.11(d);

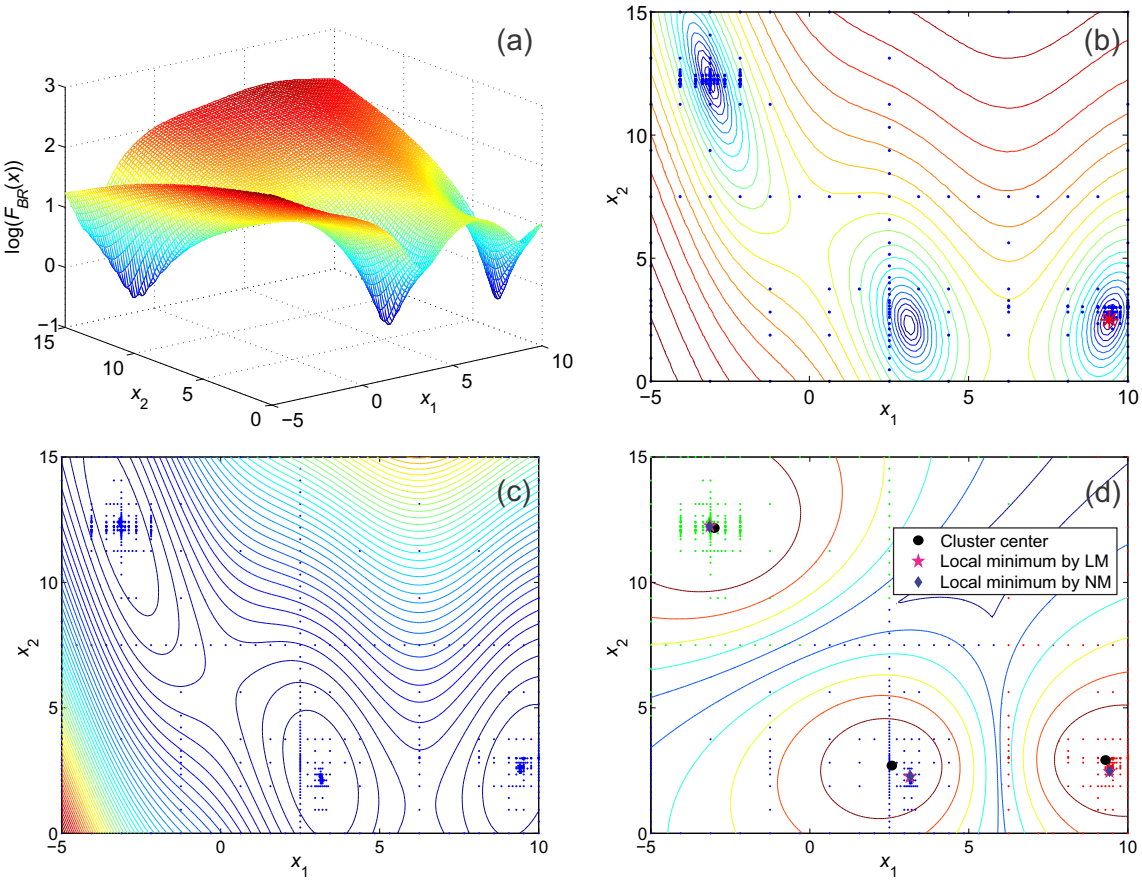

Figure 4.11. 2-dimensional Branin and Hoo Function. 3-dimensional plot (a); Contour plot and 500 evaluated HCPs (b); Contour plot and 1000 evaluated HCPs (c); HCPs are divided into three clusters by using fuzzy c-means clustering algorithm (d). The minimum of each cluster is found by using LM and NM algorithm with cluster center as a start point. The evaluated HCPs and global minimum point found by HCP are indicated with blue dots and red star, respectively.

3. Use local search algorithm, e.g. Levenberg-Marquardt (LM) algorithm [178] or Nelder-Mead (NM) algorithm [179], to find the minimum of each cluster. The start point of the local search algorithm is the center of each cluster found by the fuzzy c-means clustering algorithm (indicated with dot). In Fig. 4.11(d), the minimum of each cluster, found by LM and NM algorithm, is indicated with start and diamond, respectively. The estimated global minimum is close to the global minima given in [175].

Since the cost functions in this thesis do not have identical global minima, this method has not been employed in this research. It has been presented here to illustrate the features of HCPs for interested readers.

4.4.5 Himmelblau Function, Dim=2

The Himmelblau function F_H is defined as

$$F_H(x) = (x_1^2 + x_2 - 11)^2 + (x_1 + x_2^2 - 7)^2 \\ -5 \leqslant x_i \leqslant 5, i = 1, 2. \tag{4.11}$$

The function has four identical global minima of $\widehat{x} = (3, 2)$, $(-2.805118, 3.131312)$, $(-3.779310, -3.283186)$ and $(3.584428, -1.848126)$ with the minimum value of $F_H(\widehat{x}) = 0$ [180], as shown in Fig. 4.12(a). Fig. 4.12(b) shows one of the global minima detected by the HCPA. The four global minima are found by using the same method described in Section 4.4.4. The evaluated HCPs are divided into four clusters and minima are found by using both LM and NM algorithm, as shown in Figs. 4.12(c) and (d).

4.4.6 Mladineo Function, Dim=d

The d-dimensional Mladineo function F_{ML_d} is defined as

$$F_{ML_d}(x) = 1 + \frac{1}{d}\sum_{i=1}^{d} x_i^2 - \prod_{i=1}^{d} \cos\left[10 \log((i+1)x_i)\right] \\ 0.01 \leqslant x_i \leqslant 1, i = 1, 2, ..., d. \tag{4.12}$$

Fig. 4.13(a) shows the shape of Mladineo function with dimension $d = 2$. The function has several local minima and the region of each minimum is very small, which makes it

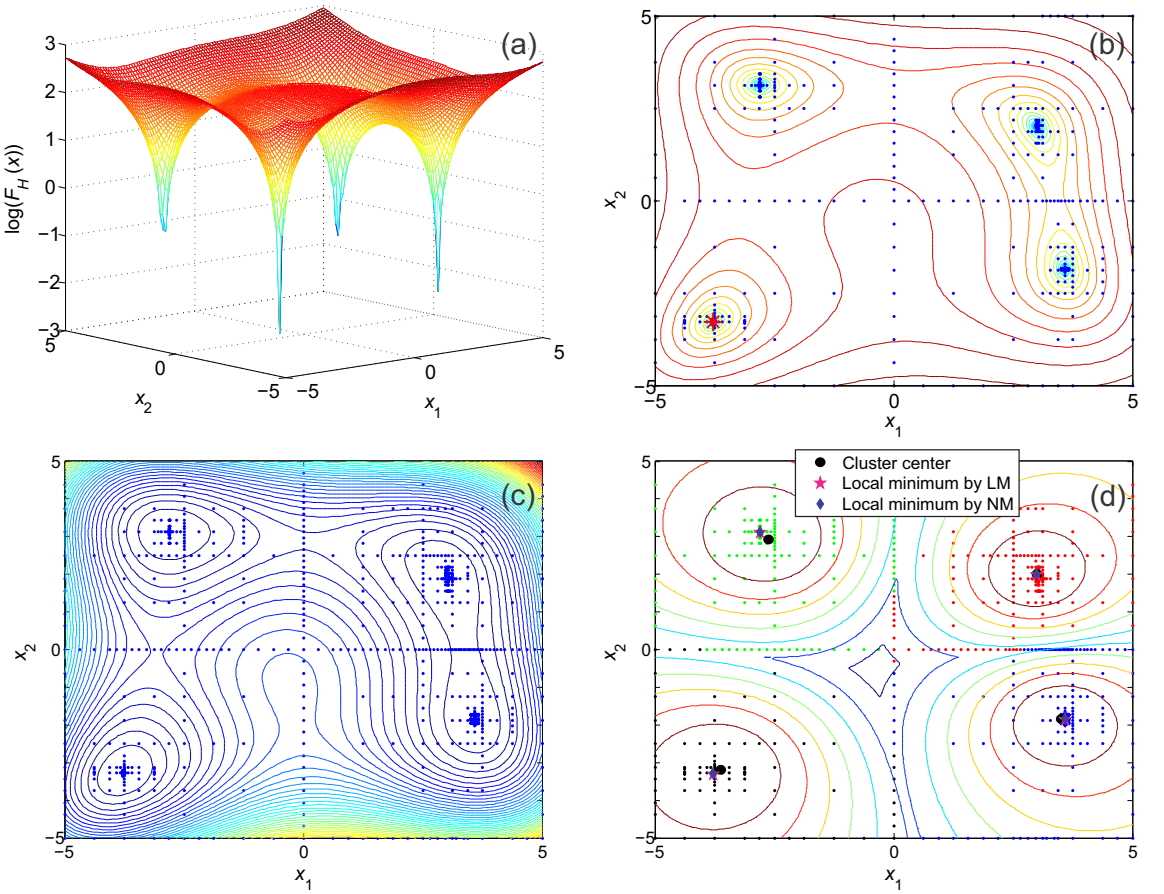

Figure 4.12. 2-dimensional Himmelblau Function. 3-dimensional plot (a); Contour plot and 500 evaluated HCPs (b); Contour plot and 1000 evaluated HCPs (c); HCPs are divided into four clusters by using fuzzy c-means clustering algorithm (d). The minimum of each cluster is found by using LM and NM algorithm with cluster centre as a start point. The evaluated HCPs and global minimum point found by HCP are indicated with blue dots and red star, respectively.

difficult for most methods. The global minimum is near $\widehat{x} = (0.011527, 0.014405)$ with the function value of $F_{ML_2}(\widehat{x}) = 0.000171$. In [181], all the methods need more than 10^6 function evaluations to achieve the specific error bound $\delta = 0.0692$. Compared with these methods, the HCPA found the point $x^* = (0.015771, 0.010514)$ with $F_{ML_2}(x^*) = 0.000231$ by using 20000 function evaluations. The error between true and estimated minimum is less than 0.00006.

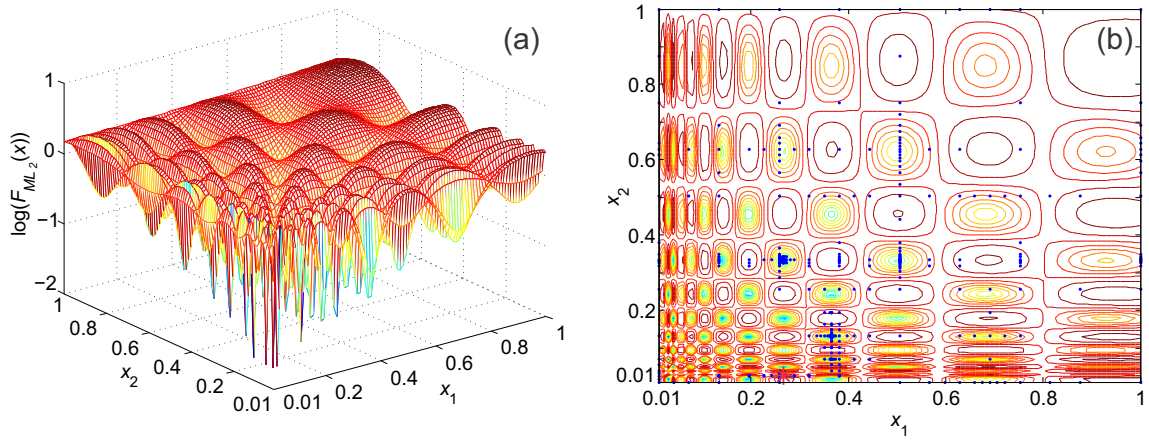

Figure 4.13. 2-dimensional Mladineo Function. 3-dimensional plot (a); Contour plot and 500 evaluated HCPs (b). The evaluated HCPs and global minimum found by HCP x^* are indicated with blue dots and red star, respectively.

4.4.7 Hartman Function, Dim=d

The d-dimensional Hartman function F_{H_d} is defined as [175]

$$F_{H_d}(x) = \sum_{i=1}^{4} c_i \exp\left[\sum_{j=1}^{d} a_{i,j}(x_j - b_{i,j})^2\right] \qquad (4.13)$$
$$0 \leqslant x_j \leqslant 1, j = 1, 2, ..., d.$$

For $d = 3$, the matrices of a, b and c are given as follows,

$$a = \begin{bmatrix} 3 & 10 & 30 \\ 0.1 & 10 & 35 \\ 3 & 10 & 30 \\ 0.1 & 10 & 35 \end{bmatrix}, \; b = \begin{bmatrix} 0.3689 & 0.1170 & 0.2673 \\ 0.4699 & 0.4387 & 0.7470 \\ 0.1091 & 0.8732 & 0.5547 \\ 0.03815 & 0.5743 & 0.8828 \end{bmatrix}, \; c = \begin{bmatrix} 1 \\ 1.2 \\ 3 \\ 3.2 \end{bmatrix}$$

The global minimum is $F_{H_3}(\hat{x}) = -3.86$ at the location of $\hat{x} = (0.114, 0.556, 0.852)$ [175]. With the standard parameters, HCPA finds the minimum values of $F_{H_3}(x^*) = -3.8628$ at the point of $x^* = (0.1146, 0.5556, 0.8525)$ after 609 function evaluations.

Table 4.2. The estimated global minimum of 4-dimensional Shekel function.

	x^*	$F_{S_m}(x^*)$
$m = 5$	(3.9999,4.0002,3.9999,4.0002)	-10.1532
$m = 7$	(4.0005,4.0005,3.9996,3.9996)	-10.4029
$m = 10$	(4.0009,4.0005,3.9996,3.9996)	-10.5364

4.4.8 Shekel Function, Dim=4

The 4-dimensional Shekel function F_{S_m} is defined as [182],

$$F_{S_m}(x) = \sum_{i=1}^{m} \frac{1}{c_i + \sum_{j=1}^{4}(x_j - a_{i,j})^2} \qquad (4.14)$$
$$0 \leqslant x_j \leqslant 10; j = 1, 2, ..., 4; 1 \leqslant m \leqslant 10.$$

The matrices a and c are given as fellows,

$$a = \begin{bmatrix} 4.0 & 4.0 & 4.0 & 4.0 \\ 1.0 & 1.0 & 1.0 & 1.0 \\ 8.0 & 8.0 & 8.0 & 8.0 \\ 6.0 & 6.0 & 6.0 & 6.0 \\ 3.0 & 7.0 & 3.0 & 7.0 \\ 2.0 & 9.0 & 2.0 & 9.0 \\ 5.0 & 5.0 & 3.0 & 3.0 \\ 8.0 & 1.0 & 8.0 & 1.0 \\ 6.0 & 2.0 & 6.0 & 2.0 \\ 7.0 & 3.6 & 7.0 & 3.6 \end{bmatrix}, \; c = \begin{bmatrix} 0.1 \\ 0.2 \\ 0.2 \\ 0.4 \\ 0.4 \\ 0.6 \\ 0.3 \\ 0.7 \\ 0.5 \\ 0.5 \end{bmatrix}.$$

The most common values for m are 5, 7 and 10. For all these three m values, the global minimum of the S_m function is near $\widehat{x} = (4, 4, 4, 4)$ with the function value of $F_{S_m}(\widehat{x}) = -10.5363$ [182]. The estimated global minima are very close to the real global minima, as shown in Table. 4.2.

4.4.9 Simplified Griewank Function, Dim=d

The Simplified Griewank function is similar as the Mladineo function, with high number of local minima. The Simplified Griewank F_{SG_d} function is defined as [183],

$$F_{SG_d}(x) = 1 + \frac{1}{d}\sum_{i=1}^{d} x_i^2 - \prod_{i=1}^{d}\cos(x_i) \qquad -1 \leqslant x_i \leqslant 4, i = 1, 2, ..., d. \tag{4.15}$$

The global minimum is $F_{SG_d}(\widehat{x}) = 0$ at the location of $\widehat{x_i} = 0$ [175]. In this example, 10-dimensional Simplified Griewank function is considered and the standard parameters are used in the estimation, i.e. $L_0 = 3$ for $d > 6$. The minimum of $F_{SG_d}(x^*) = 2.2352 \times 10^{-7}$ is found at the point of $(x_i^*) = 0.6104 \times 10^{-4}$.

4.5 Conclusion

This chapter has presented an adaptive global optimisation HCPA. The algorithm conducts search on the sparse grid based on the HCPs. Compared with full grid search or random search, the global optimisation based on HCPs significantly reduces the number of evaluated points and hence increases the efficiency. Furthermore, the HCPA employs three parameters L_0, ϵ and α to make the HCPA more flexible according to the objective function. For low dimension functions, large L_0 and small ϵ are selected to have more accurate results. While, small L_0 and large ϵ have to be used to avoid excessive computational time for high dimension functions.

In the numerical validation, the HCPA is implemented using MATLAB as a programming tool and examined by nine well-known test functions in literature. The dimensions of these functions are ranging from 2 to 10. The HCPA is able to find global minimum of most test functions. For some difficult test functions, such as Rosenbrock and Mladineo function, which have several local minima located in a small region, the estimated results of HCPA are close to the global minimum with less function evaluations compared with other algorithms in literature. In addition, this chapter also shows that functions with multiple identical global minima can be detected by combining the HCPA with the fuzzy c-means clustering algorithm and local search algorithm.

Chapter 5

Induction Motor Parameters Estimation Using HCPA

APPLICATION of inaccurate motor parameters can lead to an inefficient motor control. Although several motor estimation methods have been utilised for estimating motor parameters, it is still a challenging field to ensure a good level of confidence in the estimated parameters. This chapter proposes an offline induction motor parameters estimation method based on sparse grid optimisation algorithm. The proposed parameter estimation algorithm is implemented by matching a mathematical machine model with recorded stator current and voltage signals. This approach uses only external measurements which reduces the system complexity and cost. The parametric space has dimension of six for simulation test and seven for laboratory test. We used sampling on the sparse grid to search for a globally optimal point which gives the best match between model and measurements. The sparse grid is created using the Hyperbolic Cross Points (HCPs) and an additional heuristic is used to further reduce the total number of search points. Result of the algorithm can be further refined by using a local search method. The proposed algorithm is examined using an experimental setup where a wide range of load levels were considered. The test results indicate a very good agreement between estimated values and reference values.

5.1 Introduction

Induction motor parameters are usually obtained from manufacturer's data sheet. However, the manufacturer usually describes these parameters under starting or full-loading condition, instead of the actual operating conditions. It is well known that parameters are influenced by not only the load level but also environmental factors [10]. Especially, the stator resistance changes dramatically with temperature drift when an induction motor works at low speed and heavy loads [184]. The stator resistance variation results in the stator flux deviation and hence has severe impact on the speed estimation. Therefore, estimating the actual value of stator resistance is the most important for stable operation at very low speed [52]. Furthermore, it is also necessary to track the variation of motor parameters during normal operating conditions.

The recent development of sensorless control has led to a number of induction motor parameters estimation methods. In [16], the induction motor model has been linearized to enable direct application of a least-squares identification algorithm. This real-time estimation method provides not only parameters but also fluxes of induction motors, which could be useful for field-oriented controlled drive or methods based on nonlinear control theory. Extended Kalman Filter (EKF)-based methods have the capacity of performing simultaneous identification of states and parameters under measurement noise [64, 65]. That is the reason why EKF-based methods have been widely applied in the sensorless induction motor control although this type of methods has the major drawback of computational complexity [10]. The model reference adaptive system (MRAS) is a generic approach based on a mathematical model [68]. Within MRAS framework and with the aid of error cost function, the parameters of the model are optimised to match the model outputs with the measured outputs. The key point of this method lies in the choice of the parameter estimation algorithm which guarantees finding a global minima of the cost function [185]. The MRAS has been utilised in motor parameters estimation [13, 69] and speed sensorless motor drive [186, 187]. Among literature, some methods only emphasize identification of stator flux linage vector, stator and rotor resistance and rely on the accuracy and stability of other machine parameters, which might change during motor operation, e.g. slip, rotor inertia constant and stator magnetising inductance [188, 189]. Other methods require some special conditions or complex mathematical processing [10]. In particular, solving high order mathematical models is usually computationally intensive [65].

To overcome the aforementioned problems, this chapter proposes a motor parameter identification method using MRAS framework and the sparse grid optimisation algorithm. The offline parameter estimation method is selected by considering following facts:

1. Multiple motor parameters can be estimated at the same time. So, it avoids the errors resulting from assumption of constant machine parameters;

2. The proposed method does not require special test signals or configuration of machine;

3. The motor parameters estimation is a high dimensional task, which normally includes at least five physical parameters to be estimated. The sparse grid method is a discretization technique for high dimensional problems. The proposed estimation algorithm conducts search on sparse grid of points instead on the full grid of points or randomly selected points (Monte Carlo approach). It therefore shortens the search time and increases efficiency. It has been successfully applied in power industry, such as induction motor faults diagnostic [19], transmission line faults diagnostic [34], and modelling the pebble bed nuclear reactor [35];

4. The mathematical model of an induction motor is nonlinear. The cost function might include several local minima. Iterative algorithms based on local search techniques may be trapped in local minima. Thus, a global optimisation algorithm based on sparse grid method, namely the Hyperbolic Cross Point Algorithm (HCPA) [36], is employed to estimate motor parameters. The HCPA has rigorous mathematical base in the function approximation theory and can be adaptive by introducing very simple heuristics. Application of certain heuristics can make the HCPA adaptive and further increase the computation efficiency [19];

5. A local search method, Nelder-Mead algorithm [179], is applied to refine search result because Nelder-Mead algorithm is less sensitive to measurement noise compared to Gauss-Newton or Levenberg-Margaret algorithm. In order to avoid trapping into local minima, the global search result obtained using the HCPA is utilised as a start point of the Nelder-Mead algorithm.

This chapter is organised as fellows, Section 5.2 describes the proposed scheme of motor parameters estimation using sparse grid based optimisation algorithm. In order to

examine the scheme in a controlled environment, the simulated currents are first used to estimate the motor parameters in Section 5.3. The accuracy of the estimated parameters is discussed in terms of HCPA parameters, data window length and transient response. The experimental validation is presented in Section 5.4.

5.2 Motor parameters estimation using sparse grid based optimisation algorithm

The scheme of the proposed parameter estimation method is sketched in Fig. 5.1. The recorded three phase voltages are imported into the model, described in the Chapter 3. The stator currents $i'_{\alpha s}$ and $i'_{\beta s}$ are generated based on the motor model (for specified parameters) and the recorded stator voltages. On the other hand, the recorded stator currents are transferred from abc frame to $\alpha\beta$ frame. The measured currents $i_{\alpha\beta s}$ and simulated currents $i'_{\alpha\beta s}$ are then compared using the sum of squared residual (SR), which is utilised as the cost function F_{SR},

$$\begin{aligned} F_{SR} &= \sum_{j=1}^{N} SR(j) \\ &= \sum_{j=1}^{N} \left\{ \left[i_{\alpha s}(j) - i'_{\alpha s}(j) \right]^2 + \left[i_{\beta s}(j) - i'_{\beta s}(j) \right]^2 \right\}, \end{aligned} \tag{5.1}$$

where N is the total number of samples. The total number of samples is related to the sampling frequency and time window length. Longer time window length will increase the accuracy at the expense of increasing the computation time. The effect of the time window length is discussed in the Section 5.3.3. If the cost function is not satisfied (i.e. F_{SR} is above the threshold), F_{SR} is sent to the global optimisation algorithm and a new point in the parameter space is generated using the HCPA. Using the new set of parameters, the stator currents are generated again and then are compared with the recorded currents in the cost function. The search process continues until the cost function is below a specified threshold. As a non-intrusive parameter estimation method, the estimation processing is only based on the stator voltages and currents. It does not need any additional sensing information and therefore reduces the cost and impact on the machine. Although the proposed approach is illustrated for the three phase induction motor parameters estimation in this thesis, it is feasible to extend this approach for the other machine types by using the corresponding motor model.

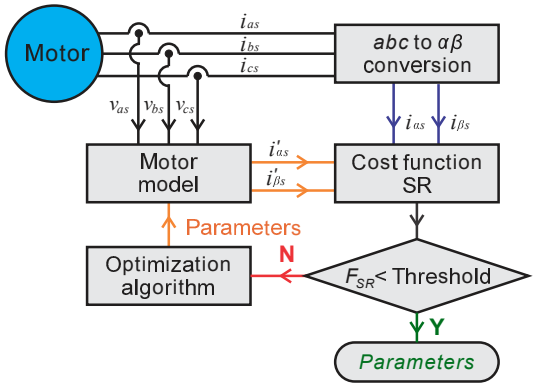

Figure 5.1. Induction motor parameters estimation scheme using global optimisation algorithm.

5.3 Simulation results and discussion

A three phase induction motor is utilised to check the method validity. The motor parameters are tabulated in Table 3.2. Since the stator winding leakage inductance (L_{ls}) is usually equal to the referred rotor winding leakage inductance (L'_{lr}) in most of induction motors, only L_{ls} will be estimated in this study. Thus, the six parameters to-be-estimated are $X = \left\{R_s, R'_r, L_{ls}, L_s, H, LL\right\}$, where LL is load level. The upper and lower boundaries of each motor parameter are tabulated in Table 5.1. Considering the fact that motor parameters might drift from the real values during the operation, the motor parameters in Table 3.2 are firstly set to the induction model to generate stator currents. The simulated currents will be utilised to estimate the motor parameters. In this case, the proposed method will be examined by eliminating the effect from motor parameters offset during the real operation.

The HCPA starts search at the point with the lowest level, i.e. the HCP with the coordinates $\{0, 0, 0, 0, 0, 0\}$. Since the HCPA is based on the domain of $[-0.5, 0.5]^d$, each element of the HCP X_i^P is scaled into its boundary using the following formula:

$$X_i = (X_i^P + 0.5)(X_i^U - X_i^L) + X_i^L, \ (i = 1, 2, ..., 6), \tag{5.2}$$

where X_i is one of the six parameters to-be-estimated; X_i^U and X_i^L are its upper and lower boundary, respectively. For example, the initial motor parameter is set to $\{10, 10, 0.032, 0.4775, 1.5, 0.5\}$ after scaling the starting HCP $\{0, 0, 0, 0, 0, 0\}$ into its boundary using Eq. (5.2). The scaled parameters are assigned to the SIMULINK model to generate stator currents. The sum of squared residual of the original and simulated stator currents are calculated by using the cost function given by Eq. (5.1). Then, new HCPs

Table 5.1. Boundaries for motor parameters

Parameter name	Variable	Range
Stator winding resistance	R_s	[5 15]
Referred rotor winding resistance	$R_r^{'}$	[5 15]
Stator winding leakage inductance	L_{ls}	[0.016 0.048]
Stator magnetising inductance	L_s	[0.3184 0.6366]
Inertia constant	H	[1 2]
Load level	LL	[0 1]

are generated based on the value of cost function using *Goodness-Criterion* Eq. (4.5). The new generated HCPs are scaled and applied to the SIMULINK model. The process iterates until it reaches the stop criteria.

5.3.1 The HCPA parameters

The stop criteria of the HCPA are the maximum *Level* $k = 15$, the maximum number of global search samples $G_p = 500$ and the maximum number of local search samples $L_p = 500$. The algorithm stops when the $k = 15$ or both the G_p and L_p reach 500. In the first study, the load level LL is set to 50% of the full load. Fig. 5.2 shows the trajectories of the estimated parameters with the adaptiveness parameter $\alpha = 1$. At the

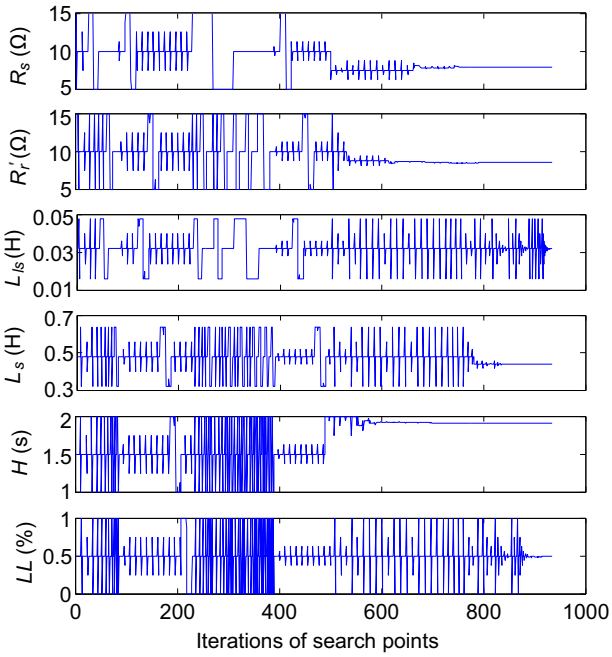

Figure 5.2. Trajectories of estimated five motor parameters and load level with the adaptiveness parameter $\alpha = 1$.

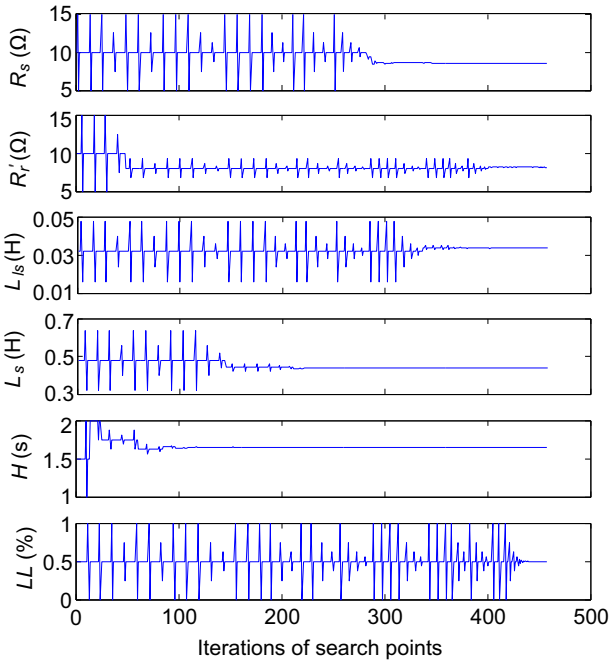

Figure 5.3. Trajectories of estimated five motor parameters and load level with the adaptiveness parameter $\alpha = 0.2$.

beginning, the HCPA is not adaptive and searches on the regions where few samples have been chosen. After the algorithm conducts the first 500 times global searches, there are unevaluated HCPs with $Level\ k < 15$. Then, the algorithm sets $\alpha = 0$ to conduct local search until $L_s = 500$ or $k = 15$. In this parameter estimation, the algorithm evaluates 934 HCPs including 500 global search and 434 local search points after it reaches the maximum $Level\ k = 15$. The estimated parameters are $R_s = 7.88$, $R_r' = 8.49$, $L_{ls} = 0.0319$, $L_s = 0.4386$, $H = 1.91$ and $LL = 48.93\%$, which are close to the corresponding parameters in Table 3.2. However, this parameter set of HCPA is not effective and leads to large number of iteration knots. To this end, the parameters of the HCP are set to $k = 10$, $\alpha = 0.2$, $\epsilon = 0.15$, $G_p = 200$ and $L_p = 300$ in the second estimation. The trajectories of estimated parameters are shown in Fig. 5.3. Compared to the estimated parameters in the first simulation, the more accurate parameters of $R_s = 8.54$, $R_r' = 8.15$, $L_{ls} = 0.0338$, $L_s = 0.4381$, $H = 1.64$ and $LL = 49.90\%$ are obtained with a total number of evaluated HCPs less than 460.

Using these parameters, the simulated stator currents are plotted and compared with the original stator currents in Fig. 5.4. The profiles of the simulated stator currents are consistent with the original currents. The stator currents are presented in the $\alpha\beta$ frame in Figs. 5.4(a) and (b), respectively. In Fig. 5.4(c), the small squared residual (SR) of i_α

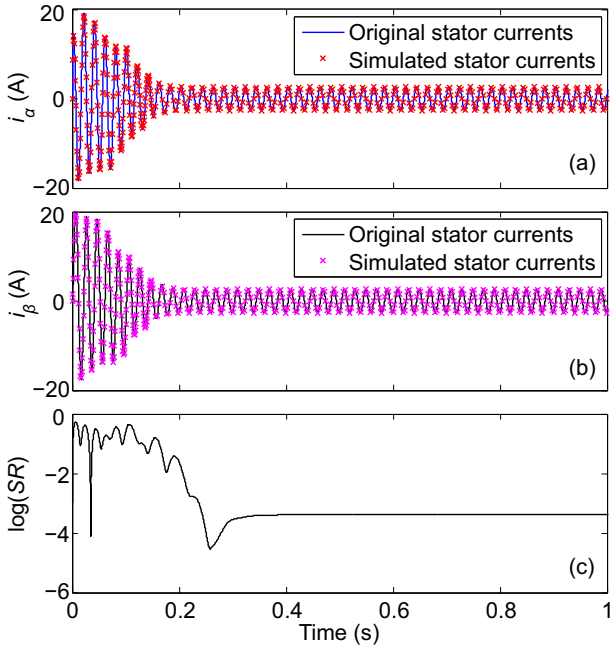

Figure 5.4. Comparison between original stator currents and simulated currents using estimated motor parameters. α coordinate (a); β coordinate (b); and squared residual (SR) in logarithmic scale (c)

and i_β indicates the accurate parameters estimation. The values of SR are plotted in logarithmic scale for the better visualization.

5.3.2 Motor parameters refinement by using local search algorithm

It is worth noting that the accuracy can be further improved by combining HCPA with a local search algorithm. Since the cost function of Eq. (5.1) is nonlinear and might include several local minima, the local search algorithm can be trapped into a local minimum if it is directly applied in the motor parameters estimation. One of the advantages of the HCPA is the adaptiveness of this algorithm. As explained in Chapter 4, the parameter α can be selected between 0 to 1 to control the adaptiveness of the algorithm according to a given task. Large value of α guarantees the algorithm to converge to a global minimum instead of one of local minima. However, the algorithm needs to evaluate more points, as shown in Fig. 5.2. On the other hand, small value of α leads to a fast convergence of the algorithm, as shown in Fig. 5.3. However, the algorithm might be trapped in a local minimum. The recommended value of is given in Table 4.1. In practice, a relative large value of is selected to find a global minimum. Then, a local search algorithm is utilized to further refine motor parameter. Our strategy of using global search result as a starting point of local search method can avoid being

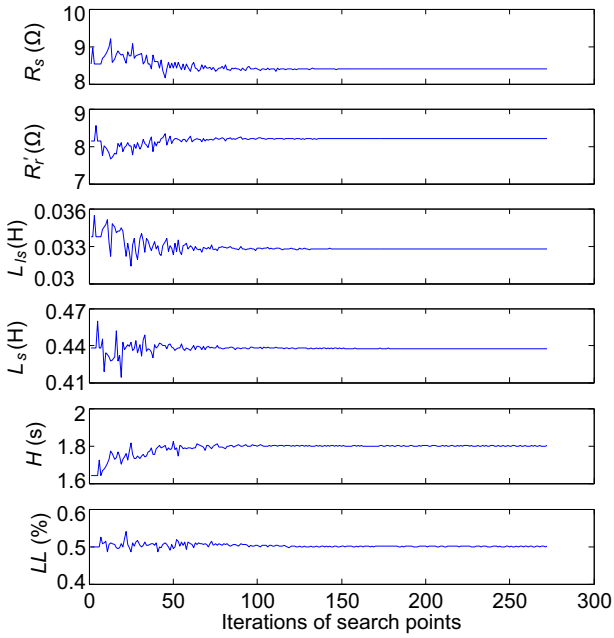

Figure 5.5. Trajectories of estimated five motor parameters and load level using the Nelder-Mead algorithm with the global search result as start point.

trapped into a local minimum, and it will further increase the parameter estimation accuracy. As an example, Fig. 5.5 shows the trajectories of estimated parameters using the Nelder-Mead algorithm [179] with the global search result of $R_s = 8.54$, $R_r^{'} = 8.15$, $L_{ls} = 0.0338$, $L_s = 0.4381$, $H = 1.64$ and $LL = 49.90\%$ as start point. The exact values of the motor parameters of $R_s = 8.4$, $R_r^{'} = 8.2$, $L_{ls} = 0.0328$, $L_s = 0.4377$, $H = 1.8$ and $LL = 50\%$ are obtained after 272 search points.

5.3.3 Impact of data window and transients response

The previous parameter estimations are based on the stator current in the period of [0 1] s. MATLAB/SIMULINK (64-Bit version) programs were implemented on a computer with Intelĩ7-3770 processor (4 cores, 3.1 GHz) and 8 GB DRAM and used 910 second of computing time. Among the total running time, SIMULINK model consumed about 90% of running time and the HCPA only occupied 10% of running time. To shorten the parameter estimation time, the time window length of currents is reduced to the period of [0 0.5] s and the sampling frequency remains the same of 10 kHz. Consequently, the running time is reduced to about half. The estimated parameter set is [8.08 8.03 0.0354 0.4384 1.58 48.82%], which is also close to the real values. Although the residuals are increased by using a shorter time window length, it reduces almost half running time and is therefore suitable for faster estimation without high accuracy

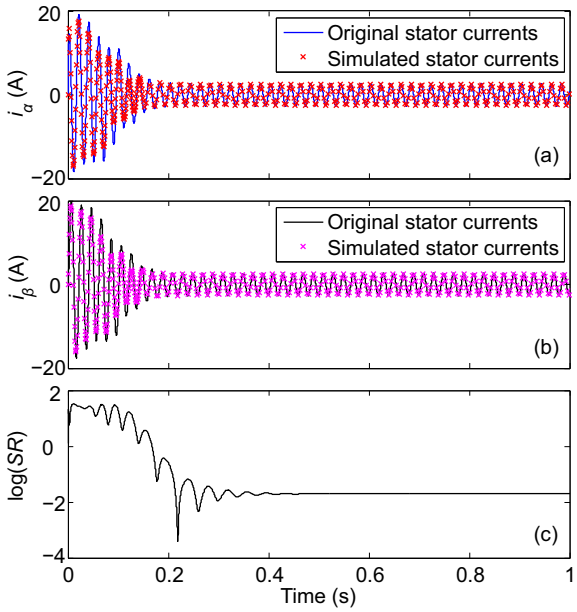

Figure 5.6. Comparison between original stator currents and simulated currents based on the steady state current from 0.5 to 1 s. α coordinate (a); β coordinate (b); and squared residual (SR) in logarithmic scale (c).

requirement. On the other hand, since the SIMULINK model consumes about 90% of total computation time, the computation efficiency of the method can be significantly improved by simplifying mathematical motor model as suggested in [16] and by implementing the algorithm on a specialized embedded controller platform. It is worthwhile to mention that the boundaries of motor parameters in Table 5.1 are very wide as found appropriate for the offline application. In an online system that updates parameters continuously, the boundaries can be narrowed which will reduce the computation time. Therefore, the proposed method can also be tailored for the online real time motor parameters estimation.

The parameters of the induction motor cannot be correctly determined unless the necessary persistency of excitation conditions is met. To ensure parameter convergence, at least $M/2$ sinusoidal harmonics are required for M parameters to be accurately estimated [190]. Since the steady state currents lack the necessary persistency of excitation, the transient data (i.e. from 0 to 0.2 s) has to be used in the parameter estimation. To illustrate this point, the parameters are estimated based on the steady state currents from 0.5 to 1 s. Although the steady state currents are correctly estimated (after 0.2 s), the transient currents are quite different (before 0.2 s), as shown in Fig. 5.6(a) and (b).

The estimated parameter set of [8.24 8.35 0.0318 0.4573 1.60 52.83%] is far from the parameter set of the SIMULINK motor model, which leads to a large residual between simulated and original stator currents, as shown in Fig. 5.6(c).

5.4 Experimental validations

After the validation of the proposed method using the simulated stator voltages and currents, a 3-phase 800 W induction motor is utilised to estimate the motor parameters under different load levels. The motor parameters are identical to the one used in the simulation study, as shown in Table 3.2. These nominal parameters are provided by the machine manufacturer as reference values. The experimental setup is similar to that described in Fig. 3.6 in Chapter 3. The stator voltage and current signals are respectively recorded using voltage transducer LEM LV 25-P [159] and the current transducer LEM HY-15 [160] via National Instruments (NI) 16-bit PCMCIA DAQCard-6036E card [161]. The load level was changed by adjusting a clutch between the motor and the loading motor. Since the proposed method is an off line parameters estimation method for commissioning test, the pulsating loads are not considered in this work.

The simulated stator currents are generated from the SIMULINK model based on the recorded stator voltage. So, the simulated current signals are synchronised with the measured voltage signals. The unsynchronised measured voltage and current signals lead to a time offset between simulated and measured current signals. Thus, an additional parameter T_D is defined and estimated to calibrate the time offset. So, there are seven parameters in total, including five physical motor parameters, load level LL in percentage and time offset T_D in s. The additional parameter T_D is in the range of [0 0.02], given a rate frequency of 50 Hz. Boundaries for physical parameters are given in Table 5.1.

The parameters of the HCP are set to $k = 10$, $\alpha = 0.2$, $\epsilon = 0.3$, $G_p = 200$ and $L_p = 100$. Fig. 5.7 shows the measured stator currents of the motor without loading and simulated currents based on estimated parameters. The comparable wave forms and relative small squared residual indicate the accurate parameter estimation. This chapter focuses on the offline tests and the parameter estimation based on a short period of recorded stator voltage and current signals (less than 1 s). The variations of motor parameters are negligible in this short period. Thus, it is feasible to use nominal parameters provided by the machine manufacturer in Table 3.2 as reference values of the

parameters. The relative error is defined as the difference between the estimated and reference parameters, e.g.

$$\Delta R_s = \frac{\text{Measured } R_s - \text{ Reference } R_s}{\text{Reference } R_s} \times 100\%. \tag{5.3}$$

It is worth mentioning that the variation of parameters can be tracked by applying the proposed method in an online real time parameter estimation. In this case, the motor parameters will be estimated based on sampled voltage and current signals at given intervals. The parameters will be updated for each new interval.

The proposed scheme is examined under different load levels of 0, 25%, 50%, 75% and 100%. The estimated motor parameters and compared with the reference parameters. In Figs. 5.8(a)-(e), the star markers represents the relative errors of these five estimated motor parameters. These relative errors are in the range of $[-10\%, 10\%]$. In Fig. 5.8(f), the start and circle markers indicate estimated load level LL and experimental setup, respectively. In Fig. 5.8(g), the recorded rotor speeds S_r (diamond markers) are compared with the calculated results using Eq. (3.17) (cross markers) from the SIMULINK induction motor model. Since the time offset T_D is only utilised to synchronise the simulated and measured current signals, it is not presented in the figure. The overall results are close to the reference values. In order to refine the estimated parameters,

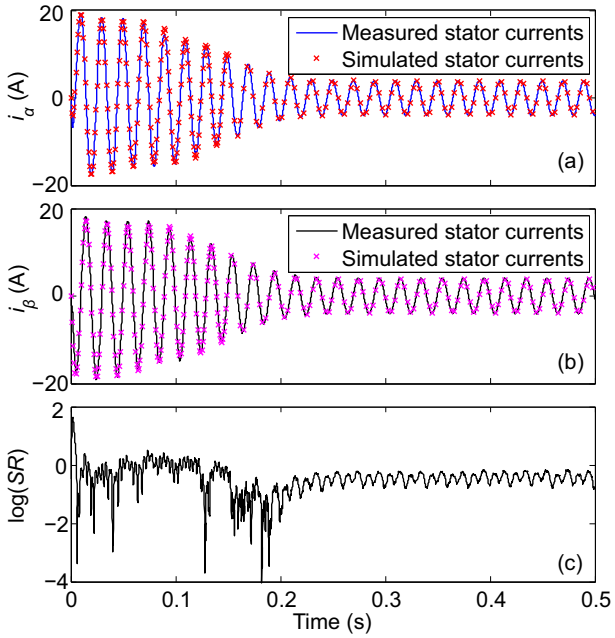

Figure 5.7. Comparison between measured and simulated stator currents using estimated motor parameters. α coordinate (a); β coordinate (b); and squared residual (SR) in logarithmic scale (c).

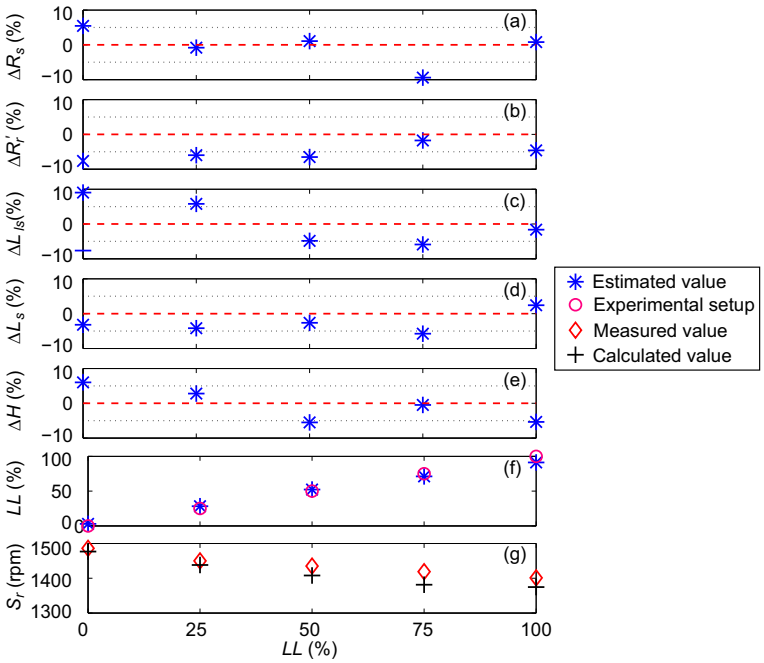

Figure 5.8. Parameters estimation results using the HCPA under different load levels. The relative error of estimated five motor parameters (a)-(e) and load level (f). The calculated and measured rotor speed are shown in (g).

the local search algorithm, Nelder-Mead algorithm, is employed with the global search result as a start point. The local search results in Fig. 5.9 indicate that the differences between estimated and reference values are less than 5%.

5.5 Conclusion

This chapter proposed a method of using global optimisation algorithm to estimate motor parameters. Combined with a SIMULINK induction machine model and a cost function, the HCPA has been employed to estimate five fundamental motor parameters, motor load level and a calibration parameter T_D. The simulation and experiment results based on a three phase 800 W induction motor demonstrate that the performance of the proposed method is satisfactory over a wide range of load levels. The relative errors of the estimated parameter values can be further reduced to less than about 5% after applying the Nelder-Mead local search method with the global search result as a start point. Furthermore, as a non-intrusive parameter estimation method, the proposed method can yield accurate parameter values without disrupting the machine's normal operation. In addition, as a general sparse grid parameter estimation

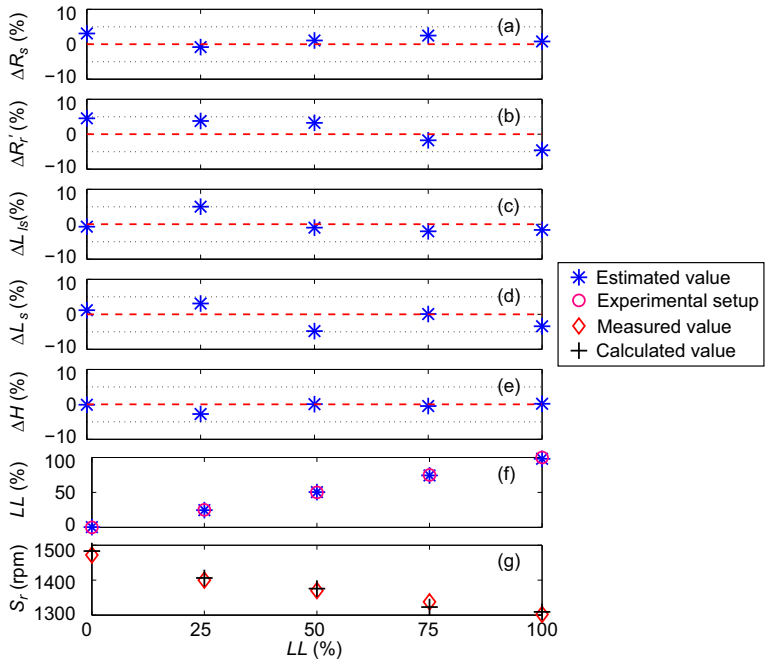

Figure 5.9. Parameters estimation results using the Nelder-Mead algorithm with the global search result as a start point. The relative error of estimated five motor parameters (a)-(e) and load level (f). The calculated and measured rotor speed are shown in (g).

technique, it can be applied to other machine types by using the corresponding machine models.

Chapter 6

Stator Winding Fault Monitoring Using Optimisation Algorithms

THIS chapter presents a simple, low-cost and effective method for an early diagnosis of stator short circuit faults. The approach relies on the combination of an induction motor mathematical model and optimisation algorithms. Kernel of the method is the efficient search for the characteristic parameters that are indicating stator short circuit faults. The system cost and complexity are minimised since the proposed method only requires voltage and current signals recorded at a machine terminal without any invasive or additional hardware circuitry. However, the main challenge is nonlinearity of the machine model and cost function. This may imply multiple local minima of a cost function implemented in the optimisation algorithm. Taking this into consideration, we investigate suitability of three optimisation algorithms, Hyperbolic Cross Point Algorithm, Genetic Algorithm and Pattern Search Algorithm as applied in the proposed condition monitoring method. Experimental results obtained from an induction motor show that the proposed diagnosis method is capable of detecting stator short circuit faults level and location under different load levels.

6.1 Introduction

Induction motors are the most widespread rotating electric machines in industry due to their efficient and cost-effective performance. An induction motor failure results in severe damage not only to the motor itself but also to motor-related equipment devices in an industrial plant. Consequently, motor condition monitoring is of great necessity to detect motor faults at an early stage in order to reduce unscheduled downtime, repair costs, and increase life span of machines.

Condition monitoring is the process of monitoring parameters that describe condition of a machine while in operation. Through the parameters monitoring process, motor failures can be diagnosed before irreversible damage has occurred. The condition monitoring can be broadly categorised into two basic types: intrusive and non-intrusive techniques [3]. The intrusive method is complex and costly because particular sensors and measurement equipments have to be employed to monitor the deviation of air-gap torque [118], magnetic field [191], vibration [192] and so on. For the non-intrusive method, the condition monitoring can be achieved by processing supply voltage and current signals. Therefore, the advantages of the non-intrusive method are reduced cost and simplicity.

The chapter is dedicated to monitor and detect the inter-turn stator winding short circuit fault of induction motors since this fault will mostly lead to turn-to-turn and turn-to-ground faults and finally result in a break down of machine. The proposed method relies on the fact that the induction motors are symmetrical structures and any kind of fault will break their symmetrical property. A change in this balance will cause a drift in characteristic parameters, which offers a method to detect motor fault by monitoring these parameters [193]. In the proposed non-intrusive method, the fault is detected by monitoring two characteristic parameters that are estimated from stator voltages and currents in the time domain. Thus, it only requires a short data window and signals recorded during machine transients.

The proposed condition monitoring approach is based on the induction motor model presented in Chapter 3 and the least squares cost function. Three optimisation algorithms, Pattern Search Algorithm (PSA) [194], Genetic Algorithm (GA) [25, 29], and Hyperbolic Cross Point Algorithm (HCPA) [36] are employed to estimate fault related characteristic parameters and motor load levels. As a direct local search algorithm, the PSA is sensitive to starting (i.e. initial) point. The algorithm might be trapped into local minima. To this end, the Latin Hypercube Sampling (LHS) method [41] is utilised

to generate a proper starting point for the PSA. In contrast, GA is one of the artificial intelligence approaches and it is based on the Darwinian theory of evolution [195]. Although GA requires longer computation time to estimate parameters, it guarantees detection of a global minimum. As we discussed in Chapter 4, the HCPA conducts search on the sparse grid consisting of the Hyperbolic Cross Points (HCPs) [36]. Unlike the conventional parameter estimation methods, HCPA enables a global minimum search for a nonlinear and multi-dimension parameter estimation function with multiple local minima in a computation-efficient and accurate way. Additional heuristics can be easily integrated with HCPA, which will reduce the unnecessary search points and hence increase the efficiency. Thus, the proposed method is feasible for condition monitoring of stator short.

In this chapter, three optimisation algorithms are applied to estimate parameters describing various stator fault conditions of an induction motor under different load levels. The chapter is organised as follows, a mathematical model of induction motor with stator short circuit fault is firstly presented in Section 6.2. The process of the stator winding condition monitoring and cost function are described in Section 6.3, where two optimisation algorithms, PSA and GA are also briefly presented. In order to eliminate the experimental error, simulated motor stator currents are firstly employed to conduct parameter estimation in Section 6.4. The parameter estimation results from HCPA and GA have been analyzed and compared in terms of accuracy and computational cost. Furthermore, the unbalanced voltage supply is also considered in the motor condition monitoring. In Section 6.5, three optimisation algorithms are utilised to monitor the stator winding fault based on current and voltage signals recorded in the laboratory environment. The obtained results are discussed in Section 6.6.

6.2 Mathematical model of induction motor with stator short circuit fault

In order to describe the stator winding short circuit fault, an additional shorted winding is added in a three phase axis of an induction motor [15,37]. Fig. 6.1 shows a stator winding short circuit fault in Phase b. Two characteristic parameters, location parameter θ_f and fault level μ_f, are normally utilised to describe stator short circuit fault in a three phase induction motor. In our study, $\theta_f = \frac{2\pi}{3} \times \{0, 1, 2\}$ represents for stator short circuit fault in phase a, b, and c, respectively.

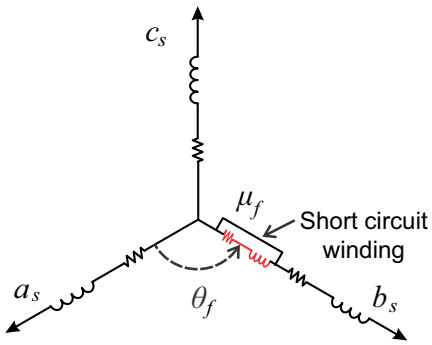

Figure 6.1. Stator winding short circuit fault in Phase b.

6.2.1 Mathematical model in abc coordinates

Applying these two characteristic parameters into the symmetrical induction motor model proposed in Chapter 3, the induction motor mathematical model with stator short circuit fault can be expressed by the following equations [2,15,37],

$$\begin{bmatrix} v_{as} \\ v_{bs} \\ v_{cs} \end{bmatrix} = R_s \begin{bmatrix} i_{as} \\ i_{bs} \\ i_{cs} \end{bmatrix} + \frac{d}{dt} \begin{bmatrix} \lambda_{as} \\ \lambda_{bs} \\ \lambda_{cs} \end{bmatrix}, \tag{6.1}$$

$$0 = R_r \begin{bmatrix} i_{ar} \\ i_{br} \\ i_{cr} \end{bmatrix} + \frac{d}{dt} \begin{bmatrix} \lambda_{ar} \\ \lambda_{br} \\ \lambda_{cr} \end{bmatrix}, \tag{6.2}$$

$$0 = R_f i_f + \frac{d}{dt} \lambda_f, \tag{6.3}$$

$$\begin{bmatrix} \lambda_{as} \\ \lambda_{bs} \\ \lambda_{cs} \end{bmatrix} = \boldsymbol{L}_{ss} \begin{bmatrix} i_{as} \\ i_{bs} \\ i_{cs} \end{bmatrix} + \boldsymbol{L}_{sr} \begin{bmatrix} i_{ar} \\ i_{br} \\ i_{cr} \end{bmatrix} + \boldsymbol{L}_{sf} i_f, \tag{6.4}$$

$$\begin{bmatrix} \lambda_{ar} \\ \lambda_{br} \\ \lambda_{cr} \end{bmatrix} = \boldsymbol{L}_{rs} \begin{bmatrix} i_{as} \\ i_{bs} \\ i_{cs} \end{bmatrix} + \boldsymbol{L}_{rr} \begin{bmatrix} i_{ar} \\ i_{br} \\ i_{cr} \end{bmatrix} + \boldsymbol{L}_{rf} i_f, \tag{6.5}$$

$$\lambda_f = \boldsymbol{L}_{fs} \begin{bmatrix} i_{as} \\ i_{bs} \\ i_{cs} \end{bmatrix} + \boldsymbol{L}_{fr} \begin{bmatrix} i_{ar} \\ i_{br} \\ i_{cr} \end{bmatrix} + L_f i_f, \tag{6.6}$$

where $R_f = \mu_f R_s$ is short circuit resistance; i_f and λ_f are short circuit current and flux, respectively; $L_f = \mu_f^2(L_{ls} + L_s)$ is short circuit inductance. The mutual inductances between stator, rotor and short-circuited windings are dependent on the rotor angle θ_r, denoted as [15],

$$\boldsymbol{L}_{sf} = \boldsymbol{L}_{fs}^T = \mu_f L_s \begin{bmatrix} \cos(\theta_f) \\ \cos(\theta_f - \frac{2\pi}{3}) \\ \cos(\theta_f + \frac{2\pi}{3}) \end{bmatrix}, \tag{6.7}$$

$$\boldsymbol{L}_{rf} = \boldsymbol{L}_{fr}^T = \mu_f L_s \begin{bmatrix} \cos(\theta_f - \theta_r) \\ \cos(\theta_f - \theta_r - \frac{2\pi}{3}) \\ \cos(\theta_f - \theta_r + \frac{2\pi}{3}) \end{bmatrix}. \tag{6.8}$$

Apart from these new variables, the remaining variables have the same definition as discussed in Chapter 3. Compared to the symmetrical induction motor model, two additional Eqs. (6.3) and (6.6) are employed to describe the short circuit current (i_f) and flux (λ_f). Two elements $\boldsymbol{L}_{sf} i_f$ and $\boldsymbol{L}_{rf} i_f$ are respectively added to Eq. (6.4) and (6.5) to include effects from stator short current.

6.2.2 Mathematical model in $\alpha\beta$ coordinates

The mathematical model is also transferred from *abc* to $\alpha\beta$ coordinates to simplify the computation. The same transformation matrices Eq. (3.12) in Chapter 3 are applied to stator and rotor variables. The transformation matrices of stator short circuit fault related variables (i_f, λ_f) are defined as [15],

$$\begin{bmatrix} i_{\alpha f} \\ i_{\beta f} \end{bmatrix} = \begin{bmatrix} \cos(\theta_f) \\ \sin(\theta_f) \end{bmatrix} i_f, \quad \begin{bmatrix} \lambda_{\alpha f} \\ \lambda_{\beta f} \end{bmatrix} = \begin{bmatrix} \cos(\theta_f) \\ \sin(\theta_f) \end{bmatrix} \lambda_f \,. \tag{6.9}$$

Applying transformation matrices to the induction motor model Eqs. (6.1)-(6.6), the motor model in $\alpha\beta$ coordinates can be expressed as,

$$\begin{bmatrix} v_{\alpha s} \\ v_{\beta s} \end{bmatrix} = R_s \begin{bmatrix} i_{\alpha s} \\ i_{\beta s} \end{bmatrix} + \frac{d}{dt} \begin{bmatrix} \lambda_{\alpha s} \\ \lambda_{\beta s} \end{bmatrix}, \tag{6.10}$$

$$0 = R_r^{'} \begin{bmatrix} i_{\alpha r}^{'} \\ i_{\beta r}^{'} \end{bmatrix} + \frac{d}{dt} \begin{bmatrix} \lambda_{\alpha r}^{'} \\ \lambda_{\beta r}^{'} \end{bmatrix} - \omega_r T_r \left(\frac{\pi}{2}\right) \begin{bmatrix} \lambda_{\alpha r}^{'} \\ \lambda_{\beta r}^{'} \end{bmatrix}, \tag{6.11}$$

$$0 = \mu_f R_s \begin{bmatrix} i_{\alpha f} \\ i_{\beta f} \end{bmatrix} + \frac{d}{dt} \begin{bmatrix} \lambda_{\alpha f} \\ \lambda_{\beta f} \end{bmatrix}, \tag{6.12}$$

$$\begin{bmatrix} \lambda_{\alpha s} \\ \lambda_{\beta s} \end{bmatrix} = L_{ls} \begin{bmatrix} i_{\alpha s} \\ i_{\beta s} \end{bmatrix} + L_m \left(\begin{bmatrix} i_{\alpha s} \\ i_{\beta s} \end{bmatrix} + \begin{bmatrix} i_{\alpha r}^{'} \\ i_{\beta r}^{'} \end{bmatrix} + \sqrt{\frac{2}{3}} \mu_f \begin{bmatrix} i_{\alpha f} \\ i_{\beta f} \end{bmatrix} \right), \tag{6.13}$$

$$\begin{bmatrix} \lambda_{\alpha r}^{'} \\ \lambda_{\beta r}^{'} \end{bmatrix} = L_{lr}^{'} \begin{bmatrix} i_{\alpha r}^{'} \\ i_{\beta r}^{'} \end{bmatrix} + L_m \left(\begin{bmatrix} i_{\alpha s} \\ i_{\beta s} \end{bmatrix} + \begin{bmatrix} i_{\alpha r}^{'} \\ i_{\beta r}^{'} \end{bmatrix} + \sqrt{\frac{2}{3}} \mu_f \frac{N_s}{N_r} \begin{bmatrix} i_{\alpha f} \\ i_{\beta f} \end{bmatrix} \right), \tag{6.14}$$

$$\begin{bmatrix} \lambda_{\alpha f} \\ \lambda_{\beta f} \end{bmatrix} = \sqrt{\frac{2}{3}} \mu_f L_m Q(\theta_f) \left(\begin{bmatrix} i_{\alpha s} \\ i_{\beta s} \end{bmatrix} + \begin{bmatrix} i_{\alpha r} \\ i_{\beta r} \end{bmatrix} \right) + \mu_f^2 (L_{ls} + \frac{2}{3} L_m) Q(\theta_f) \begin{bmatrix} i_{\alpha f} \\ i_{\beta f} \end{bmatrix} \tag{6.15}$$

where $R_r^{'} = (\frac{N_s}{N_r})^2 R_r$, $i_{\alpha\beta r}^{'} = \frac{N_r}{N_s} i_{\alpha\beta r}$, $\lambda_{\alpha\beta r}^{'} = \frac{N_s}{N_r} \lambda_{\alpha\beta r}$, $L_{lr}^{'} = (\frac{N_s}{N_r})^2 L_{lr}$ $L_m = \frac{3}{2} L_s$ and

$$Q(\theta_f) = \begin{bmatrix} cos(\theta_f)^2 & sin(\theta_f)cos(\theta_f) \\ sin(\theta_f)cos(\theta_f) & sin(\theta_f)^2 \end{bmatrix}.$$

The leakage is usually divided between stator and rotor phases, i.e. L_{ls} and L_{lr}. In [15, 196], the leakage is simplified by applying global-leakage inductance L_g referred to the stator. The induction motor model is further simplified by applying principle inductance L_p referred to the stator. Consequently, the stator-to-stator winding inductances $\boldsymbol{L}_{ss}$, rotor-to-rotor winding inductances $\boldsymbol{L}_{rr}$ and stator-to-rotor mutual inductances $\boldsymbol{L}_{sr}$ are presented as [15, 196],

$$\boldsymbol{L}_{ss} = \begin{bmatrix} L_g + L_p & -\frac{L_p}{2} & -\frac{L_p}{2} \\ -\frac{L_p}{2} & L_g + L_p & -\frac{L_p}{2} \\ -\frac{L_p}{2} & -\frac{L_p}{2} & L_g + L_p \end{bmatrix}, \tag{6.16}$$

$$\boldsymbol{L}_{rr} = \begin{bmatrix} L_p & -\frac{L_p}{2} & -\frac{L_p}{2} \\ -\frac{L_p}{2} & L_p & -\frac{L_p}{2} \\ -\frac{L_p}{2} & -\frac{L_p}{2} & L_p \end{bmatrix}, \tag{6.17}$$

$$\boldsymbol{L}_{sr} = L_p \begin{bmatrix} \cos(\theta_r) & \cos\left(\theta_r + \frac{2\pi}{3}\right) & \cos\left(\theta_r - \frac{2\pi}{3}\right) \\ \cos\left(\theta_r - \frac{2\pi}{3}\right) & \cos(\theta_r) & \cos\left(\theta_r + \frac{2\pi}{3}\right) \\ \cos\left(\theta_r + \frac{2\pi}{3}\right) & \cos\left(\theta_r - \frac{2\pi}{3}\right) & \cos(\theta_r) \end{bmatrix}, \tag{6.18}$$

Then, Eqs. (6.10)-(6.15) can be expressed as,

$$\begin{bmatrix} v_{\alpha s} \\ v_{\beta s} \end{bmatrix} = R_s \begin{bmatrix} i_{\alpha s} \\ i_{\beta s} \end{bmatrix} + \frac{d}{dt} \begin{bmatrix} \lambda_{\alpha s} \\ \lambda_{\beta s} \end{bmatrix}, \tag{6.19}$$

$$0 = R_r \begin{bmatrix} i_{\alpha r} \\ i_{\beta r} \end{bmatrix} + \frac{d}{dt} \begin{bmatrix} \lambda_{\alpha r} \\ \lambda_{\beta r} \end{bmatrix} - \omega_r T_r \left(\frac{\pi}{2}\right) \begin{bmatrix} \lambda_{\alpha r} \\ \lambda_{\beta r} \end{bmatrix}, \tag{6.20}$$

$$0 = \mu_f R_s \begin{bmatrix} i_{\alpha f} \\ i_{\beta f} \end{bmatrix} + \frac{d}{dt} \begin{bmatrix} \lambda_{\alpha f} \\ \lambda_{\beta f} \end{bmatrix}, \tag{6.21}$$

$$\begin{aligned} \begin{bmatrix} \lambda_{\alpha s} \\ \lambda_{\beta s} \end{bmatrix} &= L_g \begin{bmatrix} i_{\alpha s} \\ i_{\beta s} \end{bmatrix} + L_m \left(\begin{bmatrix} i_{\alpha s} \\ i_{\beta s} \end{bmatrix} + \begin{bmatrix} i_{\alpha r} \\ i_{\beta r} \end{bmatrix} + \sqrt{\frac{2}{3}} \mu_f \begin{bmatrix} i_{\alpha f} \\ i_{\beta f} \end{bmatrix} \right) \\ &= \begin{bmatrix} \lambda_{\alpha g} \\ \lambda_{\beta g} \end{bmatrix} + \begin{bmatrix} \lambda_{\alpha m} \\ \lambda_{\beta m} \end{bmatrix}, \end{aligned} \tag{6.22}$$

$$\begin{aligned} \begin{bmatrix} \lambda_{\alpha r} \\ \lambda_{\beta r} \end{bmatrix} &= L_m \left(\begin{bmatrix} i_{\alpha s} \\ i_{\beta s} \end{bmatrix} + \begin{bmatrix} i_{\alpha r} \\ i_{\beta r} \end{bmatrix} + \sqrt{\frac{2}{3}} \mu_f \begin{bmatrix} i_{\alpha f} \\ i_{\beta f} \end{bmatrix} \right) \\ &= \begin{bmatrix} \lambda_{\alpha m} \\ \lambda_{\beta m} \end{bmatrix}, \end{aligned} \tag{6.23}$$

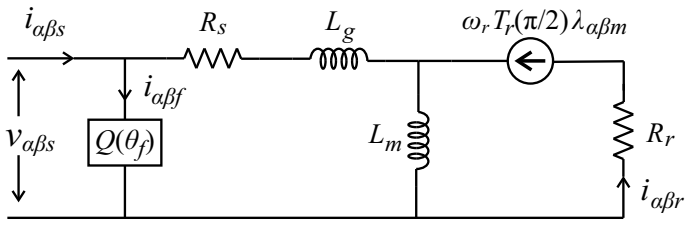

Figure 6.2. Equivalent circuit representation of an induction motor with stator short circuit fault in the $\alpha\beta$ reference frame.

$$\begin{aligned}\begin{bmatrix}\lambda_{\alpha f}\\ \lambda_{\beta f}\end{bmatrix} &= \sqrt{\frac{2}{3}}\mu_f L_m Q(\theta_f)\left(\begin{bmatrix}i_{\alpha s}\\ i_{\beta s}\end{bmatrix}+\begin{bmatrix}i_{\alpha r}\\ i_{\beta r}\end{bmatrix}\right)+\mu_f^2(L_g+\frac{2}{3}L_m)Q(\theta_f)\begin{bmatrix}i_{\alpha f}\\ i_{\beta f}\end{bmatrix}\\ &= \sqrt{\frac{2}{3}}\mu_f L_m Q(\theta_f)\left(\begin{bmatrix}i_{\alpha s}\\ i_{\beta s}\end{bmatrix}+\begin{bmatrix}i_{\alpha r}\\ i_{\beta r}\end{bmatrix}+\sqrt{\frac{2}{3}}\mu_f\begin{bmatrix}i_{\alpha f}\\ i_{\beta f}\end{bmatrix}\right)+\mu_f^2 L_g Q(\theta_f)\begin{bmatrix}i_{\alpha f}\\ i_{\beta f}\end{bmatrix}\\ &= \sqrt{\frac{2}{3}}\mu_f Q(\theta_f)\begin{bmatrix}\lambda_{\alpha m}\\ \lambda_{\beta m}\end{bmatrix}+\mu_f^2 L_g Q(\theta_f)\begin{bmatrix}i_{\alpha f}\\ i_{\beta f}\end{bmatrix}\end{aligned} \tag{6.24}$$

By neglecting L_g in Eq. 6.24, the equivalent circuit model of stator short circuit fault is shown in Fig. 6.2 [196]. Base on the model, the fault winding becomes a simple unbalanced resistance element in parallel with the magnetising inductance L_m.

6.3 Condition monitoring of stator windings using optimisation algorithms

The proposed condition monitoring of stator windings scheme conducts using SIMULINK induction motor model. The symmetric induction SIMULINK model in Chapter 3 is extended by adding the additional fault winding proposed in the previous section. The process of the stator winding condition monitoring is illustrated in Fig. 6.3 and described as follows. In order to estimate these parameters, the recorded three-phase voltage and current signals ($v_{a,b,c}$ and $i_{a,b,c}$) are firstly transferred to $v_{\alpha\beta}$ and $i_{\alpha\beta}$, respectively. The v_α and v_β signals are imported into the SIMULINK induction motor model. The output currents i'_α and i'_β are compared with measured i_α and i_β. Similarly to the cost function in Chapter 5, the difference between simulated and measured currents,

i.e. the cost function, is defined as

$$\begin{aligned} F_{SR} &= \sum_{j=1}^{N} SR(j) \\ &= \sum_{j=1}^{N} \left\{ \left[i_{\alpha s}(j) - i'_{\alpha s}(j) \right]^2 + \left[i_{\beta s}(j) - i'_{\beta s}(j) \right]^2 \right\}, \end{aligned} \tag{6.25}$$

where N is total number of the discrete stator current signals. If F_{SR} is bigger than a pre-defined threshold, the selected parameter estimation method will generate a new set of parameters and transfer to the SIMULINK model. The process iterates until the threshold is met. The inter-turn short circuit stator winding fault does not introduce any extra frequency components and only increase the amplitude of the existing frequency components [145]. In Eq. 6.25, currents are in time domain so change of amplitude at certain frequencies will introduce change of F_{SR} even if there are no new frequencies introduced by a fault. Although the approach is introduced for the diagnosis of stator faults, it is possible to adapt its use for the other faults or the combined faults as long as faults can be described by characteristic parameters. To this end, the induction motor model should be adapted to include the corresponding characteristic parameters and additional fault classification method might be necessary to detect a condition with the combined faults [15, 197].

Based on this parameter estimation method framework, the conventional local and global optimisation methods in SIMULINK Parameter Estimation Toolbox have been respectively employed to diagnose stator short circuit fault in [39]. The selection of optimisation algorithm is critical since the induction motor model is nonlinear and the cost function might include several local minima. Local optimisation algorithms might be trapped into local minima. Therefore, the estimated results are sensitive to the start points. On the contrary, the global optimisation method is not sensitive to the

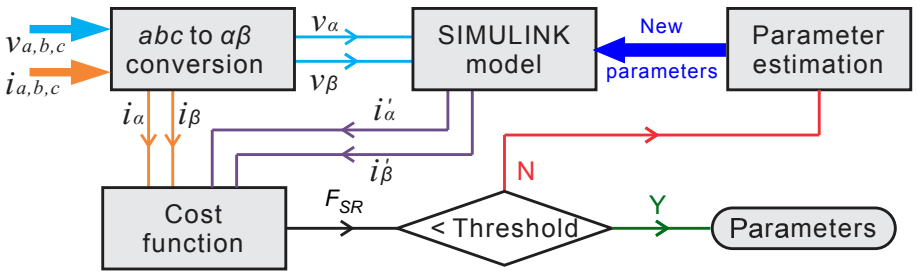

Figure 6.3. Induction motor stator winding short circuit monitoring using parameter estimation method.

start points. Although the running time is increased, the global optimisation method is highly preferred in solving the non-linear parameter estimation. In this study, the PSA, GA and HCPA are employed to illustrate the proposed induction motor fault diagnosis method. The HCPA has been presented in Chapter 4. PSA and GA are briefly described in the following sections since they can be easily found in literature.

6.3.1 Pattern Search Algorithm

The PSA is one of the direct search methods, which does not need the gradient of the cost function [194]. The PSA finds minimum by generating a sequence of points towards an optimal point. The cost function values of the sequence points either decrease or keep constant. Considering a D-dimensional cost function $f(X)$, the algorithm starts from the an initial point $X_0 = [x_1, x_2, ..., x_D]$ and initial mesh of M_0. The new pattern vectors can be generated by neither $2D$ or $DP1$ method [194]. In the case of $2D$ method, $2 \times D$ new vectors are generated, i.e.

$$\begin{bmatrix} x_1 \\ x_2 \\ ... \\ x_D \end{bmatrix} \pm \left(\underbrace{\begin{bmatrix} 1 \\ 0 \\ ... \\ 0 \end{bmatrix}, \begin{bmatrix} 0 \\ 1 \\ ... \\ 0 \end{bmatrix}, \begin{bmatrix} 0 \\ 0 \\ ... \\ 1 \end{bmatrix}}_{D} \right) \times M_0$$

Only $D + 1$ new vectors are generated in the $DP1$ method, i.e.

$$\begin{bmatrix} x_1 \\ x_2 \\ ... \\ x_D \end{bmatrix} + \left(\underbrace{\begin{bmatrix} 1 \\ 0 \\ ... \\ 0 \end{bmatrix}, \begin{bmatrix} 0 \\ 1 \\ ... \\ 0 \end{bmatrix}, \begin{bmatrix} 0 \\ 0 \\ ... \\ 1 \end{bmatrix}}_{D}, \begin{bmatrix} -1 \\ -1 \\ ... \\ -1 \end{bmatrix} \right) \times M_0$$

If the function value $f(X_i)$ is smaller than $f(X_0)$, the X_i is selected as central point X_c, which is used to generate new pattern vectors with the mesh size of $M_c \times F_M$, where M_c is the current mesh size and $F_m \geq 1$ is mesh factor. If the function values of all new generated vectors are bigger than $f(X_0)$, the central point X_c remains the same and the mesh size is reduced to M_c / F_M. The algorithm iterates until it researches stopping criteria. In our algorithm, the stopping criterion is set to $FunTol$, i.e. the difference between the function values of the previous and current central point is less than $FunTol$. As a direct search method, the parameter estimation result of the PSA depends on the starting point, as shown in the Section 6.5.1.

6.3.2 Genetic Algorithm

GA is considered as a global optimisation method that is independent of starting point [195]. The algorithm is inspired by natural evolution, such as inheritance, mutation, selection, and crossover. GA starts with creating a random initial population. The algorithm then breeds a new generation based on the existing population. The selected members, called parents, are chosen based on their fitness. Some members with lower fitness are directly passed to the next population, named elite. Children are generated either by mutation (random choosing a single parent) or crossover (combining the vector entries of a pair of parents). Then, the current population is replaced by a new generated children. The process continues until one of the stopping criteria is met. For the fair comparison, the stopping criterion of the PSA and GA is set the same value of function tolerance (*Fun Tol*).

6.4 Simulation results

The study is based on a three phase induction motor. The motor parameters are tabulated in Table 3.2. In order to eliminate the experimental error and test the HCPA and GA in controlled environment, simulated motor stator currents are firstly utilised to conduct parameter estimation. In the simulation, the motor fault level μ_f, fault location θ_f and load level LL are [0.05, 1, 0.1], i.e. 5% stator circuit short fault in phase b with 10% load level. The boundaries of these three parameters are [0 0.2], [0 2] and [0 1], respectively. The steady-state stator currents in the period of 0.5 s are employed to estimate these three parameters. The sampling frequency of the currents is 10 kHz. Thus, the discrete stator current signals include 5000 points, i.e. $N = 5000$ in the cost function given in Eq. (6.25).

6.4.1 Condition monitoring using HCPA

The HCPA is firstly utilised to estimate these three parameters. Figs. 6.4(a) and (b) compare the evaluated points by the HCPA with adaptiveness parameter α of 1 and 0, respectively. In both cases, the stopping criterion is the maximum function evaluations of 500. When $\alpha = 1$, the algorithm is not adaptive and conducts search on the region where less HCPs are evaluated, as shown in Fig. 6.4(a). This global search method prevents being trapped into local minima. However, the estimated parameter set [0.0508,

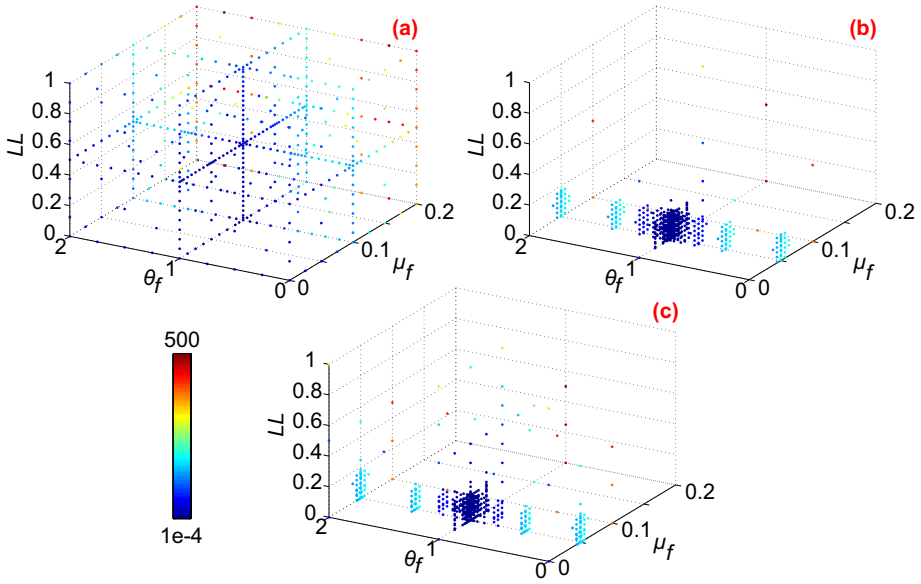

Figure 6.4. Evaluated 500 points by HCPA with different α. $\alpha = 1$ (a); $\alpha = 0$ (b); $\alpha = 0.4$ (c)

1.0000, 0.1025] is a little bit far from the real values. On the contrary, with the same function evaluations, the estimated parameter set [0.0500, 1.0000, 0.1005] is close to the real values when using the local search ($\alpha = 0$). The algorithm is adaptive and highly prefers HCPs close to small function values, as shown in Fig. 6.4(b). In this case, the algorithm might be trapped into local minima. Adopting the rule of thumb for selecting α, the value of α is chosen as 0.4 in the following studies. Fig. 6.4(c) shows the evaluated points and the global minimum of $F_{SR} = 2.4114 \times 10^{-4}$ is found at the location of $[0.0500, 1.0000, 0.1016]$. The adaptiveness parameter α offers user the flexibility of selecting a proper search method according the specified optimisation task.

6.4.2 Data window length and evaluated HCPs

The current signal data window length D_L is one of the critical factors for parameter estimation. The long data length will improve the accuracy and of course increase the SIMULINK induction motor model running time. Furthermore, large number of evaluated HCPs N_{HCP} can also improve the accuracy. This is a trade off between accuracy and time consumption. The data window length and number of evaluated HCPs have to be increased at low signal to noise ratio (SNR) environment. Fig. 6.5 shows the effect of data window length and number of evaluated HCPs on cost function values and estimated parameters under different SNR levels. The Gaussian white noise is added to the simulated voltage and current signals to generate signals with SNR of 10 dB, 20 dB

and 30 dB. Given the sampling frequency $f_s = 10$ kHz, the total number of the discrete samples are $N = f_s \times D_L$ in the cost function Eq. 6.25. In Fig. 6.5(a), the mean value of cost function is defined as $F_{SRA} = F_{SR}/N$ and the values are plotted in logarithmic scale for the better visualization. As expected, low SNR leads to large value of F_{SRA}. The mean value of cost function can be reduced by increasing either data windows length or number of evaluated HCPs.

Figs. 6.5(b), (c) and (d) show the relative errors of estimated μ_f, θ_f and LL, respectively. Ideally, the relative errors should decrease with the increase of data window length. However, insufficient number of HCPs cannot guarantee to find global minimum at low SNR environment, as shown the dashed curve in Figs. 6.5(b), (c) and (d). Although the value of F_{SRA} can be decreased by using long data window length, the relative errors of estimated parameters will not converge. In this case, the number of HCPs has to be increased to locate global minimum. With 500 HCPs, the relative errors is decreased at the cost of increasing the data window length. The relative errors of estimated parameters are less than 3% by using 500 HCPs under the condition of SNR = 20 dB.

6.4.3 Comparison between HCPA and GA

GA is heuristic search algorithm based on the Darwin theory of evolution. This search algorithm does not have any rigorous mathematical description. In contrast, the HCPA has rigorous mathematical base in the function approximation theory, as it uses a sparse grids to approximate multidimensional functions. In addition, the HCPA can be adaptive by introducing very simple heuristics that can concentrate points in the regions where solution lays. These heuristic techniques reduce the number of sampling points while preserving rigorous mathematical function approximation properties. For this induction motor condition monitoring task, the fault location parameter θ_f set is $\{0, 1, 2\}$, denoting as Phase a, b and c, respectively. Thus, it is meaningless to evaluate θ_f beyond these three values. The efficiency of the condition monitoring will be increased by only evaluating points with θ_f in the set of $\{0, 1, 2\}$. It is easy to apply extra parameter limits in the HCPA, but difficult to implement in the GA.

In this comparison we have been using the Matlab GA toolbox with the following settings: *PopulationSize=20*, *EliteCount=5*, *CrossoverFraction=0.4* and *Generations=25*. The

algorithm stops at the 25^{th} generation and the total evaluated points are about 520. The stop criteria of the HCPA and GA are about 500 evaluated points.

Table 6.1 shows the obtained results by using the GA, HCPA and improved HCPA (i.e. search θ_f in the set of $\{0, 1, 2\}$). The motor condition parameters $[\mu_f, \theta_f, LL]$ are [0.08, 2, 0.27], respectively. The programs were implemented on a computer with Intel i7-3770 processor (4 cores, 3.1 GHz) and 8 GB DRAM. The major computational load is due to SIMULINK simulation, which consumes more than 90% of the total time. The HCPA and GA are almost instantaneous compared to the SIMULINK machine simulation. The speed of HCPA is comparable with that of GA. By limiting the parameter range of θ_f, the improved HCPA uses less time to generate new points. For all of these three algorithms, the estimated parameters are close to the setup parameters.

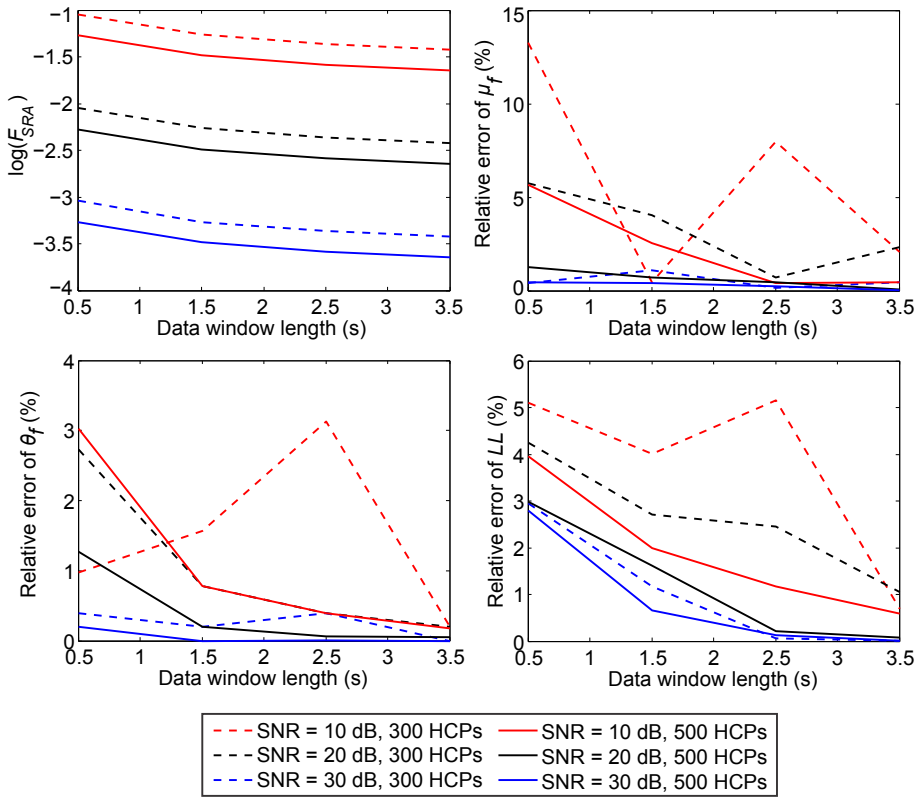

Figure 6.5. The effect of data window length and number of evaluated HCPs on cost function values and estimated parameters under different SNR levels. Mean value of cost function (a); Relative error of estimated parameters, μ_f (b), θ_f (b) and LL (c)

Table 6.1. Comparison between the GA, HCPA and improved HCPA.

		GA	HCPA	Improved HCPA
Total points		520	547	524
Total time (s)		119	131	106
Average time per point (s)		0.23	0.24	0.20
Algorithm used time		8%	10%	5%
Estimated parameters	μ_f	0.0799	0.0800	0.0800
	θ_f	2.0012	2.0000	2.0000
	LL	0.2704	0.2733	0.2699

6.4.4 Condition monitoring under unbalanced voltage

Unbalanced voltage is one of the most common disturbances in electrical systems. This asymmetry introduces negative sequence current which leads to a backward rotating field. The interaction between this unwanted backward and normal forward rotating field causes efficiency reduction, extra temperature rise, noise in machine and so on. Considering both magnitude and phase unbalance, the voltage unbalance factor (VUF) is defined as the ratio of positive (v_p) and negative (v_n) sequence voltage components [198]

$$VUF = \frac{v_p}{v_n} \times 100\%. \tag{6.26}$$

These two components are given by

$$v_p = \frac{v_a + \alpha_1 \cdot v_b + \alpha_2 \cdot v_c}{3}, \tag{6.27}$$

$$v_n = \frac{v_a + \alpha_2 \cdot v_b + \alpha_1 \cdot v_c}{3}, \tag{6.28}$$

where $\alpha_1 = 1\angle 120^\circ$ and $\alpha_2 = 1\angle 240^\circ$.

From motor condition monitoring point of view, the negative sequence current resulting from unbalanced voltage adversely affects methods based on negative sequence current [199]. As a result, a false alarm might occur. The proposed approach conducts direct characteristic parameters estimation on the mathematical induction motor model. It is therefore less sensitive to VUF. Since VUF depends on not only the magnitude shift but also the phase shift, the results presented in the followings were obtained for the worse case, including both magnitude and phase shift. For example, the three unbalanced phase voltages respectively are $304.06\angle 0^\circ$, $325.78\angle 230^\circ$ and $300.96\angle 130^\circ$, resulting in VUF = 10.06%. The setting parameters of the improved HCPA and the GA

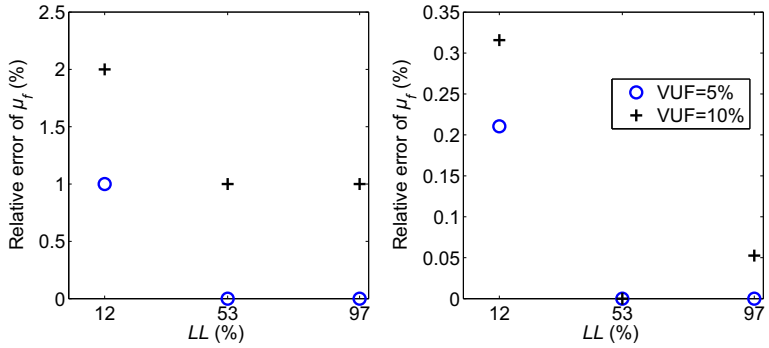

Figure 6.6. Stator winding circuit fault monitoring using the HCPA under different VUF and load level. $\mu_f = 1\%$ (a); $\mu_f = 19\%$ (b).

are the same as in the previous section and the number of evaluated points is about 500 for each algorithm.

Fig. 6.6(a) shows stator winding circuit fault monitoring result by using the improved HCPA at low fault level $\mu_f = 1\%$. The circle and cross marks represent the relative errors of the estimated μ_f at VUF of 5% and 10%, respectively. The relative error of μ_f is less than 2% at the worst case, i.e. low load level of 12%, fault level of 1% and large VUF of 10%. In other words, it is difficult to detect the fault under the condition of low fault level, low load level and large VUF. Similarly, Fig. 6.6(b) shows the result by using the improved HCPA at high fault level $\mu_f = 19\%$. As expected, the relative errors of μ_f at high fault level (Fig. 6.6(b)) are smaller than that at low fault level (Fig. 6.6(a)). Considering VUF of 5 and 10 cases, the difference of relative error of μ_f in these two cases is less than 1% under all load and fault levels. It can be concluded that the HCPA is robust to unbalanced voltage and load level. Given the 500 search points limitation, the GA has not converged under the worst case. The relative error of the estimated μ_f is as high as 60%, as shown in Fig. 6.7. The GA converges after the *Generations* is increased to 40, resulting the large number of evaluated points of 820. Therefore, the improved HCPA is more robust than GA in this example with unbalanced voltage supply.

6.5 Experimental validation

The proposed global optimisation method is experimentally validated by using a three phase 800 W induction motor, identical to the one used in the simulation study. The stator winding of the induction motor consists of 12 coils, 4 coils each phase. Each coil contains 90 turns made of enameled wire with diameter of 0.60 mm. In order

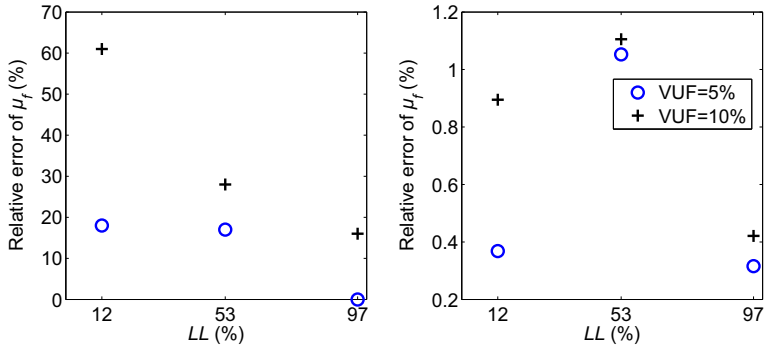

Figure 6.7. Stator winding circuit fault monitoring using the GA under different VUF and load level. $\mu_f = 1\%$ (a); $\mu_f = 19\%$ (b).

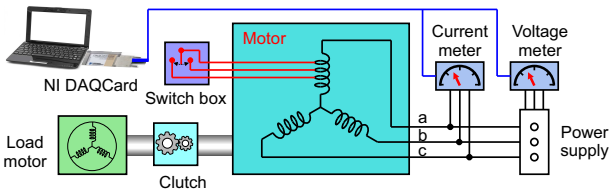

Figure 6.8. The laboratory setup for induction motor stator short circuit.

to make stator short circuit fault, the insulation layer of windings are scraped and soldered with wires. These wires are connected to a switch box which controls the stator circuit short fault level, as shown in Fig. 6.8. For example, 10% stator winding circuit fault means short circuit of 9 coil turns. The resistance introduced by the fault generating mechanism is 15 Ohms. The sampling frequency for both the current and voltage signals is 10 kHz. Another motor is utilised as a load and the load level is varied through the motor control.

The stator current signals i'_α and i'_β are generated from the induction motor model based on the measured voltage signals. The generated current signals are synchronous with the measured voltage signals. The unsynchronised measured voltage and current signals, resulted from measurement error, leads to the time offset between simulated and measured current signals, as discussed in Chapter 5. Thus, apart from two fault related characteristic parameters μ_f and θ_f and load level LL, an additional parameter, T_d, is utilised to calibrate the time offset between measured and simulated stator currents. In total, there are four parameters to be estimated and the related ranges are listed in the Table. 6.2. The range of fault level μ_f is from 0 to 0.2, i.e. from healthy condition to 20% stator short circuit fault in one coil. The fault localization θ_f of 0,1,2 stand for *Phase* a, b, c, respectively. The load level LL is defined to be in the range from

Table 6.2. Parameters to be estimated and their ranges.

Variable	Parameter name	Range
μ_f	Fault level	[0 0.2]
θ_f	Fault location	{0, 1, 2}
T_D	Offset time	[0 0.02]
LL	Motor load level	[0 1]

0 to 1 (100% load level). Since the rated frequency of the supply voltage is 50 Hz, the offset time is adjusted within one period of 0.02 s.

It is worthwhile to mention that the proposed approach is intended to apply a global optimisation algorithm for parameter estimation implemented in machine fault detection and identification. Since the mathematical model presented in this approach is replaceable, it is feasible to implement the proposed algorithm in other machine models and use for other machine types with different characteristics in practical environments.

6.5.1 Comparison between GA and PSA

The direction search algorithm, PSA, is utilised to illustrate the necessity of global optimisation algorithm in this parameter estimation task. The experiment data of 10% ($\mu_f = 0.1$) stator short circuit fault in *Phase b* ($\theta_f = 1$) is employed to evaluate the proposed diagnostic technique based on parameter estimation. The motor is under 50% loading. The parameter estimation is based the recorded current signals 0.5 s after machine starts, where the motor operates under the steady state condition.

In the first attempt, the starting point of the PSA is set to the left boundary of each parameter. Figs. 6.9(a)-(d) and (e) show the trajectories of estimated parameters and cost function value, respectively. The algorithm reaches the stopping criterion of $Fun\ Tol = 10^{-5}$, i.e. the difference between the function values of the previous and current central point is less than 10^{-5}. The cost function value is $F_{SR} = 121.7344$ and the estimated parameter are $[\mu_f = 0; \theta_f = 0; LL = 0.5300; T_s = 0.0001]$, which are far from the experimental setup. As a direct search algorithm, the search result of PSA depends on the starting point and it has been trapped into local minima. Therefore, LHS method is utilised to generate a starting point for PSA.

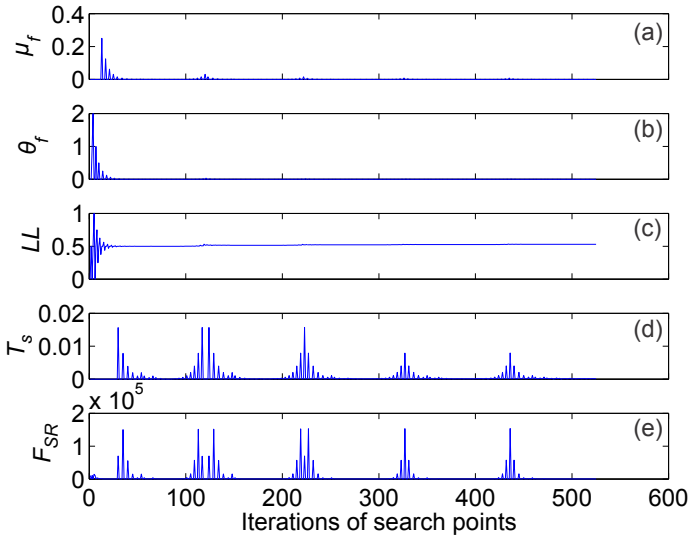

Figure 6.9. Trajectories of estimated parameters and cost function value using the PSA with left boundary of each parameter as a starting point.

The LHS is a method of sampling that can generate points with each component close to evenly spaced [41]. We use this 4 parameters estimation task as an example to illustrate the LHS method. In order to generate five start points (i.e. $SP = 5$), a matrix M_1 of 5 rows and 4 columns is firstly built by combining 4 column vectors. Each column vector has a random permutation of [1, 2, 3, 4, 5]. An example of matrix M_1 is shown below

$$M_1 = \begin{bmatrix} 2 & 5 & 4 & 2 \\ 1 & 3 & 1 & 1 \\ 3 & 2 & 5 & 4 \\ 5 & 4 & 2 & 3 \\ 4 & 1 & 3 & 5 \end{bmatrix}.$$

Then, the sampling points matrix M_{LHS} is calculated by using the equation $M_{LHS} = (M_1 - M_r)/SP$, where M_r is a random matrix with the same size as M_1. The elements of M_r are in the range of $[0, 1]$. Each element of M_{LHS} is also in the range of $[0, 1]$. In this example, the matrices M_r and M_{LHS} are shown below,

$$M_r = \begin{bmatrix} 0.6557 & 0.7577 & 0.7060 & 0.8235 \\ 0.0357 & 0.7431 & 0.0318 & 0.6948 \\ 0.8491 & 0.3922 & 0.2769 & 0.3171 \\ 0.9340 & 0.6555 & 0.0462 & 0.9502 \\ 0.6787 & 0.1712 & 0.0971 & 0.0344 \end{bmatrix};$$

$$M_{LHS} = \begin{bmatrix} 0.2689 & 0.8485 & 0.6588 & 0.2353 \\ 0.1929 & 0.4514 & 0.1936 & 0.0610 \\ 0.4302 & 0.3216 & 0.9446 & 0.7366 \\ 0.8132 & 0.6689 & 0.3908 & 0.4100 \\ 0.6643 & 0.1658 & 0.5806 & 0.9931 \end{bmatrix}.$$

The five row vectors of matrix M_{LHS} represent five new generated sampling points. Finally, each element X_i^{LHS} of row vector is rescaled to fit boundaries given in Table. 6.2 by using the following formula:

$$X_i = X_i^{LHS}(X_i^U - X_i^L) + X_i^L, \ (i = 1, 2, 3, 4), \tag{6.29}$$

where X_i is one of the four to-be-estimated parameters; X_i^U and X_i^L are its upper and lower boundary, respectively. The five starts points (SPs) are

$$\begin{bmatrix} \mu_f & \theta_f & T_D & LL \end{bmatrix};$$

$$SP_1 = \begin{bmatrix} 0.0538 & 1.6969 & 0.0132 & 0.2353 \end{bmatrix};$$

$$SP_2 = \begin{bmatrix} 0.0386 & 0.9027 & 0.0039 & 0.0610 \end{bmatrix};$$

$$SP_3 = \begin{bmatrix} 0.0860 & 0.6431 & 0.0189 & 0.7366 \end{bmatrix};$$

$$SP_4 = \begin{bmatrix} 0.1626 & 1.3378 & 0.0078 & 0.4100 \end{bmatrix};$$

$$SP_5 = \begin{bmatrix} 0.1329 & 0.3315 & 0.0116 & 0.9931 \end{bmatrix}.$$

The five generated points are close to evenly spaced inside their boundaries. After evaluated these points, the point with the minimum cost function value is selected as start point of the PSA. The large number of start points in LHS method reduces the risk of being trapped into local minima. However, it leads to longer running time to evaluate these generated points.

In this parameter estimation, the total sampling points SP is 60. Within these 60 points, the point with the minimal function value is selected as the starting point of PSA. Figs. 6.10(a)-(d) and (e) show the trajectories of estimated parameters and cost function value, respectively. After the evaluation the 60 points generated by the LHS method, the point of $[\mu_f = 0.2045; \theta_f = 0.1873; LL = 0.4086; T_s = 0.0197]$ is selected as the starting point of the PSA. The finally estimated parameter is $[\mu_f = 0.1046; \theta_f = 0.9569; LL = 0.4966; T_s = 0.0020]$, which is close to the experiment setup of 10% stator circuit fault in *Phase b* with 50% motor load level. The total 980 points are evaluated with the minimal value of the cost function $F_{SR} = 66.5986$. Since points in the

sampling points matrix are randomly generated by LHS method, the selected starting point might be close to local minima in a very rare occasion. Therefore, there is still a risk of the PSA being trapped into local minima. The risk can be reduced by increasing the number of sampling points SP. In a continuing induction motor monitoring system, the previous parameter estimation result can be used as a starting point for the next search. In this case, PAS can be directly applied in this system to shorten the parameter estimation time.

GA was employed to estimate these parameters from the same recorded data. The stopping criterion of $Fun\ Tol = 10^{-5}$ is same as that of PSA. The estimated parameters of $[\mu_f = 0.1032; \theta_f = 0.9798; LL = 0.5042; T_s = 0.0002]$ correctly indicate the motor state. The minimal value of the cost function is 52.4335, which is smaller than that of PSA. The total number of evaluated points is 1028. The more accurate result is obtained at the cost of slight increase in the number of evaluated points. Although the GA requires more computational time compared to the PSA, it guarantees robustness in parameter estimation.

The comparison was conducted under different combination of load levels and fault levels. Fig. 6.12 shows the comparison between experiment setup with parameter estimated results by using PSA and GA. In all parameter estimations, the fault location is successfully detected in *Phase b* and is not shown in the figure. The parameter T_s is not plotted since it is only utilised to calibrate the time offset. In Fig. 6.12, the red crosses represent the experiment setup. The estimated results of parameters μ_f and θ_f

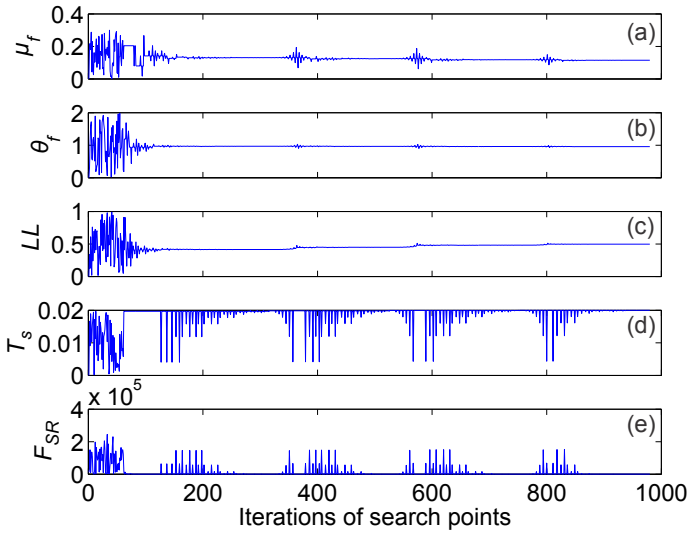

Figure 6.10. Trajectories of estimated parameters and cost function value using the PSA with the aid of LHS to generate a starting point.

by using PSA and GA are indicated with black diamonds and blue dots, respectively. The estimated parameters μ_f and θ_f have clearly indicated the motor state. In most cases, the estimated results from GA is closer to the experiment setup than these from PSA. In average, the GA evaluates about 30 points more than that of PSA.

6.5.2 Parameter estimation using HCPA

In this study, we set HPCA parameters of the fineness parameter $k = 7$, adaptive parameter $\alpha = 0.4$ and maximum number of global search samples $G_s = 500$. In this case, the algorithm conducts global search with $\alpha = 0.4$ until it reaches the criteria of maximum global search samples $G_s = 500$ or $k = 7$. In order to further improve accuracy, the algorithm switches to local search by assigning parameter $\alpha = 0$ if $G_s = 500$ is satisfied and the fineness parameter $k = 7$ is not. The algorithm stops when the fineness parameter k reaches 7 or the number of local search samples L_s exceeds 200.

The estimated results from HCPA indicate that 10.21% stator winding circuit fault occurs in Phase b and the motor is under 5.07% loading, which is close to the experiment setup. The recorded and simulated currents are plotted in Fig 6.13. The simulated currents are in good agreement with the measured currents in both transient and steady state. The measured and simulated steady state currents from 0.5 to 10 s are transferred from time to frequency domain by using fast Fourier transform (FFT) with the sampling frequency of 10 kHz, as shown in Fig. 6.14. The short circuit in the stator winding introduces a negative-sequence current. The interaction between the inducted

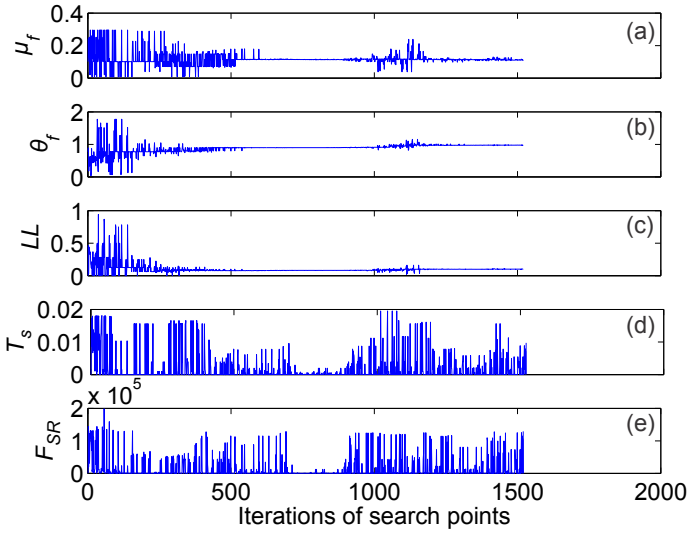

Figure 6.11. Trajectories of estimated parameters and cost function value using the GA.

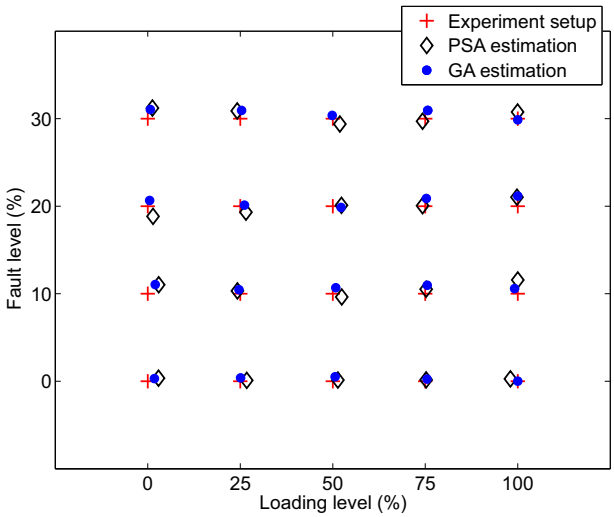

Figure 6.12. Comparison between experiment setup with parameter estimated results by using PSA and GA.

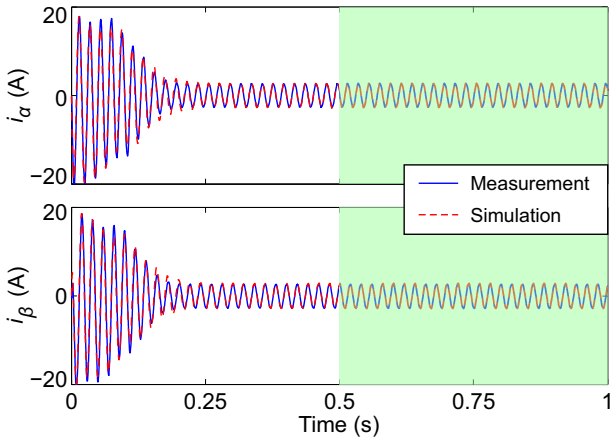

Figure 6.13. Comparison between measured current and simulated stator current in $\alpha\beta$ coordinates. The stator current signals recorded from the 5% loading of the induction motor with 10% stator winding short circuit fault occurs in Phase b. The parameter estimation is conducted based on the current in the shadow area (from 0.5 to 1 s).

rotor current and this negative-sequence current generates a pulsating torque at double mains frequency [74]. This pulsating torque results in a speed ripple and consequently produces a ripple in the main flux. Hence, a frequency component is observed in the spectra at 150 Hz ($3f$). This frequency component at $3f$ is one of the features of the stator winding short fault. However, other abnormal machine conditions, such as unbalanced voltage supplies or static eccentricity conditions could also generate this frequency component. In addition, the frequency component is difficult to be detected under the noisy environment. It is inaccurate to detect the stator winding short circuit fault only based on this frequency component, as it might raise a false alarm.

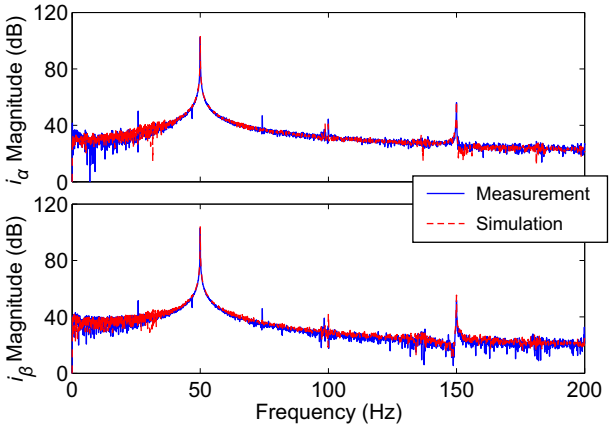

Figure 6.14. Comparison between measured current and simulated stator current spectrum in $\alpha\beta$ coordinate reference frame. The stator current signals recorded from the 5% loading of the induction motor with 10% stator winding short circuit fault that occurs in Phase b.

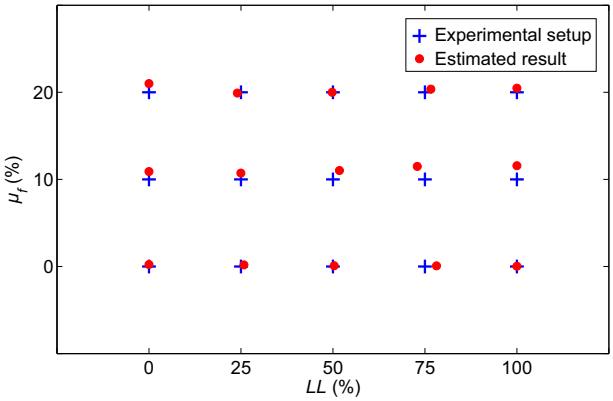

Figure 6.15. Comparison between experimental setups and estimated results under different LL and μ_f.

Fig. 6.15 presents the estimation results of the different experimental setups. The figure only shows load level (LL) and fault level (μ_f) since the fault location has been successfully located in the Phase b. In the figure, the cross and dot stand for the experiment setups and the estimated results, respectively. It has been observed that all the estimated results are close to the corresponding experiment setups.

6.6 Conclusion

This chapter presented an induction motor model based stator winding short circuit fault monitor method. The fault can be detected by monitoring the characteristic fault

parameters estimated from stator voltage and current. The proposed method is a non-intrusive scheme and only requires voltage and current signals recorded at a machine terminal without any invasive or additional hardware circuitry.

Three optimisation algorithms, PSA, GA and HCPA, are employed to estimate the fault related characteristic parameters in the proposed scheme. The experimental results reveal that the accuracy of direct search method, PSA, highly depends on the algorithm initial point in the parameter space. The risk of being trapped into local minima can be significantly reduced by introducing the LHS method. The PSA is suitable for continuing monitoring system where the new search starts from the previous result. The global optimisation method, GA, is not sensitive to initial search point and achieves accurate estimation results by guaranteed detection of global minima with a slightly increased computation time. The HCPA is robust to unbalanced voltage supply and load level change. The HCPA is comparable to the GA based technique and it shows improved robustness in the case of unbalanced voltage supply.

The effectiveness of the proposed method has been demonstrated through experimental tests under various fault and load levels. The estimated results have a good agreement with the experiment setup. Although the proposed approach is introduced for the diagnosis of stator faults in this thesis, it is feasible to extend its use for the other faults and other machine types with different characteristics in practical environments.

Chapter 7

Automated Multi-motor Condition Monitoring Based on IEC 61850

THIS chapter demonstrates a novel multi-motor condition monitoring scheme which can substantially reduce implementation cost for some industrial plants. The proposed multi-motor condition monitoring scheme builds on top of the technology implemented in modern intelligent electronic devices (IEDs) for motor protection and control. The backbone of this scheme is broadly accepted Ethernet technology and the IEC 61850 communication standard. Due to the widespread use of IEC 61850 in various industries, cost of the technology is significantly reduced while reliability has been improved.

7.1 Introduction

Monitoring of a motor condition has been used in practice to ensure reliable operation within specified thermal and mechanical limits. Application of condition monitoring technology is especially important for large motors as well as critical motors, which failure can produce major process disruptions. The benefits in implementing condition monitoring technology are: motor failure rate will be minimised, serious damage to motor itself and associated equipment will be prevented and production targets will be maximised. In many instances, downtime in industry plants could be more expensive than the cost of motor replacement. Cost of implementing condition monitoring should be balanced with cost of possible downtimes in production in order to justify purchase of such system.

In this chapter, we describe a novel multi-motor condition monitoring scheme which can substantially reduce implementation cost for some industrial plants. The backbone of this scheme is the broadly accepted Ethernet technology and the IEC 61850 communication standard [200]. Originally the IEC 61850 standard was developed for electricity transmission and distribution substation automation. In recent years, it was adapted for wind power plants [201], hydropower plants [202], distributed energy resources (DERs) [203] as well as in motor protection and control [204]. The proposed multi-motor condition monitoring scheme builds on top of the technology implemented in modern intelligent electronic devices (IEDs) for motor protection and control [204]. Typically, such IEDs are used in modern multi-motor industrial plants. In such systems, the protection functions are implemented locally in each IED associated with a single machine. The IEDs are connected to motor control centre (MCC) by using a local area network (LAN). The communication protocols of the IEC 61850 are used in the centralised motor control and motor operation monitoring functions as implemented in the MCC. The chapter proposes an additional centralised condition monitoring function that can be employed in the MCC. This function will utilise the existing IEDs and LAN infrastructure. In this way, additional cost for condition monitoring equipment is minimised.

The chapter is organised as follows. An overview of the IEC 61850 standard and topology of Ethernet communication network used in industrial plants has been presented in Section 7.2. Section 7.3 presents and discusses the proposed multi-motor condition monitoring scheme by using a specific IED (SEL 710 [204]) and describes an overall system architecture that incorporates protection, control and condition monitoring

functions. Based on the proposed system architecture, the applications used in this condition monitoring system are further discussed in Section 7.4.

7.2 Overview of the IEC 61850 standard

The IEC 61850 standard has spawned in a new generation of microprocessor-based IEDs for motor protection and control [204]. The devices built according to the IEC 61850 standard are able to exchange information with other devices using a standard Ethernet network [205, 206]. The Ethernet technologies not only can transport data in local area but also support long haul communication, thereby providing remote monitoring of status, control and data acquisition. The key features of IEC 61850 include virtualized plant model, reporting schemes, high-level communication services and standardized configuration language. These features enable designers to implement all applications (e.g. operation monitoring, control, energy management, condition monitoring, etc.) required in a multi-machine industrial plant using the same standardised hardware infrastructure. This will ultimately result in reduced cost, reduced construction and commissioning time as well as improved reliability. The IEC 61850 standard consists of 10 major sections related to general requirements, system and project management, communications requirements and configuration, and conformance testing [200, 207], as shown in Fig. 7.1. Parts 3, 4 and 5 of the IEC 61850 standard state the functional requirements for communication. An XML based configuration language, called the substation configuration language (SCL), is defined in Part 6. The SCL is used for individual device configuration as well as for retrieval and duplication of device configuration over the network when configuring a system with a large number of IEC 61850 compatible devices. It can significantly reduce the time and cost of initial system configuration. In Part 7, the concept of virtualization is described. Using this concept, a real device (i.e. IED) can be regarded as a composite of several virtual entities, named logical nodes. Each logical node contains a pre-defined set of data classes. A logical node is a virtual representation of a real functionality. Several logical nodes (might be from different IEDs) build up a logical device which is also a virtual entity. The IEC 61850 protocols facilitate communication between the logical nodes. The communication and information modelling are independent of operation and storage system, programming language and vendor. Thus, it offers enormous benefits in information exchange. The sketch in Fig. 7.2 illustrates the relationship between a physical device (i.e. IED), logical devices and logical nodes.

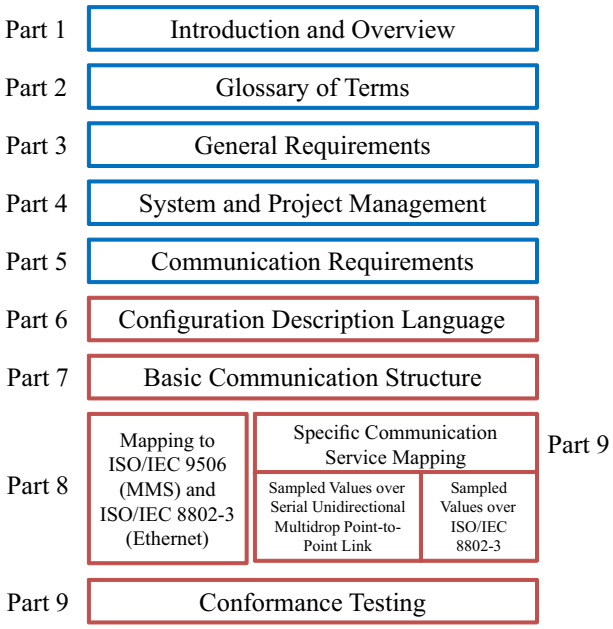

Figure 7.1. The structure of the IEC 61850 standard.

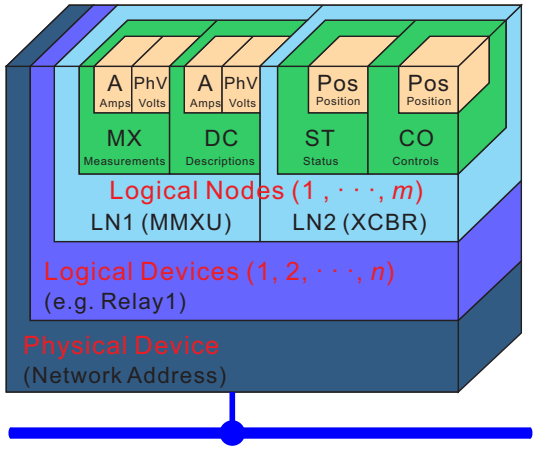

Figure 7.2. Physical device, logical devices and logical node.

Through the specific communication service mappings (SCSMs), defined in Parts 8 and 9, the data objects and services are mapped onto the ISO/IEC 9506 manufacturing messaging specification (MMS) and Ethernet data frames [200, 207]. The MMS is an international standard developed in 1980s for exchanging real-time data and control information in industrial networks. The MMS is independent of vendor and the application function being performed. The MMS uses the well-known client/server concept, which allows the implementation of the various services of the abstract communication service interface (ACSI) models defined in the IEC 61850 standard. For example, the MMS read and write services allow an application or device to read or write a variable from another application or device. The control model of IEC 61850

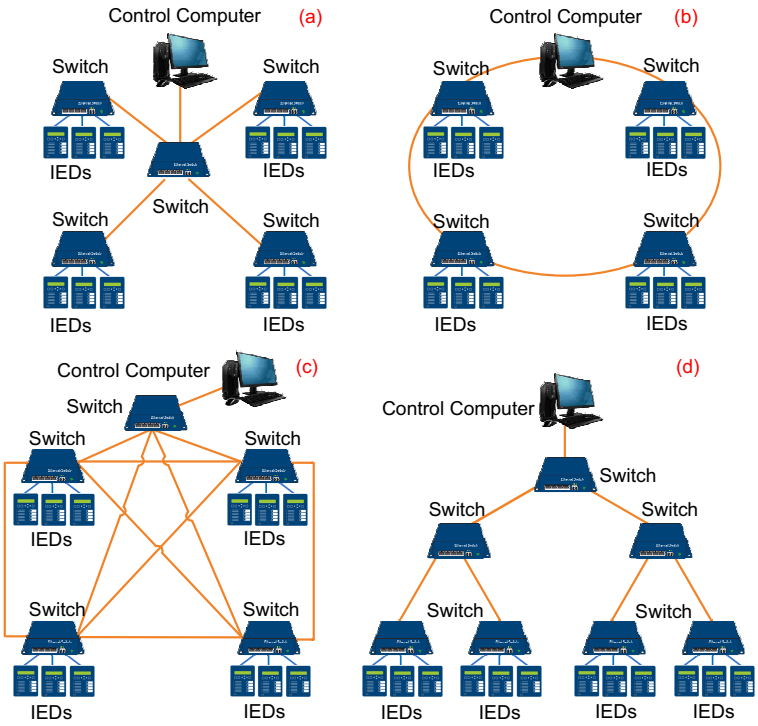

Figure 7.3. The typical Ethernet topologies. Star (a); Ring (b); Mesh (c) and Tree (d).

ACSI can be mapped to MMS read and write services. Furthermore, the various object models (e.g. service, logical device and logical node) of IEC 61850 can be mapped to specific MMS objects (e.g. vertical manufacturing device, domain and variable).

Fig. 7.3 shows typical Ethernet topologies applied in industrial networks that are comprised of the MCC (i.e. the control computers in Fig. 7.3), several IEDs and Ethernet switches [208]. The star topology (Fig. 7.3a) is the simplest architecture in the switch-based Ethernet system. The failure of any star network cable will only take down one part of network access and not the entire LAN. In a ring network (Fig. 7.3b), switch has exactly two neighbours and messages travel through a ring in the same direction. In a full mesh topology (Fig. 7.3c), switch is connected directly to the other devices. This approach offers more redundant communication channels and higher reliability but at the higher cost. The tree topology (Fig. 7.3d), which integrates multiple star topologies, is the most popular architecture in network domain management.

7.3 System architecture and implementation details

Most of commercial IEDs for motor protection and control, such as ABB REM615, SIEMENS 7SK80 and SEL 710, feature genuine support for the IEC 61850 standard and

Ethernet. The SEL 710 [204] is selected to demonstrate multi-motor condition monitoring scheme. In addition, we are using AX-S4 MMS from SISCO [209] to interface between our condition monitoring application and virtual devices in SEL 710. The AX-S4 MMS acts as an OLE (i.e. object linking and embedding) for process control (OPC) and dynamic data exchange (DDE) server, while Microsoft Windows software application packages that support OPC and/or DDE act as client. Through AX-S4 MMS, these application packages can access real-time data in networked IEDs and applications by using MMS-based Ethernet network. In Chapter 6, the condition monitoring application is developed in MATLAB and described [37, 38, 210]. The connection between our MATLAB program and the OPC server (AX-S4 MMS) is achieved via the MATLAB OPC Toolbox. Using the OPC Toolbox, our application is able to directly exchange data with the OPC server. In this way the application communicates with all virtual devices available in SEL 710.

The major parts of the condition monitoring applications are the following modules which were tested using induction motors available in our university laboratory: the broken rotor bar (BRB) detection module [20] and the diagnostic of stator faults module [37, 38]. These modules implement two types of diagnostic techniques: analysis of frequency spectrum and robust model parameter estimation based on the global optimisation using sparse grid search [38].

The condition monitoring application is designed to utilise the sequence of events recording (SER) function available at SEL 710 [204]. For each time, when an event recording is triggered, a report is created that includes the following information [204]: date and time of the event, analog inputs (currents and voltages at motor terminals) sampled at 10 kHz, digital states of selected relay word bits, event summary, and summary of IED settings. In addition, some data (measured quantities and relay word bits) associated with the logical nodes of SEL 710 (listed in appendix E of [204]) are incorporated in the application via the AX-S4 MMS and the OPC Toolbox. By using MMS, the application is able to remotely set-up the SER triggering mechanism. The SEL 710 triggers recording when either relay word bit trip asserts or when programmable logic control equation setting event report (ER) asserts [204]. The ER is set to trigger event reports for conditions other than trip conditions. These mechanisms allow for application of local and remote (via MMS) triggering. For example, when a local protection function asserts trip, the SER (including also pre-event signals) is generated and automatically transferred to the condition monitoring application. We can directly trigger

recording from the application or configure local condition-based triggers; e.g. start recording during motor start or when loading reaches a certain level. In addition, the application has access to a number of SEL 710 monitoring functions such as load profiling, motor operating statistics and motor start report.

The architecture of the infrastructure used by the multi-motor condition monitoring application is illustrated by an enterprise with the MCC and two factory plants, as shown in Fig. 7.4. The Ethernet and IEC 61850 provide interface of local IEDs for motor protection and control and the MCC. Human machine interface (HMI) is possible to implement at the factory level as well as at the MCC. In order to connect two factory plants and the MCC, switches are connected to routers, which route IP packets through WAN. In Fig. 7.4, the topologies only show star and tree architectures as examples. More switches can be added, depending on the system requirement, to improve the system redundancy. By using the AX-S4 MMS in the MCC, we can browse the logical nodes of all IEDs implemented in two factory plants and remotely control and monitor all motors. Using this technology, we are able to further add new multi-motor condition monitoring functionality. Other applications can be developed as well, e.g. reporting and scheduling. Furthermore, the remote support from vendors or integrators can be achieved through the Internet based-technologies, via VPN and remote login. In addition, smart phone offers the benefits of not only receiving the system status and alarms but also accessing to the control system and condition monitoring reports.

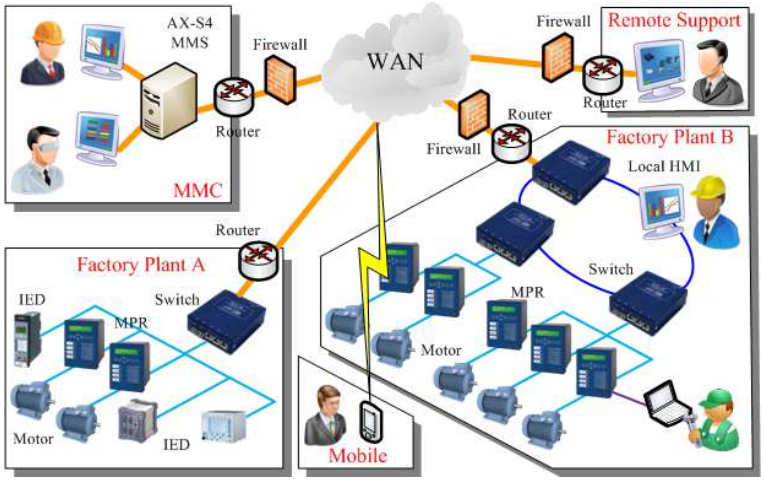

Figure 7.4. The architecture of the modern infrastructure for management of motors in two factory plants.

7.4 Application architecture

The AX-S4 MMS is utilised to illustrate the application architecture, as shown in Fig. 7.5. The IEDs stream the messages over Ethernet communications channel. These messages are received and filtered through the OPC server of AX-S4 MMS. IEC 61850 server converts the data packets to OPC format. The AX-S4 MMS offers three main input/output (I/O) interfaces.

1. The AX-S4 MMS connects with OPC server from other protocols through OPC item to IEC 61850 object mapping.
2. The DDE is allowed via OPC-DDE server I/O.
3. The substation supervisory control and data acquisition (SCADA) and HMI are connected through OPC server I/O.

The generic object oriented substation events (GOOSE) of IEC 61850 groups any format of data (status, value) into a data set. This enables high-speed integration with applications (a time period of 4 millisecond). This data base function is the core component of this system with the capability of handling real-time and historical data in high speed.

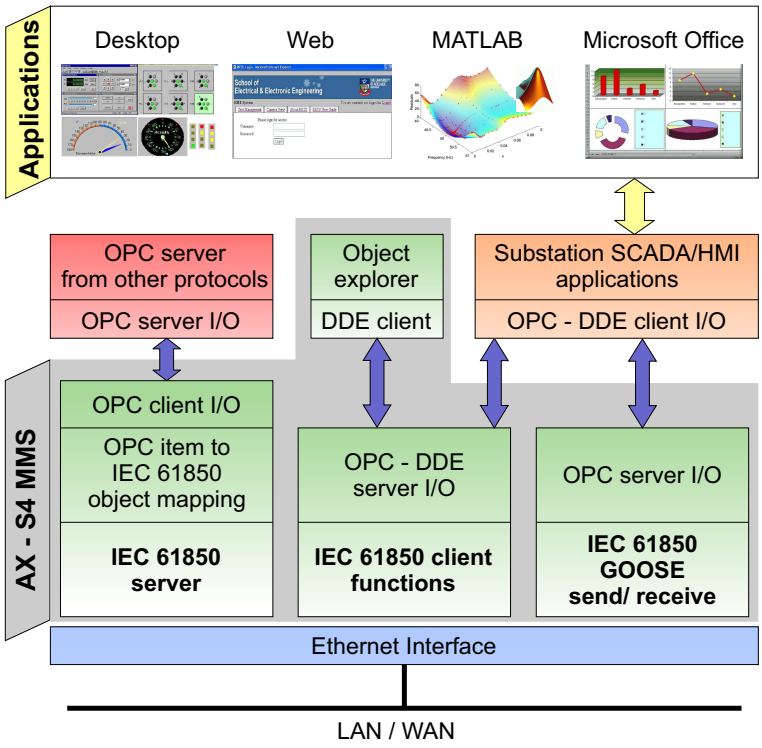

Figure 7.5. Application architecture.

The HMI solution normally consists of four applications: desktop application, web application, MATLAB application, and Microsoft Office application, as shown on the top of Fig. 7.5.

The desktop application provides remote visualization, setup and control of IEDs through a graphical user interface. Both real-time and history data are available for operators to evaluate the system performance. Data objects can be displayed in multiple formats, such a digital gauge, analog gauge, chart, or indicators.

Based on desktop application, web application can be integrated with relatively low cost. The web application offers more flexibility in term of operators' location. An operator can access database by logging in through an ordinary web portal. There is no need for additional software installation and configuration. For example, the remote relay testing system (RRTS), developed by the University of Adelaide, has the capacity to remotely set, test and monitor multi-functional digital relays [211]. Furthermore, the web application offers an integrated suite of server capabilities for central control and information sharing across an enterprise.

The MATLAB OPC toolbox provides a direct and high speed connection to the AX-S4 MMS OPC server through the interface of the OPC server I/O [212]. The node information is directly migrated from the OPC server to the MATLAB programming environment. The node information consists of induction motor model information, location, IED information (e.g. IP), and motor performance information (e.g. voltage, current, torque, speed, and temperature). This information can be utilised to diagnose induction motor faults. Based on the voltage and current signals, the faults can be detected by using the approach proposed in Chapter 6. Hence, the motor condition monitoring is achieved in the MCC.

The Microsoft Office application enables users to generate reports based on the real-time and history data. The various presentation methods provide the advantage of functioning as a visual aid to help technician, engineer and management personnel examine and interpret the data.

7.5 Conclusion

In this chapter, a practical and effective multi-motor condition monitoring scheme is proposed. The scheme is based on the modern motor protection and control IEDs

supporting the IEC 61850 standard and Ethernet. The real-time data and control information can be transferred to local and remote motor control centres by using the MMS standard. The proposed architecture of the infrastructure is illustrated by an example of an enterprise with two factory plants at different locations. In the example, IEDs (SEL 710) are employed to implement condition monitoring. The motor condition monitoring information is transferred to the condition monitoring application in the motor control centre by using AX-S4 MMS and MATLAB OPC Toolbox. By using the proposed system, motors in the multimachine plants can be remotely monitored and controlled.

Chapter 8

Conclusion and future work

THIS chapter concludes the thesis by firstly reviewing and summarising the results and findings of each chapter. The sparse grid global optimisation algorithm has been proposed to improve two applications: motor parameter estimation and condition motoring. In addition, the condition motoring application is extended from single motor to multi-motor setting. This chapter also proposes possible future research topics in this field.

8.1 Conclusion

In light of the important roles of induction motors in the industry, numerous research efforts have been devoted to ensure the efficient control, uninterrupted service and low maintenance cost. The research work presented in this thesis includes three major parts: The first and second parts of the thesis respectively conduct motor parameters estimation and condition motoring & faults diagnosis by using global optimisation algorithms, while the third part of the thesis extends single motor to multi-motor condition motoring & faults diagnosis. The aims are to provide a generic, non-invasive, low cost and reliable method for motor parameters estimation and condition motoring & faults diagnosis.

It is noted that a deep and thoughtful understanding of induction motor is generally required to create a novel solution. Thus, Chapter 2 starts with a review of induction motor working principle and structure. The basic structure of induction motor is hardly changed over the years, while the rapidly developed power electronics facilitates the precise control of motors and allows for the variable-speed operation. The modern motor control techniques are highly dependent on the accurate motor parameters, such as stator/rotor resistance, stator/rotor leakage inductance, transient stator inductance and rated magnetising inductance. The motor parameters estimation is selected as one of the research aspects in this thesis and the major methods for parameters estimation are discussed in the first part of this chapter. On the other hand, the requirements for reliable and uninterrupted service in the industry put high demand on the motor condition monitoring and fault diagnosis. The four types induction motor faults and their diagnosis methods are discussed in the second part of that chapter.

Based on the review in Chapter 2, a motor parameters estimation and condition motoring & faults diagnosis approach is proposed by using global optimisation algorithm. In the proposed approach, a global optimisation algorithm finds the most suitable parameter for the induction motor mathematical model to match the simulation and measurement results. A cost function is utilised to quantify the difference between the simulation and measurement results. Therefore, the foundation of this research lies on two major aspects, a practical and reliable mathematical model with a limited complexity and a high efficient global optimisation algorithm to converge to a global minimum. These major aspects are addressed in Chapters 3 and 4, respectively.

Chapter 3 presents a dynamic mathematical model of three phase induction motor. The model is realised in MATLAB/SIMULINK and experimentally validated by using

voltage, current and rotor speed signals recorded from an induction motor. The results indicate that the model can present both transient and steady state machine response under various load levels.

Chapter 4 describes a global optimisation algorithm based on sparse grid. The sparse grid is able to reduce the complexity for a discretization, while maintaining a comparable discretization error. Furthermore, the utilised Hyperbolic Cross Point Algorithm (HCPA) can conduct effective search on Hyperbolic Cross Points (HCPs) by adjusting its parameters that will concentrate points in the regions where solution lays. The algorithm is implemented in MATLAB program environment for the convenience of data exchange between the algorithm and SIMULINK induction model.

The algorithm MATLAB program was evaluated using nine well known optimisation test functions, whose dimensions are in the range between 2 and 10. The numerical validations show that the HCPA can find global minimum for most of the test functions. Compared with other algorithms in literature, the results of HCPA are reasonable close to the global minimum with less function evaluations for some difficult test functions, which have several local minima closely located in small region. With the aid of the fuzzy c-means clustering algorithm and local search algorithm, the HCPA can detect functions with multiple identical global minima.

In Chapter 5, the global optimisation algorithm, HCPA, is utilised to estimate motor parameters. The global optimisation algorithm is selected by considering non-linearity of motor model and cost function. In this case, the local optimisation algorithms might converge to local minima or even diverge when initial values of the parameters are far away from their real values. Although the global optimisation algorithm requires longer computational time, it guarantees the convergence of global minimum. Furthermore, the sparse grid based algorithm is able to tackle high dimensional parameters estimation tasks in a computationally effective way. In this parameters estimation task, there is total of seven parameters, including five physical parameters, loading level and a calibration parameter. As a general sparse grid parameter estimation technique, it can be applied to other machine types by using the corresponding machine models.

The proposed method only uses voltage and current signals without any invasive or additional hardware circuitry. Thus, it has the advantages of simplicity, low cost and reliability. The presented experimental validation shows that the relative errors of the estimated parameter values are less than 10% under various load levels. The relative

errors can be further reduced to less than 5% after applying the Nelder-Mead local search method with the global search result as a start point.

In Chapter 6, the symmetrical motor model is adapted to identify motor faults by including faults related characteristic parameters. Consequently, the appearance of faults will cause the drift of characteristic parameters, which offers a method to detect motor fault by monitoring these parameters. As an example, the sparse grid based global optimisation algorithm, HCPA, is utilise to estimated the characteristic parameters related to stator short circuit fault. In the proposed non-intrusive method, the fault is detected by monitoring two characteristic parameters estimated (fault level and fault location) from stator voltages and currents in the time domain. Thus, it only needs a short length of voltage and current signals recorded at switch board without disrupting the machine's normal operation.

The advantages of the HCPA has been highlighted through the comparison with a direct search method, pattern search algorithm (PSA) and an artificial intelligence (AI)-based global optimisation algorithm, genetic algorithm (GA). PSA might be trapped into a local minimum since it depends on the start point. Latin hypercube sampling (LHS) method can be additionally employed to generate a start point, which reduces the risk of being trapped into local minima. AI-based global optimisation algorithms do not have any rigorous mathematical description and hence it is difficult to apply constraints to concentrate the regions where solution lays. On the contrary, the efficiency of HCPA is improved by applying constraint to search only preprocessed fault location. The laboratory experiments show that both GA and HCPA are not sensitive to initial search point and achieve accurate estimation results. The HCPA is comparable to the GA based technique and it shows improved robustness in the case of unbalanced voltage supply.

Chapter 7 extends the single motor condition monitoring to multimotor condition monitoring scheme. The widely used intelligent electronic devices (IEDs), Ethernet technology and IEC 61850 communication standard make this scheme easily applicable for large companies with several plants at different geographic locations. The overall system cost is minimised by utilising the existing IEDs and LAN/WAN infrastructure.

In the two factory plants example, the IEDs, SEL-710 motor protection relay from Schweitzer Engineering Laboratories, are employed to implement multimotor condition monitoring. The AX-S4 MMS from SISCO acts as an object linking and embedding

(OLE) for process control (OPC) and dynamic data exchange (DDE) server to interface condition monitoring application with virtual devices in SEL-710. The connection between the motor condition monitoring MATLAB/SIMULINK applications in Chapter 6 and the OPC server is achieved via the MATLAB OPC Toolbox. Using the OPC Toolbox, our applications are able to exchange data with all virtual devices available in SEL 710 to achieve remotely condition monitoring and control. Apart from the MATLAB applications, desktop, web and Microsoft office applications can be developed to provide the advantage of functioning as a visual aid in helping technician, engineer and management personnel examine and interpret the data.

8.2 Future work

This thesis proposed a generic approach of applying sparse grid based global optimisation algorithm to parameters estimation. Although the proposed approach is only applied for three phase induction motor in this study, it is feasible to extend its use for other electric machine types, e.g. DC motor, synchronous motor, generators, in practical environments. Some of the possible research directions are the following.

- **Real-time motor parameters estimation**: The research has only focused on the offline parameter estimation for commissioning test. The computation efficiency of the proposed method has to be improved and the method can be considered for online applications. Since motor simulation consumes about 90% of total computation time, the computation efficiency of the method can be significantly improved by simplifying mathematical model and by implementing the algorithm on a specialized embedded controller platform. Apart from the computation efficiency improvement, it is essential to examine the compatibility of the proposed approach with the most popular advanced controllers, i.e. feeding those controllers with the parameters found by the proposed method. More efforts are necessary to address this task as well as experimental validation.

- **Real-time Motor condition monitoring and fault diagnosis**: In this thesis, the stator winding short circuit fault is employed to demonstrate that motor faults can be detected by estimating the corresponding characteristic parameters of the motor model using global optimisation method. The proposed technique can be used to detect other faults after the corresponding faults characteristic parameters are added into the current motor model. For example, the broken rotor bar

fault can be detected by estimating characteristic parameters, number of broken bars and location. The approach is able to detect multi-faults and combined faults as long as faults can be described by characteristic parameters. To this end, additional fault classification method might be necessary to detect a condition with the combined faults. In particular, fault classification is still one of the challenge fields in motor fault diagnosis.

- **Multi-Devices condition monitoring**: The work in this thesis has demonstrated an example of multimotor condition monitoring scheme based on IEDs and IEC 61850. This represents a first step towards remote condition monitor and control, not only for electric motor but also for other IEDs connected machines. The research opens a number of directions that could provide the next steps along the path to further low-cost industry remote control and monitor. Various applications can be developed to improve the capabilities for central monitoring, control, information sharing and management across technicians, engineers and managers in the enterprise.

Bibliography

[1] C. I. Hubert, *Electric machines: theory, operation, applications, adjustment and control*. Merrill, 1991, ch. 2.

[2] P. C. Krause, O. Wasynczuk, and S. D. Sudhoff, *Analysis of Electric Machinery*. New York: IEEE Press, 1996.

[3] P. Vas, *Parameter Estimation, Condition Monitoring, and Diagnosis of Electrical Machines*. Clarendron Press Oxfords, 1993, ch. 3.

[4] W. Thomson, "A review of on-line condition monitoring techniques for three phase squirrel cage induction motors-past, present and future," in *SDEMPED'99, Gijon, Spain*, vol. 33, no. 1, Sep. 1999, pp. 3–18.

[5] H. Su and K.-T. Chong, "Induction machine condition monitoring using neural network modeling," *IEEE Trans. Ind. Electron.*, vol. 54, no. 1, pp. 241–249, 2007.

[6] P. Tavner, L. Ran, J. Penman, and H. Sedding, *Condition Monitoring of Rotating Electrical Machines*. IET, 2008.

[7] S. Nandi, S. Ahmed, H. Toliyat, and R. Mohan Bharadwaj, "Selection criteria of induction machines for speed-sensorless drive applications," *IEEE Trans. Ind. Appl.*, vol. 39, no. 3, pp. 704–712, May 2003.

[8] A. Nabae, K. Otsuka, H. Uchino, and R. Kurosawa, "An approach to flux control of induction motors operated with variable-frequency power supply," *IEEE Trans. Ind. Appl.*, vol. IA-16, no. 3, pp. 342–350, 1980.

[9] I. Takahashi and T. Noguchi, "A new quick-response and high-efficiency control strategy of an induction motor," *IEEE Trans. Ind. Appl.*, vol. IA-22, no. 5, pp. 820–827, 1986.

[10] H. Toliyat, E. Levi, and M. Raina, "A review of RFO induction motor parameter estimation techniques," *IEEE Trans. Energy Convers.*, vol. 18, no. 2, pp. 271–283, June 2003.

[11] E. Laroche, E. Sedda, and C. Durieu, "Methodological insights for online estimation of induction motor parameters," *IEEE Trans. Control Syst. Technol.*, vol. 16, no. 5, pp. 1021–1028, 2008.

[12] S. Nandi, H. A. Toliyat, and X. Li, "Condition monitoring and fault diagnosis of electrical motors - a review," *IEEE Trans. Energy Convers.*, vol. 20, no. 4, pp. 719–729, 2005.

[13] S. Wang, V. Dinavahi, and J. Xiao, "Multi-rate real-time model-based parameter estimation and state identification for induction motors," *IET Electr. Power Appl.*, vol. 7, no. 1, pp. 77–86, 2013.

[14] X. Chang, V. Cocquempot, and C. Christophe, "A model of asynchronous machines for stator fault detection and isolation," *IEEE Trans. Ind. Electron.*, vol. 50, no. 3, pp. 578–584, 2003.

[15] S. Bachir, S. Tnani, J. Trigeassou, and G. Champenois, "Diagnosis by parameter estimation of stator and rotor faults occurring in induction machines," *IEEE Trans. Ind. Electron.*, vol. 53, no. 3, pp. 963–973, 2006.

[16] J. Stephan, M. Bodson, and J. Chiasson, "Real-time estimation of the parameters and fluxes of induction motors," *IEEE Trans. Ind. Appl.*, vol. 30, no. 3, pp. 746–759, May 1994.

[17] B. Mirafzal, G. Skibinski, and R. Tallam, "Determination of parameters in the universal induction motor model," *IEEE Trans. Ind. Appl.*, vol. 45, no. 1, pp. 142–151, Jan 2009.

[18] C. De Angelo, G. Bossio, S. Giaccone, M. Valla, J. Solsona, and G. Garcia, "Online model-based stator-fault detection and identification in induction motors," *IEEE Trans. Ind. Electron.*, vol. 56, no. 11, pp. 4671–4680, 2009.

[19] F. Duan and R. Živanović, "Condition monitoring of an induction motor stator windings via global optimization based on the Hyperbolic Cross Points," *IEEE Trans. Ind. Electron.*, vol. PP, no. 99, pp. 1–9, 2014.

[20] S. Chen and R. Živanović, "Estimation of frequency components in stator current for the detection of broken rotor bars in induction machines," *Measurement*, vol. 43, no. 7, pp. 887–900, 2010.

[21] F. Duan and R. Živanović, "Induction motor fault diagnostics using global optimization algorithm," in *AUPEC09 - 19th Australasian Universities Power Engineering Conference*, Adelaide, Australia, Sep. 2009, pp. 1–4.

[22] F. Filippetti, M. Martelli, G. Franceschini, and C. Tassoni, "Development of expert system knowledge base to on-line diagnosis of rotor electrical faults of induction motors," in *IEEE Industry Applications Society Annual Meeting*, vol. 1, 1992, pp. 92–99.

[23] I. Lasurt, A. Stronach, and J. Penman, "A fuzzy logic approach to the interpretation of higher order spectra applied to fault diagnosis in electrical machines," in *19th International Conference of the North American, Fuzzy Information Processing Society (NAFIPS)*, 2000, pp. 158–162.

[24] M. Bouzid, G. Champenois, N. Bellaaj, L. Signac, and K. Jelassi, "An effective neural approach for the automatic location of stator interturn faults in induction motor," *IEEE Trans. Ind. Electron.*, vol. 55, no. 12, pp. 4277–4289, 2008.

[25] H. Razik, M. de Rossiter Correa, and E. da Silva, "A novel monitoring of load level and broken bar fault severity applied to squirrel-cage induction motors using a genetic algorithm," *IEEE Trans. Ind. Electron.*, vol. 56, no. 11, pp. 4615–4626, 2009.

[26] P. Pillay, R. Nolan, and T. Haque, "Application of genetic algorithms to motor parameter determination for transient torque calculations," *IEEE Trans. Ind. Appl.*, vol. 33, no. 5, pp. 1273–1282, Sep 1997.

[27] E. Bim, "Fuzzy optimization for rotor constant identification of an indirect FOC induction motor drive," *IEEE Trans. Ind. Electron.*, vol. 48, no. 6, pp. 1293–1295, Dec 2001.

[28] P. Vas, *Artificial-Intelligence-Based Electrical Machines and Drives*. Oxford Univ. Press, 1999.

[29] F. Filippetti, G. Franceschini, C. Tassoni, and P. Vas, "Recent developments of induction motor drives fault diagnosis using AI techniques," *IEEE Trans. Ind. Electron.*, vol. 47, no. 5, pp. 994–1004, 2000.

[30] T. Gerstner and M. Griebel, "Numerical integration using sparse grids," *Numerical Algorithms*, vol. 18, no. 3-4, pp. 209–232, 1998.

[31] M. Holtz, "Sparse grid quadrature," in *Sparse Grid Quadrature in High Dimensions with Applications in Finance and Insurance*, ser. Lecture Notes in Computational Science and Engineering. Springer Berlin Heidelberg, 2011, vol. 77, pp. 51–76.

[32] J. Garcke, M. Griebel, and M. Thess, "Data mining with sparse grids," *Computing*, vol. 67, no. 3, pp. 225–253, 2001.

[33] H.-J. Bungartz, A. Heinecke, D. Pflger, and S. Schraufstetter, "Option pricing with a direct adaptive sparse grid approach," *Journal of Computational and Applied Mathematics*, vol. 236, no. 15, pp. 3741 – 3750, 2012.

[34] R. Živanović, "Global sensitivity analysis of transmission line fault-locating algorithms using sparse grid regression," *Reliability Engineering & System Safety*, vol. 107, pp. 132 – 138, 2012.

[35] R. Živanović and P. M. Bokov, "Cross-section parameterization of the pebble bed modular reactor using the dimension-wise expansion model," *Annals of Nuclear Energy*, vol. 37, no. 12, pp. 1763 – 1773, 2010.

[36] E. Novak and K. Ritter, "Global optimization using Hyperbolic Cross Points," in *State of the Art in Global Optimization*, C. Floudas and P. Pardalos, Eds. Kluwer Academic Publishers, 1972, pp. 19–33.

[37] F. Duan and R. Živanović, "A model for induction motor with stator faults," in *22th Australasian Universities Power Engineering Conference*, Bali, Indonesia, Sep. 2012, pp. 1–4.

[38] ——, "Diagnosis of induction machine stator faults by parameter estimation techniques based on direct search on sparse grid," in *The 9th IET International Conference on Advances in Power System Control, Operation and Management*, Hong Kong, China, Nov. 2012, pp. 1–6.

[39] ——, "Induction motor stator faults diagnosis by using parameter estimation algorithms," in *9th IEEE International Symposium on Diagnostics for Electrical Machines, Power Electronics & Drives*, Valencia, Spain, Aug. 2013, pp. 1–5.

[40] ——, "Automated multi-motor condition monitoring based on IEC 61850," in *5th Annual International Energy Conversion Congress and Exhibition*, Melbourne, Australia, Jun. 2013, pp. 1–5.

[41] R. L. Iman, *Latin Hypercube Sampling*. John Wiley & Sons, Ltd, 2008.

[42] F. Giri, *AC Electric Motors Control: Advanced Design Techniques and Applications*. Wiley, 2013, ch. 2.

[43] "Ieee standard test procedure for polyphase induction motors and generators," *IEEE Std 112-1991*, 1991.

[44] A. Ukil, R. Bloch, and A. Andenna, "Estimation of induction motor operating power factor from measured current and manufacturer data," *IEEE Trans. Energy Convers.*, vol. 26, no. 2, pp. 699–706, June 2011.

[45] J. Pedra, "On the determination of induction motor parameters from manufacturer data for electromagnetic transient programs," *IEEE Trans. Power Syst.*, vol. 23, no. 4, pp. 1709–1718, Nov 2008.

[46] P. Kini and R. Bansal, "Effect of voltage and load variations on efficiencies of a motor-pump system," *IEEE Trans. Energy Convers.*, vol. 25, no. 2, pp. 287–292, June 2010.

[47] R. Kerkman, J. D. Thunes, T. Rowan, and D. Schlegel, "A frequency-based determination of transient inductance and rotor resistance for field commissioning purposes," *IEEE Trans. Ind. Appl.*, vol. 32, no. 3, pp. 577–584, May 1996.

[48] M. Bertoluzzo, G. Buja, and R. Menis, "Self-commissioning of RFO IM drives: one-test identification of the magnetization characteristic of the motor," *IEEE Trans. Ind. Appl.*, vol. 37, no. 6, pp. 1801–1806, Nov 2001.

[49] A. Proca and A. Keyhani, "Identification of variable frequency induction motor models from operating data," *IEEE Trans. Energy Convers.*, vol. 17, no. 1, pp. 24–31, Mar 2002.

[50] K. Akatsu and A. Kawamura, "Sensorless very low-speed and zero-speed estimations with online rotor resistance estimation of induction motor without signal injection," *IEEE Trans. Ind. Appl.*, vol. 36, no. 3, pp. 764–771, May 2000.

[51] J. Maes and J. Melkebeek, "Speed-sensorless direct torque control of induction motors using an adaptive flux observer," *IEEE Trans. Ind. Appl.*, vol. 36, no. 3, pp. 778–785, May 2000.

[52] J. Holtz and J. Quan, "Sensorless vector control of induction motors at very low speed using a nonlinear inverter model and parameter identification," *IEEE Trans. Ind. Appl.*, vol. 38, no. 4, pp. 1087–1095, 2002.

[53] A. Khambadkone and J. Holtz, "Vector-controlled induction motor drive with a self-commissioning scheme," *IEEE Trans. Ind. Electron.*, vol. 38, no. 5, pp. 322–327, Oct 1991.

[54] S.-I. Moon and A. Keyhani, "Estimation of induction machine parameters from standstill time-domain data," *IEEE Trans. Ind. Appl.*, vol. 30, no. 6, pp. 336–342, Nov 1994.

[55] C. Wang, D. Novotny, and T. Lipo, "An automated rotor time-constant measurement system for indirect field-oriented drives," *IEEE Trans. Ind. Appl.*, vol. 24, no. 1, pp. 151–159, Jan 1988.

[56] A. Boglietti, P. Ferraris, M. Lazzari, and F. Profumo, "Induction motor equivalent circuit parameters determination from standard tests made with inverter supply," in *Sixth International Conference on Electrical Machines and Drives*, Sep 1993, pp. 271–276.

[57] Y.-N. Lin and C.-L. Chen, "Automatic im parameter measurement under sensorless field-oriented control," *IEEE Trans. Ind. Electron.*, vol. 46, no. 1, pp. 111–118, Feb 1999.

[58] E. Levi, M. Sokola, and S. Vukosavic, "A method for magnetizing curve identification in rotor flux oriented induction machines," *IEEE Trans. Energy Convers.*, vol. 15, no. 2, pp. 157–162, Jun 2000.

[59] H. Toliyat and A. Hosseiny, "Parameter estimation algorithm using spectral analysis for vector controlled induction motor drives," in *IEEE International Symposium on Industrial Electronics*, 1993, pp. 90–95.

[60] R. Gabriel and W. Leonhard, "Microprocessor control of induction motor," in *Proc. Int. Semiconductor Power Conversion Conf.*, 1982, pp. 385–396.

[61] H. Sugimoto and S. Tamai, "Secondary resistance identification of an induction-motor applied model reference adaptive system and its characteristics," *IEEE Trans. Ind. Appl.*, vol. IA-23, no. 2, pp. 296–303, March 1987.

[62] P. Vas, *Sensorless Vector and Direct Torque Control*. Oxford Univ. Press, 1993.

[63] L.-C. Zai, C. Demarco, and T. Lipo, "An extended Kalman filter approach to rotor time constant measurement in PWM induction motor drives," *IEEE Trans. Ind. Appl.*, vol. 28, no. 1, pp. 96–104, Jan 1992.

[64] L. Salvatore, S. Stasi, and L. Tarchioni, "A new EKF-based algorithm for flux estimation in induction machines," *IEEE Trans. Ind. Electron.*, vol. 40, no. 5, pp. 496–504, 1993.

[65] M. Barut, S. Bogosyan, and M. Gokasan, "Experimental evaluation of braided EKF for sensorless control of induction motors," *IEEE Trans. Ind. Electron.*, vol. 55, no. 2, pp. 620–632, 2008.

[66] G. Yang and T.-H. Chin, "Adaptive-speed identification scheme for a vector-controlled speed sensorless inverter-induction motor drive," *IEEE Trans. Ind. Appl.*, vol. 29, no. 4, pp. 820–825, Jul 1993.

[67] K. Kubota, K. Matsuse, and T. Nakano, "Dsp-based speed adaptive flux observer of induction motor," *IEEE Trans. Ind. Appl.*, vol. 29, no. 2, pp. 344–348, Mar 1993.

[68] D. Marcetic and S. Vukosavic, "Speed-sensorless AC drives with the rotor time constant parameter update," *IEEE Trans. Ind. Electron.*, vol. 54, no. 5, pp. 2618–2625, 2007.

[69] V. Vasic, S. Vukosavic, and E. Levi, "A stator resistance estimation scheme for speed sensorless rotor flux oriented induction motor drives," *IEEE Trans. Energy Convers.*, vol. 18, no. 4, pp. 476–483, Dec 2003.

[70] P. Zhang, Y. Du, T. Habetler, and B. Lu, "A survey of condition monitoring and protection methods for medium-voltage induction motors," *IEEE Trans. Ind. Appl.*, vol. 47, no. 1, pp. 34–46, Jan 2011.

[71] A. H. Bonnett, "Analysis of winding failures in three-phase squirrel cage induction motors," *IEEE Trans. Ind. Appl.*, vol. IA-14, no. 3, pp. 223–226, May. 1978.

[72] S. Williamson and K. Mirzoian, "Analysis of cage induction motors with stator winding faults," *IEEE Trans. Power App. Syst.*, vol. PAS-104, no. 7, pp. 1838–1842, July 1985.

[73] G. Kliman, R. Koegl, J. Stein, R. Endicott, and M. Madden, "Noninvasive detection of broken rotor bars in operating induction motors," *IEEE Trans. Energy Convers.*, vol. 3, no. 4, pp. 873 –879, Dec. 1988.

[74] J. Hsu, "Monitoring of defects in induction motors through air-gap torque observation," *IEEE Trans. Ind. Appl.*, vol. 31, no. 5, pp. 1016–1021, 1995.

[75] M. El Hachemi Benbouzid, "A review of induction motors signature analysis as a medium for faults detection," *IEEE Trans. Ind. Electron.*, vol. 47, no. 5, pp. 984–993, 2000.

[76] A. Siddique, G. Yadava, and B. Singh, "A review of stator fault monitoring techniques of induction motors," *IEEE Trans. Energy Convers.*, vol. 20, no. 1, pp. 106–114, Mar. 2005.

[77] R. Tallam, S.-B. Lee, G. Stone, G. Kliman, J.-Y. Yoo, T. Habetler, and R. Harley, "A survey of methods for detection of stator-related faults in induction machines," *IEEE Trans. Ind. Appl.*, vol. 43, no. 4, pp. 920–933, July 2007.

[78] R. Schoen, T. Habetler, F. Kamran, and R. Bartfield, "Motor bearing damage detection using stator current monitoring," *IEEE Trans. Ind. Appl.*, vol. 31, no. 6, pp. 1274–1279, Nov 1995.

[79] J. Stack, R. Harley, and T. Habetler, "An amplitude modulation detector for fault diagnosis in rolling element bearings," *IEEE Trans. Ind. Electron.*, vol. 51, no. 5, pp. 1097–1102, Oct 2004.

[80] M. Blodt, P. Granjon, B. Raison, and G. Rostaing, "Models for bearing damage detection in induction motors using stator current monitoring," *IEEE Trans. Ind. Electron.*, vol. 55, no. 4, pp. 1813–1822, April 2008.

[81] G. Kliman and J. Stein, "Induction motor fault detection via passive current monitoring," in *Int. Conf. Electrical Machines, Cambridge, MA.*, Aug 1990, pp. 13–17.

[82] M. Ballal, Z. Khan, H. Suryawanshi, and R. Sonolikar, "Adaptive neural fuzzy inference system for the detection of inter-turn insulation and bearing wear faults in induction motor," *IEEE Trans. Ind. Electron.*, vol. 54, no. 1, pp. 250–258, Feb 2007.

[83] W. Zhou, B. Lu, T. Habetler, and R. Harley, "Incipient bearing fault detection via motor stator current noise cancellation using Wiener filter," *IEEE Trans. Ind. Appl.*, vol. 45, no. 4, pp. 1309–1317, July 2009.

[84] M. Prieto, G. Cirrincione, A. Espinosa, J. Ortega, and H. Henao, "Bearing fault detection by a novel condition-monitoring scheme based on statistical-time features and neural networks," *IEEE Trans. Ind. Electron.*, vol. 60, no. 8, pp. 3398–3407, Aug 2013.

[85] A. Bellini, F. Filippetti, C. Tassoni, and G. Capolino, "Advances in diagnostic techniques for induction machines," *IEEE Trans. Ind. Electron.*, vol. 55, no. 12, pp. 4109–4126, 2008.

[86] F. Immovilli, C. Bianchini, M. Cocconcelli, A. Bellini, and R. Rubini, "Bearing fault model for induction motor with externally induced vibration," *IEEE Trans. Ind. Electron.*, vol. 60, no. 8, pp. 3408–3418, Aug 2013.

[87] X. Jin, M. Zhao, T. Chow, and M. Pecht, "Motor bearing fault diagnosis using trace ratio linear discriminant analysis," *IEEE Trans. Ind. Electron.*, vol. 61, no. 5, pp. 2441–2451, May 2014.

[88] M. Amar, I. Gondal, and C. Wilson, "Vibration spectrum imaging: A bearing fault classification approach," *IEEE Trans. Ind. Electron.*, vol. PP, no. 99, pp. 1–9, 2014.

[89] B. Yazici and G. Kliman, "An adaptive statistical time-frequency method for detection of broken bars and bearing faults in motors using stator current," *IEEE Trans. Ind. Appl.*, vol. 35, no. 2, pp. 442–452, Mar 1999.

[90] J.-H. Jung, L. Jong-Jae, and B.-H. Kwon, "Online diagnosis of induction motors using MCSA," *IEEE Trans. Ind. Electron.*, vol. 53, no. 6, pp. 1842–1852, 2006.

[91] L. Frosini and E. Bassi, "Stator current and motor efficiency as indicators for different types of bearing faults in induction motors," *IEEE Trans. Ind. Electron.*, vol. 57, no. 1, pp. 244–251, Jan 2010.

[92] M. Seera and C. P. Lim, "Online motor fault detection and diagnosis using a hybrid FMM-CART model," *IEEE Trans. Neural Netw. Learn. Syst.*, vol. 25, no. 4, pp. 806–812, Apr. 2014.

[93] F. Immovilli, A. Bellini, R. Rubini, and C. Tassoni, "Diagnosis of bearing faults in induction machines by vibration or current signals: A critical comparison," *IEEE Trans. Ind. Appl.*, vol. 46, no. 4, pp. 1350–1359, July 2010.

[94] C. Riley, B. Lin, T. Habetler, and R. Schoen, "A method for sensorless on-line vibration monitoring of induction machines," *IEEE Trans. Ind. Appl.*, vol. 34, no. 6, pp. 1240–1245, Nov 1998.

[95] M. Devaney and L. Eren, "Detecting motor bearing faults," *IEEE Instrumentation Measurement Magazine*, vol. 7, no. 4, pp. 30–50, Dec 2004.

[96] E. Esfahani, S. Wang, and V. Sundararajan, "Multisensor wireless system for eccentricity and bearing fault detection in induction motors," *IEEE/ASME Trans. Mechatronics*, vol. 19, no. 3, pp. 818–826, June 2014.

[97] A. Bonnett and G. Soukup, "Rotor failures in squirrel cage induction motors," *IEEE Trans. Ind. Appl.*, vol. IA-22, no. 6, pp. 1165–1173, Nov 1986.

[98] M. Benbouzid and G. Kliman, "What stator current processing-based technique to use for induction motor rotor faults diagnosis?" *IEEE Trans. Energy Convers.*, vol. 18, no. 2, pp. 238–244, 2003.

[99] F. Filippetti, G. Franceschini, and C. Tassoni, "Neural networks aided on-line diagnostics of induction motor rotor faults," *IEEE Trans. Ind. Appl.*, vol. 31, no. 4, pp. 892–899, Jul 1995.

[100] H. Çalış and A. Çaklır, "Rotor bar fault diagnosis in three phase induction motors by monitoring fluctuations of motor current zero crossing instants," *Electric Power Systems Research*, vol. 77, no. 5-6, pp. 385–392, 2007.

[101] R. Supangat, N. Ertugrul, W. Soong, D. Gray, C. Hansen, and J. Grieger, "Detection of broken rotor bars in induction motor using starting-current analysis and effects of loading," *IEE Proc. Electric Power Applications,*, vol. 153, no. 6, pp. 848–855, Nov 2006.

[102] J. Wang, S. Liu, R. X. Gao, and R. Yan, "Current envelope analysis for defect identification and diagnosis in induction motors," *Journal of Manufacturing Systems*, vol. 31, no. 4, pp. 380–387, 2012.

[103] B. Ayhan, M.-Y. Chow, and M.-H. Song, "Multiple discriminant analysis and neural-network-based monolith and partition fault-detection schemes for broken rotor bar in induction motors," *IEEE Trans. Ind. Electron.*, vol. 53, no. 4, pp. 1298 –1308, Jun. 2006.

[104] O. Mohammed, N. Abed, and S. Ganu, "Modeling and characterization of induction motor internal faults using finite-element and discrete wavelet transforms," *IEEE Trans. Magn.*, vol. 42, no. 10, pp. 3434–3436, Oct 2006.

[105] J. Cusido, L. Romeral, J. Ortega, J. Rosero, and A. Garcia Espinosa, "Fault detection in induction machines using power spectral density in wavelet decomposition," *IEEE Trans. Ind. Electron.*, vol. 55, no. 2, pp. 633–643, Feb 2008.

[106] S. Kia, H. Henao, and G.-A. Capolino, "A high-resolution frequency estimation method for three-phase induction machine fault detection," *IEEE Trans. Ind. Electron.*, vol. 54, no. 4, pp. 2305–2314, 2007.

[107] Y.-H. Kim, Y.-W. Youn, D.-H. Hwang, J.-H. Sun, and D.-S. Kang, "High-resolution parameter estimation method to identify broken rotor bar faults in induction motors," *IEEE Trans. Ind. Electron.*, vol. 60, no. 9, pp. 4103–4117, Sept 2013.

[108] A. Trzynadlowski and E. Ritchie, "Comparative investigation of diagnostic media for induction motors: a case of rotor cage faults," *IEEE Trans. Ind. Electron.*, vol. 47, no. 5, pp. 1092–1099, Oct 2000.

[109] Z. Liu, X. Yin, Z. Zhang, D. Chen, and W. Chen, "Online rotor mixed fault diagnosis way based on spectrum analysis of instantaneous power in squirrel cage induction motors," *IEEE Trans. Energy Convers.*, vol. 19, no. 3, pp. 485–490, Sept 2004.

[110] G. Didier, E. Ternisien, O. Caspary, and H. Razik, "Fault detection of broken rotor bars in induction motor using a global fault index," *IEEE Trans. Ind. Appl.*, vol. 42, no. 1, pp. 79–88, Jan 2006.

[111] M. Drif and A. J. M. Cardoso, "The use of the instantaneous-reactive-power signature analysis for rotor-cage-fault diagnostics in three-phase induction motors," *IEEE Trans. Ind. Electron.*, vol. 56, no. 11, pp. 4606–4614, Nov 2009.

[112] A. Ceban, R. Pusca, and R. Romary, "Study of rotor faults in induction motors using external magnetic field analysis," *IEEE Trans. Ind. Electron.*, vol. 59, no. 5, pp. 2082–2093, May 2012.

[113] A. da Silva, R. Povinelli, and N. Demerdash, "Rotor bar fault monitoring method based on analysis of air-gap torques of induction motors," *IEEE Trans. Ind. Informat.*, vol. 9, no. 4, pp. 2274–2283, Nov 2013.

[114] J. Milimonfared, H. Kelk, S. Nandi, A. Minassians, and H. Toliyat, "A novel approach for broken-rotor-bar detection in cage induction motors," *IEEE Trans. Ind. Appl.*, vol. 35, no. 5, pp. 1000–1006, Sep 1999.

[115] S. M. A. Cruz, A. Stefani, F. Filippetti, and A. Marques Cardoso, "A new model-based technique for the diagnosis of rotor faults in RFOC induction motor drives," *IEEE Trans. Ind. Electron.*, vol. 55, no. 12, pp. 4218–4228, Dec 2008.

[116] C. Yang, T. Kang, D. Hyun, S. Lee, J. Antonino-Daviu, and J. Pons-Llinares, "Reliable detection of induction motor rotor faults under the rotor axial air duct influence," *IEEE Trans. Ind. Appl.*, vol. 50, no. 4, pp. 2493–2502, July 2014.

[117] A. Bellini, F. Filippetti, G. Franceschini, C. Tassoni, and G. Kliman, "Quantitative evaluation of induction motor broken bars by means of electrical signature analysis," *IEEE Trans. Ind. Appl.*, vol. 37, pp. 1248 –1255, Sep. 2001.

[118] D. Dorrell, W. Thomson, and S. Roach, "Analysis of airgap flux, current, and vibration signals as a function of the combination of static and dynamic airgap eccentricity in 3-phase induction motors," *IEEE Trans. Ind. Appl.*, vol. 33, no. 1, pp. 24–34, Jan. 1997.

[119] J. Cameron, W. Thomson, and A. Dow, "Vibration and current monitoring for detecting airgap eccentricity in large induction motors," *IEE Proceedings B Electric Power Applications*, vol. 133, no. 3, pp. 155–163, May 1986.

[120] S. Nandi, R. Bharadwaj, and H. Toliyat, "Performance analysis of a three-phase induction motor under mixed eccentricity condition," *IEEE Trans. Energy Convers.*, vol. 17, no. 3, pp. 392–399, Sep 2002.

[121] S. Nandi, S. Ahmed, and H. Toliyat, "Detection of rotor slot and other eccentricity related harmonics in a three phase induction motor with different rotor cages," *IEEE Trans. Energy Convers.*, vol. 16, no. 3, pp. 253–260, Sep 2001.

[122] D. Morinigo-Sotelo, L. Garcia-Escudero, O. Duque-Perez, and M. Perez-Alonso, "Practical aspects of mixed-eccentricity detection in PWM voltage-source-inverter-fed induction motors," *IEEE Trans. Ind. Electron.*, vol. 57, no. 1, pp. 252–262, Jan 2010.

[123] X. Huang, T. Habetler, and R. Harley, "Detection of rotor eccentricity faults in a closed-loop drive-connected induction motor using an artificial neural network," *IEEE Trans. Power Electron.*, vol. 22, no. 4, pp. 1552–1559, July 2007.

[124] J. Faiz and M. Ojaghi, "Instantaneous-power harmonics as indexes for mixed eccentricity fault in mains-fed and open/closed-loop drive-connected squirrel-cage induction motors," *IEEE Trans. Ind. Electron.*, vol. 56, no. 11, pp. 4718–4726, Nov 2009.

[125] J. Hong, D. Hyun, S. B. Lee, and C. Kral, "Offline monitoring of airgap eccentricity for inverter-fed induction motors based on the differential inductance," *IEEE Trans. Ind. Appl.*, vol. 49, no. 6, pp. 2533–2542, Nov 2013.

[126] G. Kliman, W. Premerlani, R. Koegl, and D. Hoeweler, "A new approach to on-line turn fault detection in AC motors," in *IEEE Industry Applications Soc. Annual Meeting Conf.*, vol. 1, Oct 1996, pp. 687–693.

[127] S. Grubic, J. Aller, B. Lu, and T. Habetler, "A survey on testing and monitoring methods for stator insulation systems of low-voltage induction machines focusing on turn insulation problems," *IEEE Trans. Ind. Electron.*, vol. 55, no. 12, pp. 4127–4136, Dec 2008.

[128] J. Kohler, J. Sottile, and F. Trutt, "Alternatives for assessing the electrical integrity of induction motors," *IEEE Trans. Ind. Appl.*, vol. 28, no. 5, pp. 1109–1117, Sep 1992.

[129] J. Sottile, J. and J. Kohler, "An on-line method to detect incipient failure of turn insulation in random-wound motors," *IEEE Trans. Energy Convers.*, vol. 8, no. 4, pp. 762–768, Dec 1993.

[130] S. M. A. Cruz and A. J. M. Cardoso, "Stator winding fault diagnosis in three-phase synchronous and asynchronous motors, by the extended Park's vector approach," *IEEE Trans. Ind. Appl.*, vol. 37, no. 5, pp. 1227–1233, 2001.

[131] ——, "Multiple reference frames theory: A new method for the diagnosis of stator faults in three-phase induction motors," *IEEE Trans. Energy Convers.*, vol. 20, no. 3, pp. 611–619, Sep. 2005.

[132] A. da Silva, R. Povinelli, and N. Demerdash, "Induction machine broken bar and stator short-circuit fault diagnostics based on three-phase stator current envelopes," *IEEE Trans. Ind. Electron.*, vol. 55, no. 3, pp. 1310–1318, March 2008.

[133] T. Wolbank, K. Loparo, and R. Wohrnschimmel, "Inverter statistics for online detection of stator asymmetries in inverter-fed induction motors," *IEEE Trans. Ind. Appl.*, vol. 39, no. 4, pp. 1102–1108, July 2003.

[134] M. Cash, T. Habetler, and G. Kliman, "Insulation failure prediction in AC machines using line-neutral voltages," *IEEE Trans. Ind. Appl.*, vol. 34, no. 6, pp. 1234–1239, Nov 1998.

[135] S. Cheng, P. Zhang, and T. Habetler, "An impedance identification approach to sensitive detection and location of stator turn-to-turn faults in a closed-loop multiple-motor drive," *IEEE Trans. Ind. Electron.*, vol. 58, no. 5, pp. 1545–1554, May 2011.

[136] J. Kohler, J. Sottile, and F. Trutt, "Condition monitoring of stator windings in induction motors. I. Experimental investigation of the effective negative-sequence impedance detector," *IEEE Trans. Ind. Appl.*, vol. 38, no. 5, pp. 1447–1453, Sep 2002.

[137] S. Nandi and H. Toliyat, "Novel frequency-domain-based technique to detect stator interturn faults in induction machines using stator-induced voltages after switch-off," *IEEE Trans. Ind. Appl.*, vol. 38, no. 1, pp. 101–109, Jan 2002.

[138] J. Sottile, F. Trutt, and J. Kohler, "Condition monitoring of stator windings in induction motors. II. Experimental investigation of voltage mismatch detectors," *IEEE Trans. Ind. Appl.*, vol. 38, no. 5, pp. 1454–1459, Sep 2002.

[139] S.-B. Lee, R. Tallam, and T. Habetler, "A robust, on-line turn-fault detection technique for induction machines based on monitoring the sequence component impedance matrix," *IEEE Trans. Power Electron.*, vol. 18, no. 3, pp. 865–872, May 2003.

[140] R. Maier, "Protection of squirrel-cage induction motor utilizing instantaneous power and phase information," *IEEE Trans. Ind. Appl.*, vol. 28, no. 2, pp. 376–380, Mar 1992.

[141] M. Drif and A. Cardoso, "Stator fault diagnostics in squirrel cage three-phase induction motor drives using the instantaneous active and reactive power signature analyses," *IEEE Trans. Ind. Informat.*, vol. 10, no. 2, pp. 1348–1360, May 2014.

[142] B. Mirafzal, R. Povinelli, and N. A. O. Demerdash, "Interturn fault diagnosis in induction motors using the pendulous oscillation phenomenon," *IEEE Trans. Energy Convers.*, vol. 21, no. 4, pp. 871–882, Dec 2006.

[143] B. Mirafzal and N. A. O. Demerdash, "On innovative methods of induction motor interturn and broken-bar fault diagnostics," *IEEE Trans. Ind. Appl.*, vol. 42, no. 2, pp. 405–414, March 2006.

[144] A. Ukil, S. Chen, and A. Andenn, "Detection of stator short circuit faults in three-phase induction motors using motor current zero crossing instants," *Electric Power System Research*, vol. 81, no. 4, pp. 1036 – 1044, 2011.

[145] G. Joksimovic and J. Penman, "The detection of inter-turn short circuits in the stator windings of operating motors," *IEEE Trans. Ind. Electron.*, vol. 47, no. 5, pp. 1078–1084, 2000.

[146] S. Nandi, "A detailed model of induction machines with saturation extendable for fault analysis," *IEEE Trans. Ind. Appl.*, vol. 40, no. 5, pp. 1302–1309, Sept 2004.

[147] C. Kallesoe, R. Izadi-Zamanabadi, P. Vadstrup, and H. Rasmussen, "Observer-based estimation of stator-winding faults in delta-connected induction motors: A linear matrix inequality approach," *IEEE Trans. Ind. Appl.*, vol. 43, no. 4, pp. 1022–1031, July 2007.

[148] J. Vitrià, P. Radeva, and I. Aguiló, *Recent Advances in Artificial Intelligence Research and Development*. IOS Press, 2004, vol. 113.

[149] F. Filippetti, G. Franceschini, C. Tassoni, and P. Vas, "AI techniques in induction machines diagnosis including the speed ripple effect," *IEEE Trans. Ind. Appl.*, vol. 34, no. 1, pp. 98–108, 1998.

[150] M.-Y. Chow and S. Yee, "Methodology for on-line incipient fault detection in single-phase squirrel-cage induction motors using artificial neural networks," *IEEE Trans. Energy Convers.*, vol. 6, no. 3, pp. 536–545, Sep 1991.

[151] F. Zidani, M. Benbouzid, D. Diallo, and M.-S. Nait-Said, "Induction motor stator faults diagnosis by a current concordia pattern-based fuzzy decision system," *IEEE Trans. Energy Convers.*, vol. 18, no. 4, pp. 469–475, Dec 2003.

[152] P. Goode and M. yuen Chow, "Using a neural/fuzzy system to extract heuristic knowledge of incipient faults in induction motors. Part I-Methodology," *IEEE Trans. Ind. Electron.*, vol. 42, no. 2, pp. 131–138, Apr 1995.

[153] G. Frantz, "Signal core: A short history of the digital signal processor," *IEEE Solid-State Circuits Magazine*, vol. 4, no. 2, pp. 16–20, 2012.

[154] C. Ong, *Dynamic Simulation of Electric Machinery: Using MATLAB/SIMULINK*. Prentice Hall PTR, 1998, ch. 6.

[155] B. Robyns, B. Francois, P. Degobert, and J. Hautier, *Vector Control of Induction Machines: Desensitisation and Optimisation Through Fuzzy Logic*. Springer, 2012.

[156] A. Proca, A. Keyhani, and J. Miller, "Sensorless sliding-mode control of induction motors using operating condition dependent models," *IEEE Trans. Energy Convers.*, vol. 18, no. 2, pp. 205–212, June 2003.

[157] G. Garcia Soto, E. Mendes, and A. Razek, "Reduced-order observers for rotor flux, rotor resistance and speed estimation for vector controlled induction motor drives using the extended Kalman filter technique," *IEE Proceedings Electric Power Applications*, vol. 146, no. 3, pp. 282–288, 1999.

[158] A. Trzynadlowski, *The Field Orientation Principle in Control of Induction Motors*. Kluwer Academic Publishers, Boston, 1994, ch. 1.

[159] LEM. [Online]. Available: http://www.lem.com/docs/products/lv%2025-p.pdf

[160] LEM. [Online]. Available: http://www.lem.com/docs/products/hy_sp1_e.pdf

[161] National Instruments. [Online]. Available: http://sine.ni.com/nips/cds/view/p/lang/en/nid/11914

[162] C. Zenger, "Sparse grids," in *Parallel Algorithms for Partial Differential Equations (W. Hackbusch, ed.)*, 1991, p. 590.

[163] R. Bellmann, *Adaptive Control Processes: A Guided Tour*. Princeton University Press, 1961.

[164] H.-J. Bungartz and M. Griebel, "Sparse grids," *Acta Numerica*, vol. 13, pp. 147–269, May 2004.

[165] K. Frank, S. Heinrich, and S. Pereverzev, "Information complexity of multivariate fredholm integral equations in Sobolev classes," *Journal of Complexity*, vol. 12, no. 1, pp. 17–34, 1996.

[166] M. Griebel, P. Oswald, and T. Schiekofer, "Sparse grids for boundary integral equations," *Numerische Mathematik*, vol. 83, no. 2, pp. 279–312, 1999.

[167] W. Sickel and F. Sprengel, "Interpolation on sparse grids and tensor products of Nikol'skij−Besov spaces," *Journal of Computational Analysis and Applications*, vol. 1, no. 3, pp. 263–288, 1999.

[168] M. Griebel and S. Knapek, "Optimized tensor-product approximation spaces," *Constructive Approximation*, vol. 16, no. 4, pp. 525–540, 2000.

[169] J. Garcke and M. Griebel, "On the computation of the eigenproblems of Hydrogen and Helium in strong magnetic and electric fields with the sparse grid combination technique," *Journal of Computational Physics*, vol. 165, no. 2, pp. 694 – 716, 2000.

[170] R. Byrd, C. Dert, A. Rinnooy Kan, and R. Schnabel, "Concurrent stochastic methods for global optimization," *Mathematical Programming*, vol. 46, no. 1-3, pp. 1–29, 1990.

[171] E. Novak and K. Ritter, "High dimensional integration of smooth functions over cubes," *Numerische Mathematik*, vol. 75, no. 1, pp. 79–97, 1996.

[172] T. Gerstner and M. Griebel, "Numerical integration using sparse grids," *Numerical Algorithms*, vol. 18, no. 3-4, pp. 209–232, 1998.

[173] F. Sprengel, "A unified approach to error estimates for interpolation on full and sparse Gauss−Chebyshev grids," *Rostocker Math. Kolloq*, vol. 51, pp. 51–64, 1997.

[174] M. Griebel, W. Huber, U. Rde, and T. Strtkuhl, "The combination technique for parallel sparse-grid-preconditioning or -solution of PDE's on workstation networks," in *Parallel Processing: CONPAR 92-VAPP V*, ser. Lecture Notes in Computer Science, L. Boug, M. Cosnard, Y. Robert, and D. Trystram, Eds. Springer Berlin Heidelberg, 1992, vol. 634, pp. 217–228.

[175] L. C. W. Dixon and G. P. Szegö, "The global optimization problem: An introduction," in *Towards Global Optimization 2*. North-Holland, Amsterdam, 1978.

[176] V. Picheny, T. Wagner, and D. Ginsbourger, "A benchmark of kriging-based infill criteria for noisy optimization," *Structural and Multidisciplinary Optimization*, vol. 48, no. 3, pp. 607–626, 2013.

[177] F. Höppner, F. Klawonn, R. Kruse, and T. Runkler, *Fuzzy Cluster Analysis: Methods for Classification*. John Wiley and Sons, 1999.

[178] K. Levenberg, "A method for the solution of certain non-linear problems in least squares," *The Quarterly of Applied Mathematics*, vol. 2, pp. 164–168, 1944.

[179] J. Nelder and R. Mead, "A simplex method for function minimization," *Computer Journal*, vol. 7, no. 4, pp. 308–313, 1965.

[180] D. Himmelblau, *Applied Nonlinear Programming*. McGraw-Hill, 1972.

[181] P. Hansen and B. Jaumard, "Lipschitz optimization," in *Handbook of Global Optimization*, R. Horst and P. M. Pardalos, Eds. Kluwer, Dordrecht, 1995, pp. 407–493.

[182] J. Shekel, "Test functions for multimodal search techniques," in *Fifth Annual Princeton Conference on Information Science and Systems*, 1971.

[183] A. Griewank, "Generalized descent for global optimization," *Journal of Optimization Theory and Applications*, vol. 34, no. 1, pp. 11–39, 1981.

[184] H. Kojabadi, L. Chang, and R. Doraiswami, "A novel adaptive observer for very fast estimation of stator resistance in sensorless induction motor drives," in *2003 IEEE 34th Annual Power Electronics Specialist Conference, 2003. PESC '03.*, vol. 3, 2003, pp. 1455–1459.

[185] J. De Kock, F. van der Merwe, and H. Vermeulen, "Induction motor parameter estimation through an output error technique," *IEEE Trans. Energy Convers.*, vol. 9, no. 1, pp. 69–76, 1994.

[186] R. Cardenas and R. Pena, "Sensorless vector control of induction machines for variable-speed wind energy applications," *IEEE Trans. Energy Convers.*, vol. 19, no. 1, pp. 196–205, March 2004.

[187] V. Verma, C. Chakraborty, S. Maiti, and Y. Hori, "Speed sensorless vector controlled induction motor drive using single current sensor," *IEEE Trans. Energy Convers.*, vol. 28, no. 4, pp. 938–950, 2013.

[188] I.-J. Ha and S.-H. Lee, "An online identification method for both stator and rotor resistances of induction motors without rotational transducers," *IEEE Trans. Ind. Electron.*, vol. 47, no. 4, pp. 842–853, Aug 2000.

[189] M. Depenbrock, "Speed sensorless control of induction motors at very low stator frequencies," in *Proc. European Conf. Power Electronics and Applications*, 1999.

[190] K. J. Åström and B. Wittenmark, *Adaptive Control*, 2nd ed. Addison-Wesley, 1995, ch. 2.

[191] K. Gyftakis, D. Spyropoulos, J. Kappatou, and E. Mitronikas, "A novel approach for broken bar fault diagnosis in induction motors through torque monitoring," *IEEE Trans. Energy Convers.*, vol. 28, no. 2, pp. 267–277, 2013.

[192] A. Sadoughi, M. Ebrahimi, and E. Razaei, "A new approach for induction motor broken bar diagnosis by using vibration spectrum," in *International Joint Conference SICE-ICASE, 2006.*, Oct. 2006, pp. 4715 –4720.

[193] G. Joksimovic, J. Riger, T. Wolbank, N. Peric, and M. Vasak, "Stator-current spectrum signature of healthy cage rotor induction machines," *IEEE Trans. Ind. Electron.*, vol. 60, no. 9, pp. 4025–4033, 2013.

[194] M. Avriel, *Nonlinear Programming: Analysis and Methods*. Courier Dover Publications, 2003.

[195] M. Mitchell, *An Introduction to Genetic Algorithms*. MIT Press, 1999.

[196] S. Bachir, S. Tnani, G. Champenois, and J. Trigeassou, "Diagnosis of induction machines by parameter estimation," in *Control Methods for Electrical Machines*, R. Husson, Ed. Wiley-ISTE, 2003, ch. 8, pp. 245–270.

[197] T. Boukra, A. Lebaroud, and G. Clerc, "Statistical and neural-network approaches for the classification of induction machine faults using the ambiguity plane representation," *IEEE Trans. Ind. Electron.*, vol. 60, no. 9, pp. 4034–4042, Sep. 2013.

[198] R. Dugan, M. McGranaghan, and H. Beaty, *Electrical Power Systems Quality*. New York: McGraw-Hill, 1996.

[199] R. Tallam, T. Habetler, and R. Harley, "Transient model for induction machines with stator winding turn faults," *IEEE Trans. Ind. Appl.*, vol. 38, no. 3, pp. 632–637, 2002.

[200] *Communication networks and systems in substations*, IEC Std. IEC 61 850.

[201] *Communications for monitoring and control of wind power plants*, IEC Std. IEC 61 400-25, 2006.

[202] *Hydroelectric Power plants communication for monitoring and control*, IEC Std. IEC 61 850 Part 7-410, 2006.

[203] *DER logical nodes*, IEC Std. IEC 61 850 Part 7-420, 2008.

[204] *SEL-710 Motor Protection Relay Instruction Manual*, Schweitzer Engineering Laboratories, WA 99163, USA.

[205] S. Jun-ping, S. Wan-xing, W. Sun-an, and K. gong Wu, "Substation automation high speed network communication platform based on MMS+TCP/IP+Ethernet," in *International Conference on Power System Technology*, vol. 2, 2002, pp. 1296–1300.

[206] A. Raza, K. Ullah, S. Ahmed, S. Ahmed, H.-S. Jang, and H.-S. Yang, "Gigabit ethernet based substation under IEC 61850 standard," in *2nd International Conference on Computer, Control and Communication, IC4 2009.*, 2009, pp. 1–6.

[207] R. Mackiewicz, "Overview of IEC 61850 and benefits," in *IEEE Power Engineering Society General Meeting, 2006.*, 2006, pp. 1–8.

[208] A. S. Tanenbaum, *Computer Networks*, 4th ed. Merrill, 2002.

[209] *AX-S4 MMS*, Systems Integration Specialists Company, Inc. (SISCO), MI, USA. [Online]. Available: http://www.sisconet.com/axs4mms.htm

[210] S. Chen and R. Živanović, "Modelling and simulation of stator and rotor fault conditions in induction machines for testing fault diagnostic techniques," *European Transactions on Electrical Power*, vol. 20, no. 5, pp. 611–629, 2010.

[211] M. Musaruddin, M. Zaporoshenko, and R. Zivanovic, "Remote protective relay testing," in *AUPEC08 - 18th Australasian Universities Power Engineering Conference*, 2008, pp. 1–4.

[212] Mathworks. [Online]. Available: http://www.mathworks.com/products/opc/